

**DEMONSTRATION OF FUEL RESISTANT
TO PELLET-CLADDING INTERACTION
PHASE 2 — SECOND SEMIANNUAL REPORT
JULY — DECEMBER 1979**

COMMONWEALTH RESEARCH CORPORATION
SUBCONTRACT 3-20-46
U.S. DEPARTMENT OF ENERGY
PRIME CONTRACT DE-AC02-77ET34001

GENERAL  ELECTRIC

8009160 436

GEAP-25163-2
UC-78
March 1980
DRF No. J11-102

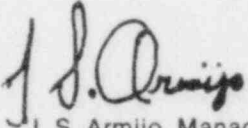
**DEMONSTRATION OF FUEL RESISTANT TO
PELLET-CLADDING INTERACTION**

PHASE 2

Second Semiannual Report, July—December 1979

Compiled by
H.S. Rosenbaum
Program Manager

Approved:


J. S. Armijo, Manager
Core Materials Technology

Prepared for the
Commonwealth Research Corporation under Subcontract 3-20-46
U.S. Department of Energy
Prime Contract DE-AC02-77ET34001
(Formerly Contract EN-77-C-02-4473)

*Printed in the United States of America
Available from
National Technical Information Service
U.S. Department of Commerce
5285 Port Royal Road
Springfield, VA 22161*

Price: Printed Copy \$4.00; Microfiche \$2.25

LEGAL NOTICE

This report was prepared by General Electric as an account of work sponsored by the U.S. Department of Energy ("DOE"). Neither DOE, members of DOE, nor GE, nor any person acting on behalf of either, including Commonwealth Edison Company and Commonwealth Research Corporation:

- A. *Makes any warranty or representations, express or implied, with respect to the accuracy, completeness, or usefulness of the information contained in this report, or that the use of any information, apparatus, method, or process disclosed in this report may not infringe privately owned rights; or*

- B. *Assumes any liabilities with respect to the use of, or for damages resulting from the use of, any information, apparatus, method, or process disclosed in this report.*

TABLE OF CONTENTS

	Page
ABSTRACT.....	ix
CONTRIBUTING AUTHORS.....	xi
HIGHLIGHTS.....	xiii
ACKNOWLEDGEMENTS.....	xv
1. INTRODUCTION.....	1-1
2. TASK I. NUCLEAR DESIGN AND CORE MANAGEMENT.....	2-1
2.1 Objectives.....	2-1
2.2 Introduction.....	2-1
2.3 Energy Utilization Plan (EUP).....	2-5
2.4 Power Ramp Simulation.....	2-6
3. TASK II. SUPPORT TESTS.....	3-1
3.1 Objectives.....	3-1
3.2 Subtask II.1 Laboratory Tests.....	3-1
3.2.1 Subtask II.1.1 Characterization and Stability.....	3-1
3.2.2 Subtask II.1.2 PCI Simulation Tests.....	3-12
3.3 Subtask II.2 Licensing Tests.....	3-18
3.3.1 Loss-of-Coolant-Accident Simulation.....	3-18
3.4 Subtask II.3 Fuel Irradiation Tests.....	3-24
3.4.1 Segmented Rod Irradiation Tests.....	3-24
3.4.2 Fuel with Cladding Perforation.....	3-45
4. TASK III. DEMONSTRATION.....	4-1
4.1 Objectives.....	4-1
4.2 Subtask III.1 Design and Licensing of Demonstration Fuel.....	4-1
4.3 Subtask III.2 Fabrication of Demonstration Fuel.....	4-1
4.3.1 Zr-liner.....	4-1
4.3.2 Cu-barrier.....	4-1
4.4 Subtask III.3 Irradiation and Evaluation.....	4-2
5. TASK IV. LEAD TEST ASSEMBLIES.....	5-1
DISTRIBUTION.....	1

LIST OF ILLUSTRATIONS

Figure	Title	Page
2.2-1	Ramp Cell Locations, Cycles 6 and 7.....	2-2
2.2-2	Ramp Cell Locations, Cycles 8 and 9. Driver Fuel Indicated by D.....	2-3
2.2-3	Allowable Pre-Ramp Locations for Special Barrier Bundles.....	2-4
2.4-1	Operational Strategy.....	2-7
2.4-2	Typical EOC Ramping Schedule, Cycle 6/7.....	2-8
3.2-1	Perforated Rod Simulator Test Apparatus.....	3-3
3.2-2	The Refreshed Autoclave System Shown Schematically.....	3-4
3.2-3	Photomicrographs of (a) low oxygen sponge and (b) crystal bar zirconium lined tubing before testing, (1), and after being tested in the simulator at 350 °C in 7.0 MPa (1000 psig) steam for 3 days.....	3-5
3.2-4	Photomicrographs of (1) low oxygen sponge and (2) crystal bar zirconium lined tubing after being tested in the simulator at 350 °C in 7.0 MPa (1000 psig) steam for 12 days. (a) and (b) represent different locations of the same samples.....	3-7
3.2-5	Corrosion Weight Gains for Zr-liner Cladding and Reference Zircaloy-2 as a Function of Time at 350 °C and 400 °C in 7.0 MPa (1000 psig) Steam in the Simulator.....	3-8
3.2-6	Photomicrographs of (a) low oxygen sponge and (b) crystal bar zirconium lined tubing after being tested in the refreshed autoclave at (1) 350 °C and (2) 400 °C in 7.0 MPa (1000 psig) Steam for 3 Days.....	3-10
3.2-7	Photomicrographs and photomicrographs of specimens after being tested in the refreshed autoclave at 350 °C, 7.0 MPa (1000 psig) for 13 days: (a) inner surface visual appearance; specimens labeled L have the low oxygen sponge Zr-liner while those labeled X have the crystal bar Zr-liner; (b) crystal bar liner in the as-received condition; (c) crystal bar liner in the belt ground condition; low oxygen sponge in (d) as received; (e) 1 min etched; (f) belt ground conditions.....	3-11
3.2-8	Comparison of Knoop microhardness impressions for irradiated crystal bar zirconium liner and Zircaloy-2 cladding. (Fluence = 1.5×10^{21} n/cm ² (E > 1 MeV), Irradiation Temperature ≈ 288 °C).....	3-13
3.2-9	Knoop Microhardness vs. Fast Neutron Fluence for Zirconium and Zircaloy-2.....	3-14
3.2-10	Remote Expanding Mandrel Loading System (REMLS).....	3-16
3.3-1	Temperature as a Function of Time for Simulated LOCA Testing.....	3-19
3.3-2	Typical Computer Output for LOCA Test.....	3-21
3.3-3	LOCA Specimens Tested at 5.2 Mpa Hoop Stress Original Tubing Outer Diameter = 12.3 mm.....	3-22

3.3-4	LOCA Specimens Tested at 6.9 MPa Hoop Stress	3-23
3.4-1	Ramp Test Sequence to Investigate Effect of Short (6 Hours) Standardization Phase. Ramp Test Sequence A	3-28
3.4-2	Ramp Test Sequence B	3-29
3.4-3	Recorder Chart Output, SRP-2/21	3-30
3.4-4	Ramp Sequence A — Effect of Standardization Time	3-32
3.4-5	Copper Barrier (Nonbonded) — Total Experience	3-33
3.4-6	Ramp Sequence B Results	3-35
3.4-7	Nondestructive Test Results — Cu-barrier Rod SRP-2/1	3-37
3.4-8	Nondestructive Test Results — Zr-liner Rod SRP-3/35	3-39
3.4-9	Nondestructive Test Data — Reference Rod SRP-2/14	3-41
3.4-10	SRP Segment Cladding Strain Due to Power Ramp Testing	3-44
3.4-11	Fabrication Flow in the High Power Region of Zr-liner Fuel Rod SRP-3/35	3-46
3.4-12	Microcracks in the High Power and High Strain Region of Zr-liner Fuel Rod SRP-3/35	3-47
3.4-13	Locations of Microcracks on Inner Surface of Zr-liner Fuel Rod SRP-3/35	3-48
3.4-14	Perforated Fuel Test Rod	3-49
3.4-15	Correlation Between Loop Activity and Loop Pressure During Steady State Operation	3-52
3.4-16	Correlation Between Loop Activity and Loop Pressure Shortly After Reactor Shutdown	3-53
3.4-17	Trend of Loop 2 Coolant Activity Through First Two Cycles	3-54
4.3-1	Example of Low-Oxygen Sponge Zirconium-Lined Tubeshell Showing the Zircaloy-Zirconium Interface Prior to Tube Reduction	4-2
4.3-2	Electroless Copper Plated on Oxidized Zircaloy, Viewed in Tapered Section. (a) WLM (b) CRD	4-3
4.3-3	Same as Figure 4.3-2 at 1000 \times	4-4
4.3-4	Scanning Electron Micrographs of Copper Surfaces Electroless Plated on Oxidized Zircaloy. (a) WLM (b) CRD	4-5
4.3-5	Copper Electroless Plated on Oxidized Zircaloy Viewed on Polished Cross Sectioned and Etched. (a) WLM (b) CRD	4-6
4.3-6	Zircaloy Tubing Surfaces After Removal of Copper in Dilute aq. HNO ₃ . (a) WLM (b) CRD	4-7

LIST OF TABLES

Table	Title	Page
2.3-1	Initial Energy Utilization Plan for PCI-Resistant Fuel Demonstration in Quad-Cities Unit 2	2-5
2.4-1	Reload Bundle Requirements for Demonstration Cycles (Preliminary)	2-6
2.4-2	Preliminary Reference Loading Pattern Cycle Exposure Capabilities	2-7
2.4-3	Peak LHGR Achieved During Ramping	2-8
3.2-1	Weight Gain Data of Samples Tested in the Simulator at 350 and 400 °C	3-6
3.2-2	The Weight Gain (mg/dm ²) of Cladding Samples Tested in the Recirculating Autoclave at 350 and 400 °C	3-9
3.2-3	Weight Gain (mg/dm ²) of Samples Tested in the Re-circulating Autoclave Test Conditions: 350 °C, 7.0 MPa (1000 psig), 13 Days	3-9
3.2-4	Tensile Tests of Zirconium Irradiated at 327 °C to Fluence 6.8×10^{26} n/cm ² (E > 1 MeV)	3-15
3.3-1	LOCA Test Summary	3-24
3.4-1	SRP Irradiation Status	3-25
3.4-2	Description of Fuel Rods Ramp Tested in 1979	3-26
3.4-3	1979 SRP Ramp Test, Program Result Summary	3-31
3.4-4	1978 Ramp Tests — Nondestructive PIE Results Summary	3-36
3.4-5	Cladding Strains — Zr-Liner Rods	3-43
3.4-6	Correlation Between Microcracks and Cladding Duty in SRP-3/35	3-45
3.4-7	Perforated Rod Design Details	3-50
3.4-8	Special Reactor Startup Procedure	3-50
3.4-9	Water Sample Activity Analysis — Data Summary	3-55

ABSTRACT

This program has as its ultimate objective the demonstration of an advanced fuel design that is resistant to the failure mechanism known as fuel pellet-cladding interaction (PCI). Two fuel concepts are being developed for possible demonstration within this program: (a) Cu-barrier fuel and (b) Zr-liner fuel. These advanced fuels (known collectively as "barrier fuels") have special fuel cladding designed to avoid the harmful effects of localized stress and reactive fission products during reactor service. Within the work scope of this program one of these concepts will be selected for demonstration in a commercial power reactor.

In the current report period the nuclear design of the demonstration was begun. The design calls for 132 bundles of barrier fuel to be inserted into the core of Quad Cities Unit 2 at the Beginning of Cycle 6. The nuclear design uses the scheme which was developed in PHASE 1 of this program. Near the end of Cycles 6, 7, 8 and 9, sixteen bundles of demonstration fuel will be power ramped to demonstrate resistance to PCI. Thus, 64 bundles will be ramped in this manner.

Laboratory and in-reactor tests were started to evaluate the stability of Zr-liner fuel which remains in service after a defect has occurred which allows water to enter the rod. Results to date on intentionally defected fuel indicate that the Zr-liner fuel is not rapidly degraded despite ingress of water.

Irradiation tests of barrier fuel, including power ramping, have shown that Zr-liner fuel has excellent PCI resistance at burnup levels to 16.6 MWd/kg U despite plastic deformation in excess of 0.5% induced by the severe power ramp test. Cu-barrier fuel with copper plated onto etched Zircaloy (no intermediate oxide diffusion barrier) tends to lose its resistance to PCI at exposures >14 MWd/kg U. However, it continues to perform better than does reference fuel.

Four lead test assemblies of barrier fuel (two of Zr-liner and two of Cu-barrier) are presently under irradiation in Quad Cities Unit 1 and have achieved a burnup of approximately 6.5 MWd/kg U thus far.

CONTRIBUTING AUTHORS

- R. B. Adamson, Nuclear Fuel and Services Engineering Department, (NFSED)
- D. E. Allen, Wilmington Manufacturing Department, (WMD)
- J. A. Baumgartner, Nuclear Fuel and Services Engineering Department, (NFSED)
- R. E. Blood, Nuclear Fuel and Services Engineering Department, (NFSED)
- R. E. Brown, Nuclear Fuel and Services Engineering Department, (NFSED)
- B. Cheng, Nuclear Fuel and Services Engineering Department, (NFSED)
- J. H. Davies, Nuclear Fuel and Services Engineering Department, (NFSED)
- D. K. Dennison, Nuclear Fuel and Services Engineering Department, (NFSED)
- R. E. Donaghy, Wilmington Manufacturing Department, (WMD)
- E. L. Esch, Nuclear Fuel and Services Engineering Department, (NFSED)
- W. J. Grubb, Corporate Research and Development, (CRD)
- C. C. Guitton, Nuclear Fuel and Services Engineering Department, (NFSED)
- J. O. Hegland, Nuclear Fuel and Services Engineering Department, (NFSED)
- G. H. Henderson, Nuclear Fuel and Services Engineering Department, (NFSED)
- R. D. Jones, Nuclear Fuel and Services Engineering Department, (NFSED)
- R. J. Mack, Wilmington Manufacturing Department, (WMD)
- H. H. Paustian, Nuclear Fuel and Services Engineering Department, (NFSED)
- M. B. Reynolds, Nuclear Fuel and Services Engineering Department, (NFSED)
- E. Rosicky, Nuclear Fuel and Services Engineering Department, (NFSED)
- J. R. Thompson, Nuclear Fuel and Services Engineering Department, (NFSED)
- R. P. Tucker, Nuclear Fuel and Services Engineering Department, (NFSED)
- S. B. Wisner, Nuclear Fuel and Services Engineering Department, (NFSED)

HIGHLIGHTS

- Power ramp testing of barrier fuel continues to show superior PCI resistance compared to the reference conventional fuel.
- The Zr-liner fuel tested at lead burnup (16.6 MWd/kg U) successfully sustained diametral plastic strain of approximately 0.5%; comparable reference fuel failed at much lower plastic strain in these ramp tests.
- Many crack nuclei were found on the inner surface of the highly strained regions of the Zr-liner cladding. These crack nuclei were uniformly limited in length to approximately $12 \mu\text{m}$. Thus, while cracks nucleated at high powers they did not propagate into the zirconium liner despite the large strain.
- Although Cu-barrier fuel out-performs reference fuel, the design with copper plated onto etched Zircaloy (i.e. no oxide layer between copper and Zircaloy) is not immune to PCI failures at burnups >14 MWd/kg U. The tests are consistent with the hypothesis that interdiffusion of copper with Zircaloy tends to reduce the resistance to PCI.
- Laboratory tests of the stability of Zr-liner fuel indicate that under conditions which simulate a fuel cladding perforation the zirconium liner oxidizes rapidly and that the reaction slows markedly when the oxide/metal interface enters the Zircaloy.
- An in-reactor test of deliberately perforated Zr-liner fuel is in progress with early results showing no sign of rapid degradation of the cladding.
- Four lead test assemblies (LTA's) of barrier fuel are under irradiation in the core of Quad Cities Unit 1 since February 1979, and they have achieved a burnup of approximately 6.5 MWd/kg U through December 1979. These assemblies include both Cu-barrier and Zr-liner fuel.

ACKNOWLEDGEMENTS

The help of the following people is gratefully acknowledged:

J. S. Armijo of the GE Nuclear Fuel and Services Engineering Department for his continued encouragement and leadership.

M. L. Ishikawa of the Japan Atomic Energy Research Institute for his help in implementing the RIA tests which were reported in this program.

W. V. Johnston and R. VanHouten of the Fuel Behavior Research Branch of the U.S. Nuclear Regulatory Commission for their continued interest in this program and for their help in effecting safety tests for barrier fuel.

W. M. Kiefer of the Commonwealth Edison Company for his continued interest and for his participation in the Program Steering Committee.

P. M. Lang of the U.S. Department of Energy for his support and for his participation in the Program Steering Committee.

A. S. Mehner of the U.S. Department of Energy (on leave from EG&G Idaho, Inc.) for his encouragement and for helpful discussions.

D. R. O'Boyle of the Commonwealth Edison Company for his active support from the beginning of this program and for his critical review of the manuscript of this report.

1. INTRODUCTION

An important mechanism for fuel failure in power reactors involves the direct interaction between the irradiated uranium fuel, including its inventory of fission products, and the Zircaloy fuel sheath. This fuel failure mechanism is known as "fuel/cladding interaction" or "pellet-cladding interaction" (PCI). This fuel failure mechanism is known to occur in all types of power reactors fueled with uranium oxide which is sheathed in Zircaloy. Building upon the General Electric Company's efforts from 1969 to 1977 to understand the PCI phenomenon and to develop potential remedies, this program was designed to exploit two remedies which General Electric (GE) had already identified as having good potential for success: (a) Cu-barrier fuel and (b) Zr-liner fuel. These fuel concepts are known collectively as barrier fuel, and they have been previously described.¹⁻⁴

This program leads ultimately to the large-scale demonstration of one of the two remedy concepts discussed here: Cu-barrier or Zr-liner. The overall program has been divided into three phases:

- PHASE 1. Design and Supporting Tests
- PHASE 2. Large-Scale Demonstration
- PHASE 3. Demonstration Extending to High Burnup

PHASE 1 now has been completed and its final report issued.² PHASE 1 included:

1. A generic nuclear engineering study to show that the demonstration is feasible in a reactor of the BWR/3 type.
2. Laboratory and reactor tests to verify the PCI resistance of the Cu-barrier and the Zr-liner fuel types.
3. Laboratory tests of barrier cladding under simulated loss-of-coolant accident (LOCA) conditions.
4. Design, licensing documentation, fabrication and preirradiation characterization of four lead test assemblies (LTA's) for irradiation in the Quad Cities Nuclear Power Station Unit 1, beginning in Cycle 5. Irradiation of the LTA's was begun in February 1979.

PHASE 2 continues the work of PHASE 1, and includes:

1. Selection of the fuel design for the demonstration.
2. Nuclear design and core management of the demonstration, expanding from the generic feasibility study in PHASE 1 to a specific reactor and target cycle, including bundle nuclear designs. As presently contemplated, the reactor and target cycle are Quad Cities Unit 2, beginning with Cycle 6 (tentatively scheduled to begin in January 1982).
3. Design, licensing documentation, and manufacturing of the demonstration fuel.
4. The demonstration *per se*; i.e., the irradiation (including specially designed power ramps to demonstrate PCI resistance). As presently perceived, PHASE 2 will include the irradiation through 1984 and is intended to include two full demonstration cycles and end-of-cycle ramps (depending on reactor schedule).
5. Continued irradiation and evaluation of the four LTA's.
6. Continued testing of barrier fuel to assure PCI resistance at burnup levels relevant to the demonstration.

PHASE 3 is intended to extend the demonstration to high burnup. It is contingent on successful completion of PHASE 2, and details of the scope have yet to be defined.

The first semiannual progress report for PHASE 2 has been issued previously¹ and includes work done in the first half of calendar year 1979. This is the second semiannual progress report for PHASE 2; it includes work during July-December 1979.

The task structure of PHASE 2 is as follows:

Task I. Nuclear Design and Core Management

- Design of the core and the licensing of the demonstration including the mode of operation to power ramp the demonstration of fuel bundles in the test cells.
- Core management activities associated with the demonstration (but excluding that effort which would be normally required in the absence of the demonstration).

Task II. Support Tests

Subtask II.1 Laboratory Tests

- Characterization of barrier fuel and assessment of barrier stability.
- Simulated PCI tests.

Subtask II.2 Licensing Tests

- Tests to assess behavior of barrier fuel under accident conditions: (a) reactivity-initiated accident (RIA) and (b) loss-of-coolant accident (LOCA).

Subtask II.3 Fuel Irradiation Tests

- Power ramp tests in a test reactor to evaluate the PCI resistance of barrier fuel at various burnup levels.
- Stability of barrier fuel with a through-wall defect.

Task III. Demonstration

Subtask III.1 Design and Licensing of Demonstration Fuel

- Design and licensing activities associated with the barrier fuel itself.
- Integration of design and fabrication.

Subtask III.2 Fabrication of Demonstration Fuel

- Fabrication of 132 demonstration bundles of barrier fuel.

Subtask III.3 Irradiation and Evaluation

- Monitoring power history.
- Evaluation of performance of the demonstration fuel and analysis leading to engineering inferences.

Task IV. Lead Test Assemblies

- Evaluation of the in-reactor performance of the LTA's including correlations with power history.

2. TASK I. NUCLEAR DESIGN AND CORE MANAGEMENT (H. H. Paustian and R. E. Brown, NFSED)

2.1 OBJECTIVES

1. Design the demonstration irradiation for a specific reactor and target cycle (tentatively Quad Cities-2, Cycle 6) including technical evaluation of the fuel loading pattern and the reactor operational mode to effect both the demonstration and the efficient production of electricity as dictated by the needs of the Commonwealth Edison Company (CECo).
2. Develop and implement a core management plan for the demonstration irradiation.
3. Design the demonstration fuel bundles.
4. Provide the nuclear licensing support required for the demonstration irradiation and the associated reactor operating plan.
5. Work with CECo
 - a) to define the operational constraints imposed by the reactor owner-operator, and
 - b) to obtain mutually satisfactory arrangements required to conduct the demonstration irradiation.

2.2 INTRODUCTION

In PHASE 1 a generic nuclear design was done^{2,3} to determine the feasibility of a large-scale demonstration of PCI-resistant fuel in an operating commercial power reactor of type BWR/3. The generic design involved 132 bundles of the PCI-resistant fuel (i.e., barrier fuel), of which 64 were to be power ramped. These 64 bundles were divided into four groups of 16 with one group to be ramped at the end of each of four successive reactor cycles. Thus, taking Quad Cities Unit 1, Cycles 6-9 as an example of a BWR/3 core on which to base the generic study, one group of 16 bundles would be ramped at the end of Cycle 6, another at the end of Cycle 7, etc. In each of these cycles the bundles to be ramped were placed into four particular cells (one cell in each quarter core); these cells comprised a single cruciform control blade and four demonstration bundles surrounded by a buffer zone of one row of low reactivity conventional fuel bundles. In each cycle the control blade in these assemblies was held ~70-100% inserted until very near the end of the cycle, when the blade was withdrawn in increments of 0.457 m (1.50 feet) to effect a controlled and localized power ramp.

This generic design was studied in PHASE 1, and calculations were performed to evaluate cycle exposure capability, reactivity margins, critical control rod patterns, core response to assumed accidents and transients, and core response to the power ramping of the demonstration fuel assemblies.^{2,3}

Having shown in PHASE 1 the feasibility of a large-scale demonstration in an operating reactor, attention has been turned to the detailed design required for the demonstration in a specific reactor and cycles, Quad Cities Unit 2, Cycles 6 through 9. However, the basic concept utilizing special ramp cells surrounded by a buffer zone was retained from the generic study. The locations and configurations of the special ramp cells are shown in Figure 2.2-1. In the later demonstration cycles (Cycles 8 and 9) it is possible that fresh fuel bundles will have to be used within the ramp cells to boost the power to obtain a good demonstration of PCI resistance during the power ramps. In that event each quarter core would have two special ramp cells, each with two demonstration fuel bundles and two fresh driver fuel bundles as shown in Figure 2.2-2. In accord with the generic study the demonstration bundles which are to be ramped in a particular cycle are loaded in the special ramp cells at the beginning of that cycle; bundles which are scheduled to be ramped in subsequent cycles are loaded near the core periphery in the locations indicated in Figure 2.2-3.

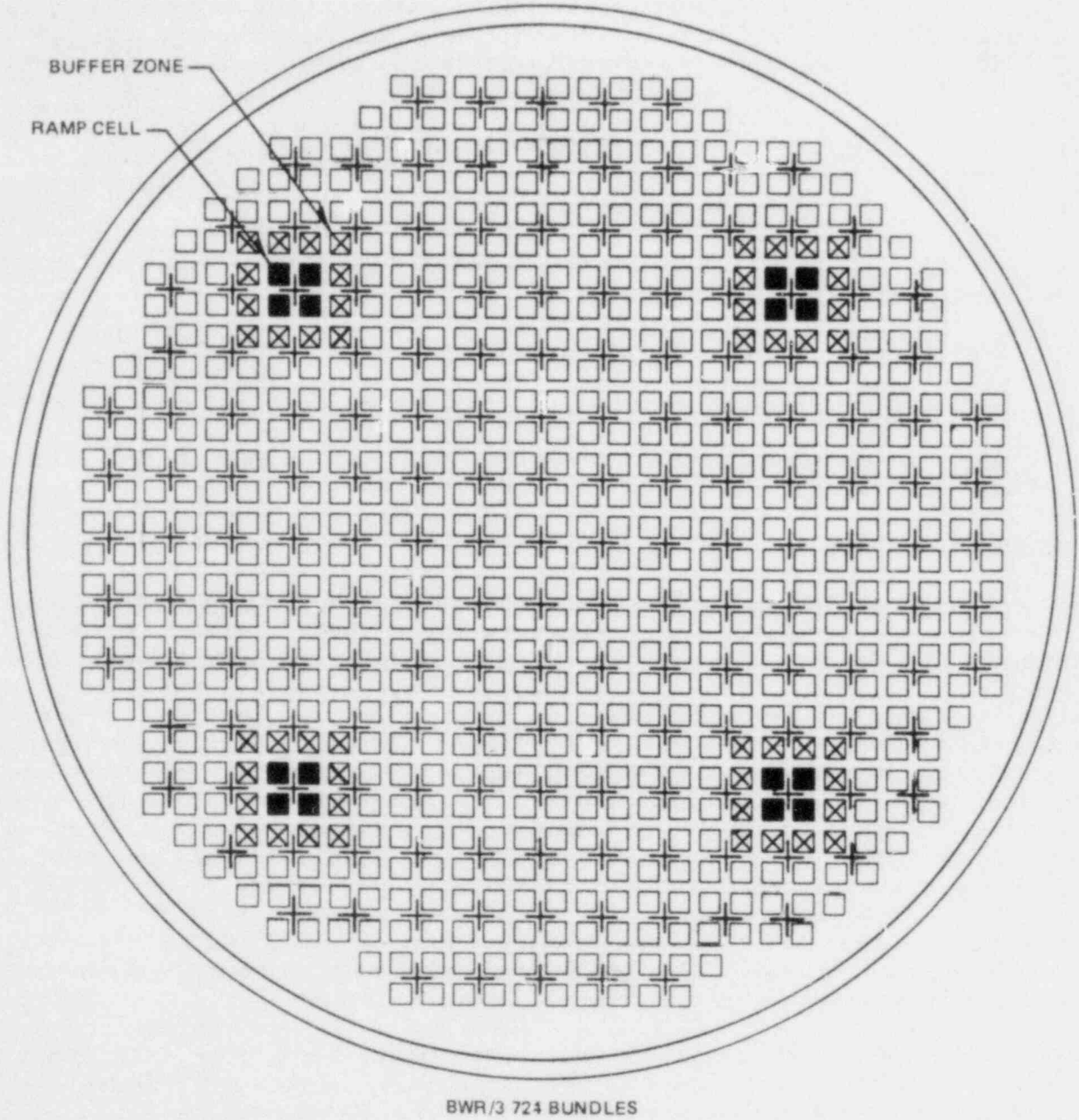
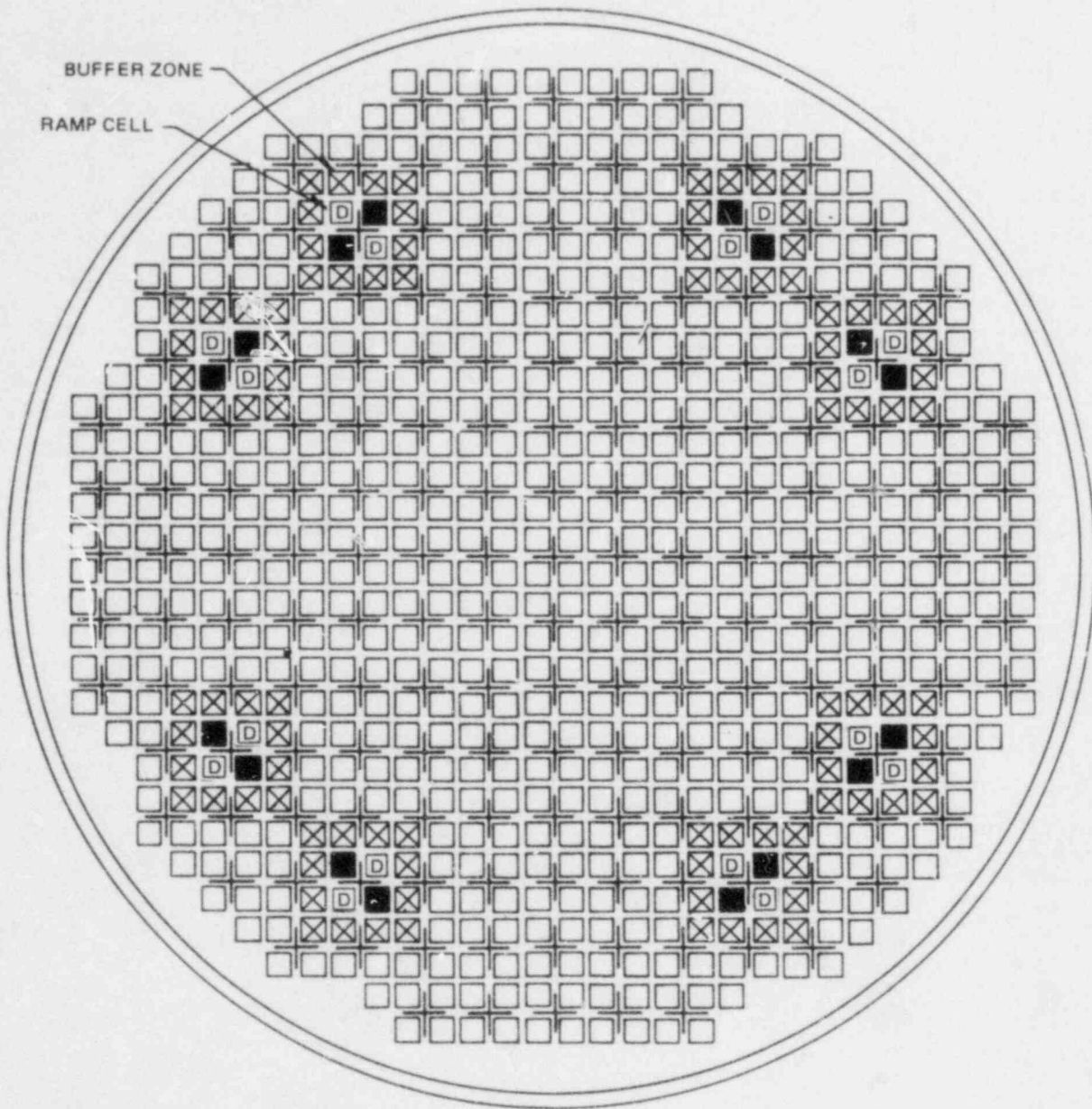
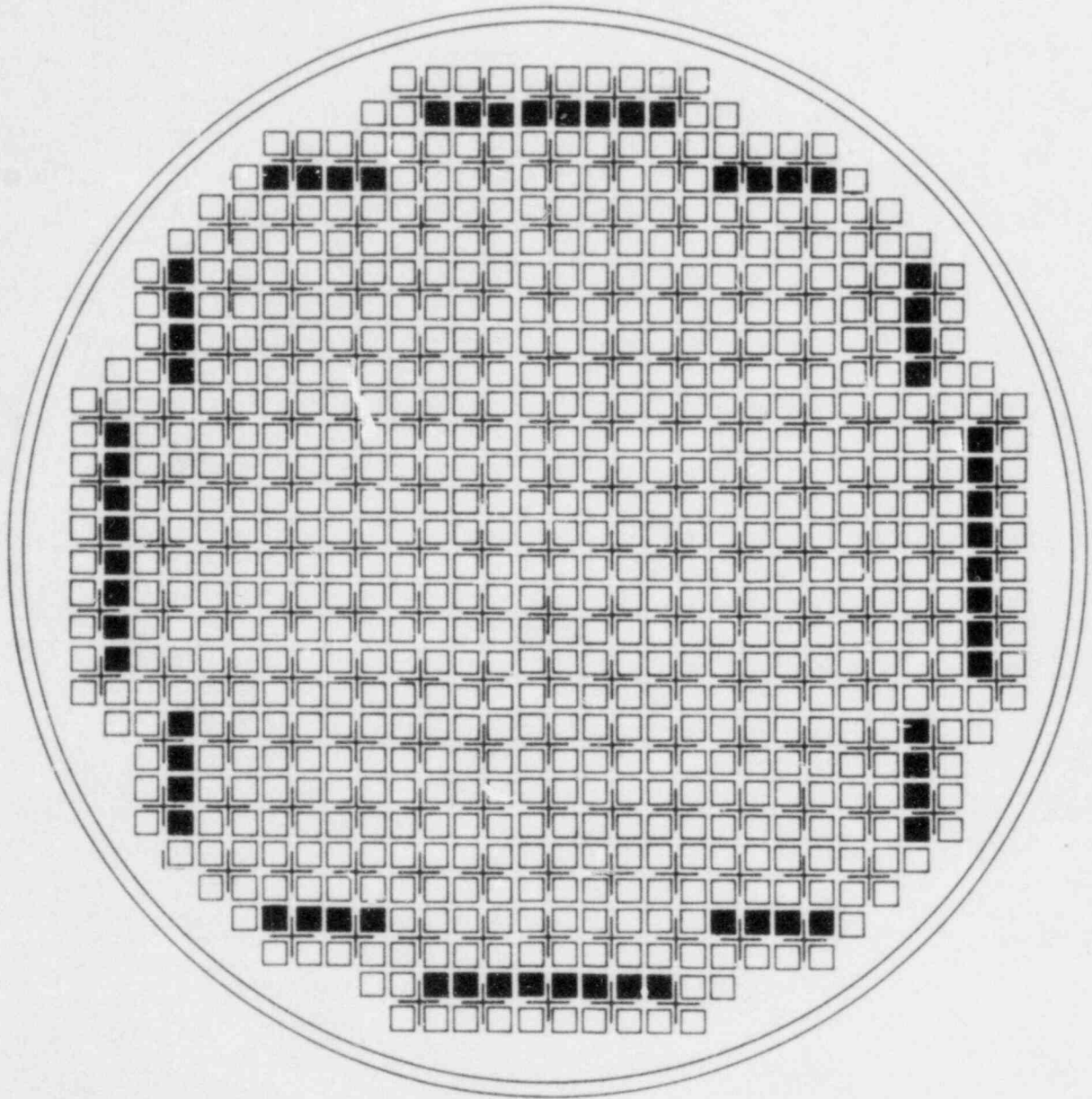


Figure 2.2-1. Ramp Cell Locations, Cycles 6 and 7



BWR/3 724 BUNDLES

Figure 2.2-2. Ramp Cell Locations, Cycles 8 and 9. Driver Fuel Indicated by D



■ ALLOWABLE BUNDLE LOCATIONS

Figure 2.2-3. Allowable Pre-Ramp Locations for Special Barrier Bundles

At the beginning of the design work in PHASE 2 it is convenient to define the nomenclature that will be used. The cells for which the end of cycle power ramps are planned are called "ramp cells". The 132 bundles of barrier fuel (*i.e.* the PCI-resistant fuel) to be demonstrated are called the "demonstration fuel bundles". Of these, the 64 scheduled for power ramps in the special ramp cells are called "special demonstration bundles" or "special barrier bundles"; while the 68 remaining are called "standard demonstration bundles" or "standard barrier bundles". In the generic study the special demonstration bundles had a special nuclear design to increase the power change near the wide-wide corner of the bundle (*i.e.* those fuel rods nearest the control blade axis) during the end-of-cycle power ramp. Somewhat different nomenclature was used in the PHASE 1 reports^{2,4}.

A prerequisite to the nuclear design is a realistic energy utilization plan (EUP). A reference EUP was obtained from CECO, and preliminary reference loading patterns for Cycles 6 through 9 were derived. Simulated power ramping studies for each of the four demonstration cycles (6 through 9) were also done. Each of these is discussed in the following paragraphs.

2.3 ENERGY UTILIZATION PLAN (EUP)

Table 2.3-1 shows the energy utilization plan which is anticipated for the demonstration. Note that these are full-power cycle exposure capabilities; no end-of-cycle power coastdowns are included. Quad-Cities Unit 2 has just completed an end-of-cycle coastdown for Cycle 4, and a similar end-of-cycle coastdown is anticipated for Cycle 5. Thus, at the beginning of Cycle 6 the fuel remaining from previous cycles has relatively low reactivity. In the current analyses of the demonstration it was assumed that no coastdown would occur in Cycles 6-9. Cycles 10 through 13 are listed because it is anticipated that by the end of Cycle 13, all of the demonstration fuel will have been removed from the core and all effects of the demonstration will have been removed. It is likely that PHASE 3 of this program will involve retaining some of the demonstration fuel for extended burnup, but extended burnup has not been considered in the fuel cycle comparisons. Thus, by considering cycles through Cycle 13, any fuel cycle comparisons done between the demonstration loading patterns and a normal loading pattern will be on a consistent basis. The normal loading considered here is one involving the control cell core concept.⁵

This Energy Utilization Plan includes higher cycle exposure capability requirements than did the EUP utilized in the PHASE 1 generic study.³ Thus, it was necessary to significantly revise the loading strategies developed in PHASE 1. However, the test cell locations, buffer zone locations, and incubation of the special demonstration bundles one row from the core periphery, were retained. In the preliminary reference loading patterns, the same number of bundles and enrichment of the special demonstration bundles to be ramped were also retained. The size of the reload batches and in some cases the enrichment of the reload fuel were changed, however, to meet the EUP. The demonstration fuel loading patterns have progressed through a number of iterations, as the EUP was evolved and as Cycle 4 was coasted down beyond previously calculated end-of-cycle exposures. The detailed design is being developed, and some changes in loading patterns can be expected.

Table 2.3-1
INITIAL ENERGY UTILIZATION PLAN FOR PCI-RESISTANT
FUEL DEMONSTRATION IN QUAD-CITIES UNIT 2

	Cycle	Cycle Exposure Capability (MWd/kg U)
Demonstration Cycles	6	6.3
	7	7.5
	8	7.5
	9	7.5
	10	7.5
	11	7.5
	12	7.5
	13	7.5

2.4 POWER RAMP SIMULATION

To find what modifications would be required in standard bundle designs to raise peaking to values where the resulting linear heat generation rates in the fuel would adequately demonstrate its PCI resistance, one of the loading patterns was selected for ramping calculations. Table 2.4-1 shows the reload bundle requirements of the loading patterns used in the ramping simulations. Table 2.4-2 shows the cycle exposure capability obtained from these loadings. The ramping simulations were done using the three-dimensional coupled thermohydraulic-nuclear BWR core simulator program. A Haling analysis was done with the ramp cell blades withdrawn to Notch Position 18 (48 = fully withdrawn) until the end of full-power capability with those blades inserted was reached. This point is called EOC' (see Figure 2.4-1). The ramp cell blades were then withdrawn in 0.457 m (1.50 ft) increments interspersed with periods of coastdown such that reactor power would not exceed 100% following the ramp. To estimate the powers obtained in fuel after rod pull, xenon was held constant following the rod pull. It was then allowed to reach its new equilibrium level and was then followed by the next coastdown interval. This procedure was repeated until all ramp cell blades were fully withdrawn. Figures 2.4-1 and 2.4-2 illustrate the operating strategy.

Table 2.4-3 shows the maximum power obtained in the ramped special demonstration bundles for each of the four demonstration cycles. Note that these estimated peak power levels include the effect on bundle local power distributions of extended periods of exposure accumulation with the adjacent control rod inserted (control blade history or CBH). Based on the work in PHASE 1 it can be anticipated that special nuclear design of the demonstration bundles can increase the peak power levels attainable by 10-15%. Such bundle designs are in progress.

Table 2.4-1
RELOAD BUNDLE REQUIREMENTS FOR DEMONSTRATION CYCLES (PRELIMINARY)

Cycle	No. of Reload Bundles	Cladding	Enrichment (Bundle Avg)	Comments
6	16	Barrier	2.39	Special demonstration bundles to be power ramped
	16		2.65	
	32		2.82	
	68		2.82	
	100		2.82	
7	168	Conventional	2.65	
8	184	Conventional	2.65	
9	56	Conventional	2.65	
	152	Conventional	2.82	

Table 2.4-2
PRELIMINARY REFERENCE LOADING PATTERN CYCLE EXPOSURE CAPABILITIES

Cycle	Total No. of Reload Bundles	Cycle Exposure* from BOC to EOC' (MWd/kg U)	Cycle Exposure* from EOC' to EOC (MWd/kg U)	Total Cycle Exposure (MWd/kg U)
6	232	6.28	0.19	6.47
7	168	7.43	0.15	7.58
8	184	7.08	0.30	7.38
9	208	7.27	0.37	7.64

*Haling analyses with ramp cell blades withdrawn to notch position 18 from BOC to EOC' and with all ramp cell blades completely withdrawn from EOC' to EOC. See Figure 2.4-1.

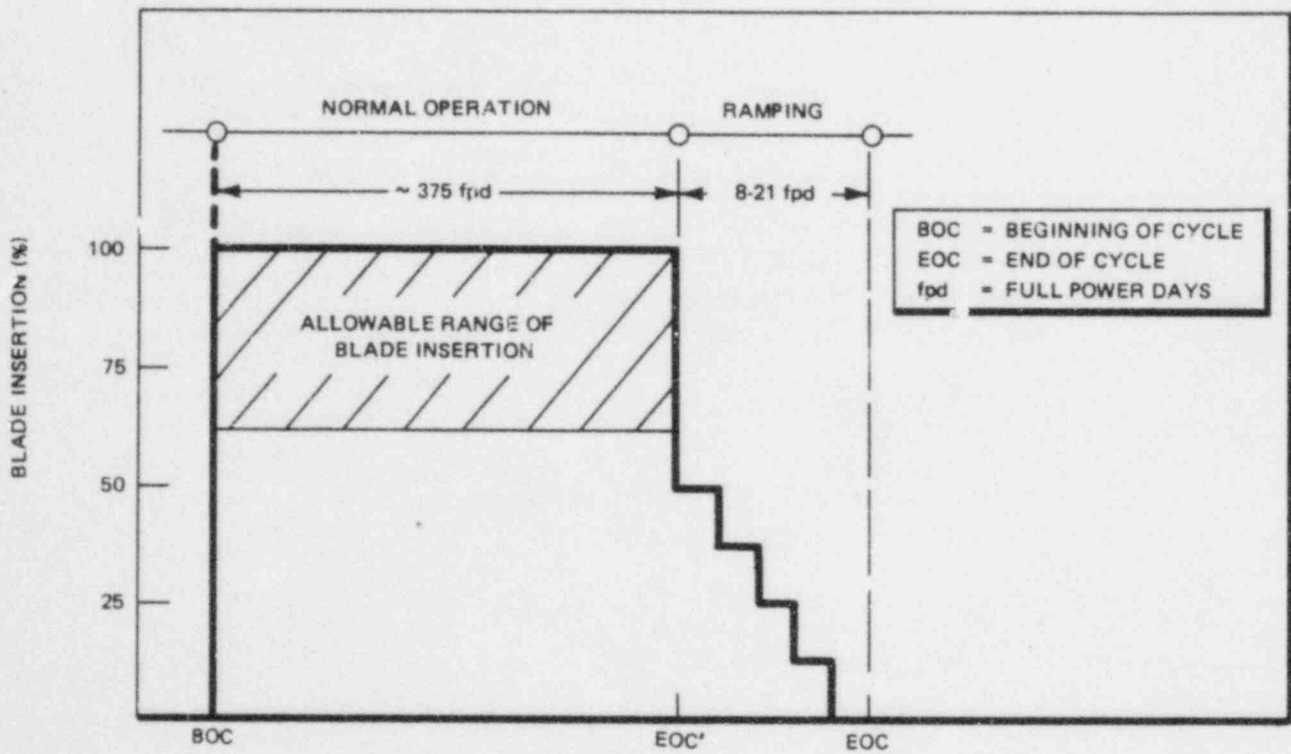


Figure 2.4-1. Operational Strategy

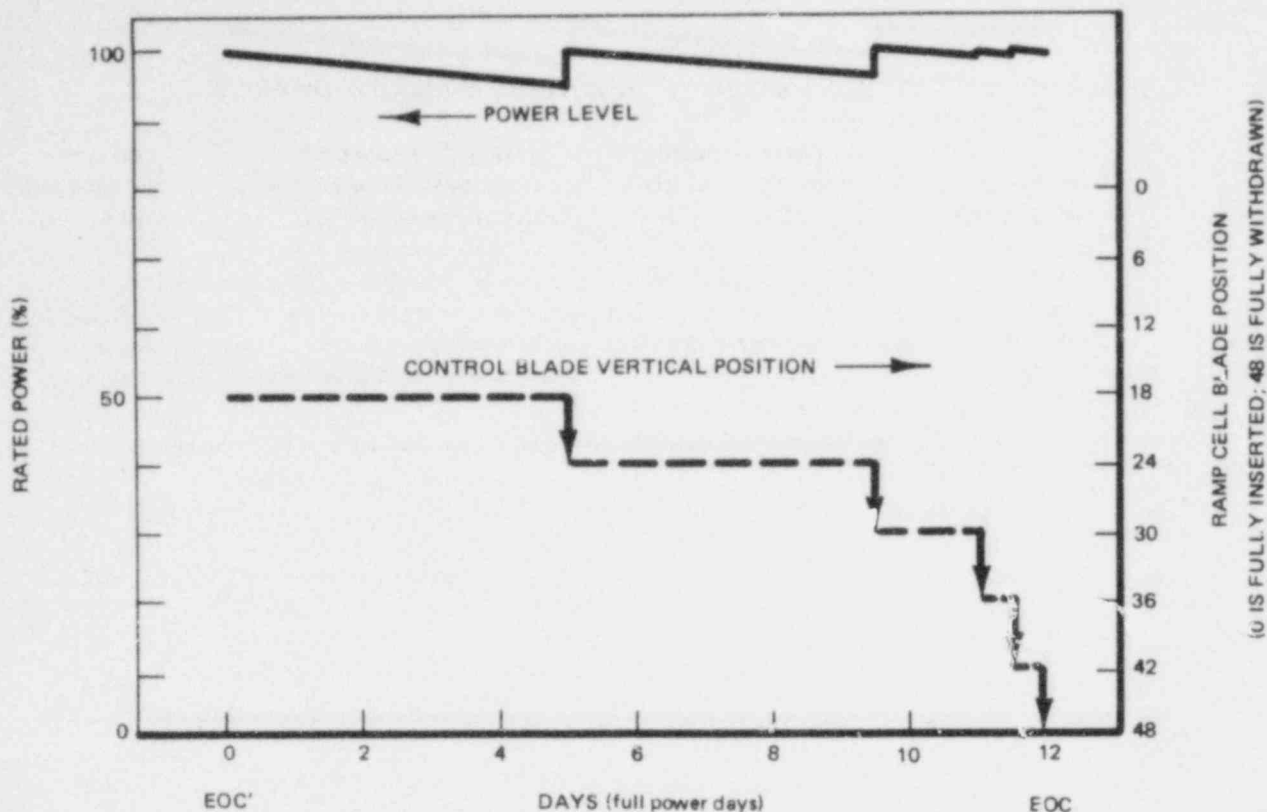


Figure 2.4-2. Typical EOC Ramping Schedule, Cycle 6/7

Table 2.4-3
PEAK LHGR ACHIEVED DURING RAMPING

Cycle	Blade Movement for Highest Peak LHGR	Peak Bundle Location ^a	Axial Fuel Segment ^b	Nodal Exposure (MWd/kg U)	W-W Corner Rod Linear Heat Generation Rate After Blade Movement kW/m (kW/ft)
6	24 to 30	(8, 8)	11	5.7	35.1 (10.7)
7	24 to 30	(8, 8)	11	10.0	33.1 (10.1)
8	30 to 36	(9, 6)	8	18.1	30.5 (9.3)
9	24 to 30	(9, 6)	11	26.5	26.6 (8.1)

^a Utilizing the 4-fold symmetry of the core, the bundle locations are designated by considering the upper left quadrant (see Figures 2.2-1 and 2.2-2) and counting bundle rows from left to right and then from top to bottom.

^b Axial fuel segments correspond to core node designations which are numbered from the bottom 1 to 24. Thus, the axial segment 1 corresponds to the bottom 6 inches (153 mm) of the core; segment 24 is the uppermost 6-inch (153-mm) segment of the fuel column.

ACKNOWLEDGEMENTS

The contributing authors gratefully acknowledge the contributions of their colleagues to the work reported in Section 2:

R. L. Crowther and P. J. Savoia for their encouragement and direction.

P. Wei for performing the nuclear analyses of the bundle designs and for assistance in the ramping simulations.

J. S. Gunz and D. K. Cheng for their assistance in developing the nuclear assumptions and reference point for the start of the nuclear design.

3. TASK II. SUPPORT TESTS

3.1 OBJECTIVES

1. Assess the long-term stability of the advanced fuel and develop supporting information needed for licensing.
2. Develop materials performance data needed to support the demonstration in a commercial power reactor.
3. Assess Cu-barrier and Zr-liner fuel performance under Loss of Coolant Accident (LOCA) and Reactivity Initiated Accident (RIA) conditions.
4. Determine the capability of the advanced fuel to resist PCI.
5. Assess the in-reactor behavior of barrier fuel with cladding perforation.
6. Develop data needed to justify recommendation of a primary PCI-resistant fuel design for the demonstration and to maintain a viable backup design.

3.2 SUBTASK II.1 LABORATORY TESTS

3.2.1 Subtask II.1.1 Characterization and Stability

3.2.1.1 Oxidation of Zirconium-Lined Zircaloy (B. Cheng, J. O. Hegland, and R. B. Adamson, NFSED)

3.2.1.1.1 Introduction

The use of a metallurgically bonded zirconium liner on the inner surface of Zircaloy-2 fuel cladding has been shown in ex-reactor mandrel tests (Subtask II.1.2) and by in-reactor power ramp tests (Subtask II.3) to increase resistance to PCI. Since zirconium can oxidize more rapidly than Zircaloy-2 in steam and water environments in the temperature range of interest⁶ (288-400°C), it is important to determine whether the Zr-liner fuel can remain stable in the event that the cladding is breached and water (steam) has entered the fuel rod. In this subtask laboratory tests are used to study this effect under conditions where parameters of the experiment can be varied, and in Subtask II.3.2 an in-reactor experiment is in progress.

The ingress of H₂O into a fuel rod is expected to result in a steam/hydrogen mixture. The entering water (initially at approximately 288°C, 7.0 MPa) will be flashed into the vapor phase as it encounters the hotter fuel rod interior. The outer surface temperature of the UO₂ pellets will be ~650°C, while the inner surface temperature of the fuel cladding (i.e. that of the zirconium liner) will be in the range 300-400°C. Oxidation of the fuel and the zirconium is expected to occur and some hydrogen will be produced.

The aim of the present experiment was to study the corrosion resistance of zirconium-lined cladding in an environment which simulates that in a failed fuel rod. The corrosion resistance of the barrier cladding in pure steam was also investigated.

3.2.1.1.2 Experimental Procedure

Full ring specimens 2.5 cm long were prepared from both the crystal bar and low oxygen sponge Zr-liner cladding. The specimens lined with crystal bar zirconium were from a single tube, as were those lined with low oxygen sponge zirconium. These tubes were manufactured by General Electric's Wilmington Manufacturing Department (WMD) in 1977. The inner surface was grit-blasted and etched.

After samples were cut from the tubes, they were cleaned in soapy water in an ultrasonic bath for 5-10 min. and then etched to remove ~ 0.003 mm (~ 0.0001 in.) of zirconium.

The experimental apparatus, which produces a test condition simulating that of a fuel rod with a cladding perforation is shown schematically in Figure 3.2-1. A reservoir of water is maintained at 288°C, 7.0 MPa (1000 psig). Two separate temperature chambers are interconnected: UO_2 pellets are maintained at temperature T_1 and the barrier tubing test specimens are held at T_2 . Temperature T_1 is 650°C and T_2 is the test temperature of interest in the range 300-400°C. Initially, the UO_2 is equilibrated at T_1 and the barrier tubing specimens at T_2 ; both chambers have an environment of He at 0.3 MPa (3 atm). The test starts with the admission of steam from the water reservoir into the chambers with UO_2 and cladding tube specimens. The flow of steam is through an orifice, which is typically 0.13 mm diameter. The steam reacts with the cladding at T_2 while simultaneously reacting with the uranium at T_1 . The entire test is in a relatively small volume where H_2 remains to affect the reactions. The environment changes as the reactions proceed. The tests were conducted with T_1 at 650°C and T_2 at 350-400°C for various durations.

Corrosion tests were also carried out in a refreshed autoclave shown schematically in Figure 3.2-2. The test temperature and pressure were 350-400°C and 7.0 MPa (1000 psig), respectively. Due to the nature of the recirculation system, the hydrogen generated from corrosion of the test samples left the autoclave rapidly and was removed from the feedwater with argon, which was bubbled through the water in the feedwater tank.

Corrosion rates in both tests mentioned above were determined by weight changes and by metallographic examination.

3.2.1.1.3 Results and Discussion

(A) Simulation Tests

The specimens tested in the simulator at 350°C for 3, 12 and 36 days all exhibited white powdery appearance on the inner zirconium liner surfaces. The outer surfaces of all specimens and the reference Zircaloy-2 tubing specimens showed the typical black oxide color. The weight gain data shown in Table 3.2-1 indicated that the low oxygen sponge liner has slightly better corrosion resistance than does the crystal bar liner.

Metallographic examination of untested specimens showed that the thicknesses of the barriers (Zr-liner) were 0.0025 ± 0.0001 and 0.0026 ± 0.00007 inches (63.5 ± 2.5 and 66.0 ± 1.8 μm) for crystal bar and low oxygen sponge samples, respectively, Figure 3.2-3. Conversion of the zirconium liners completely to zirconium oxide gives weight gains of ~ 1460 and 1520 mg/dm² for the crystal bar and the low oxygen sponge specimens, respectively. In comparison with the data shown in Table 3.2-1, it can be seen that both types of barrier were completely oxidized in 36 days at 350°C, whereas the 3 and 12 day tests resulted only in partial oxidation of the liners. The weight gain data are consistent with the results obtained from metallographic examination, Figures 3.2-3 and 3.2-4. One interesting feature observed in the photomicrographs shown in Figure 3.2-3 is that zirconium hydrides tended to concentrate at the vicinity of the interface between the zirconium liner and the Zircaloy.

The weight gain data, Figure 3.2-5, showed a linear relation with test duration for the 3 and 12 day tests. The reaction rate of the crystal bar liner is slightly higher than that of the low oxygen sponge liner. Extrapolations of both lines intercept the dashed line at 18.5 and 24.5 days for crystal bar and low oxygen sponge-based liner, respectively. The dashed line represents the weight gain of a completely oxidized zirconium liner of 0.065 mm (0.00255 in.) in thickness. Since the weight gain data from the 36 day test are nearly the same as the value estimated to have reached after only 18.5 and 24.5 days for crystal bar and low oxygen sponge liners, respectively, it appears that the corrosion reaction was stopped at the zirconium-Zircaloy interface, and no significant reaction occurred for 12-18 days after the complete oxidation of the barriers.

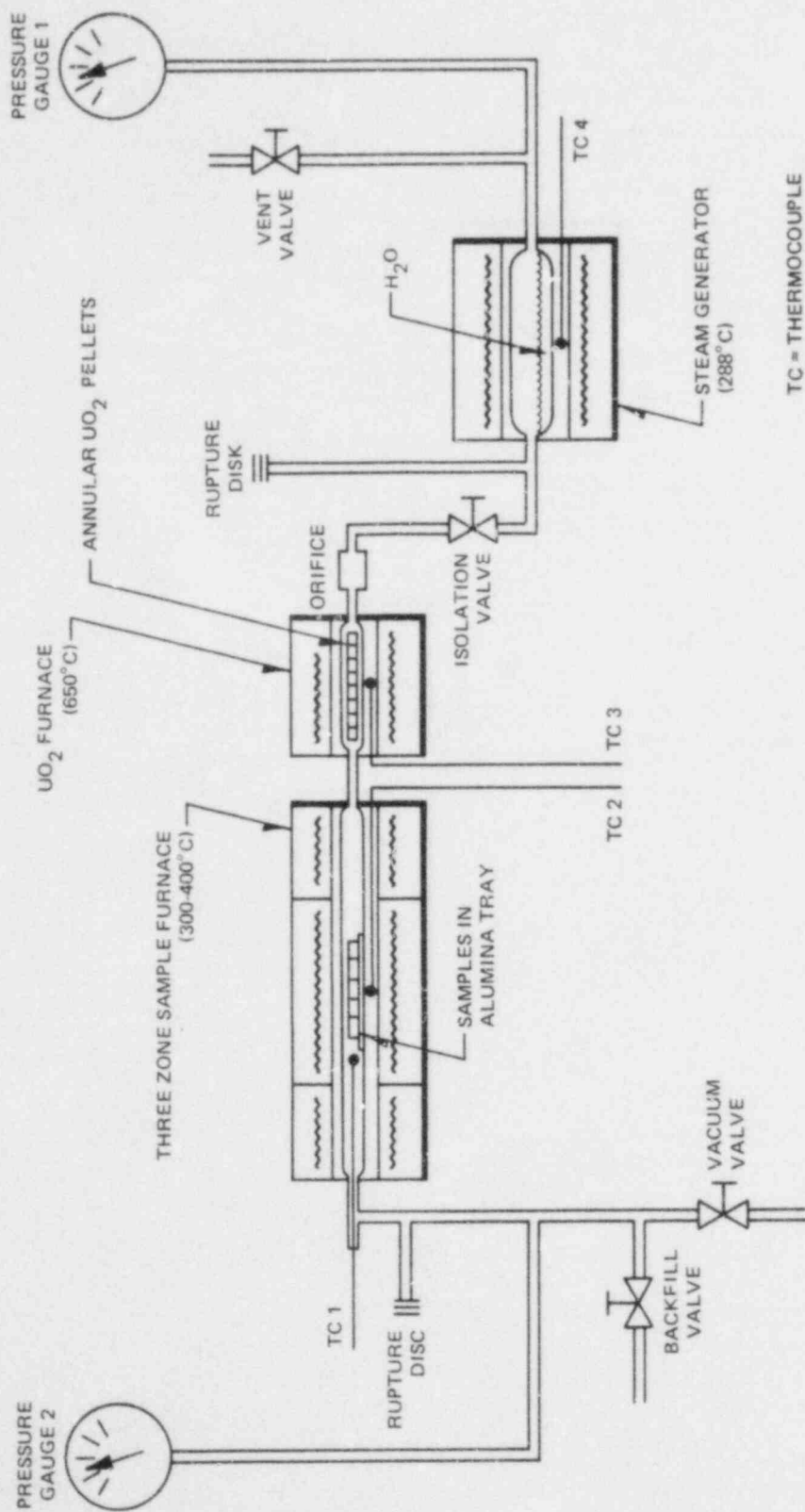


Figure 3.2-1. Perforated Rod Simulator Test Apparatus

1. LOW PRESSURE CENTRIFUGAL PUMP
2. FLOW METER
3. DE-IONIZER
4. CONDUCTIVITY METER
5. HIGH PRESSURE POSITIVE DISPLACEMENT PUMP
6. FILTER
7. THERMOCOUPLE
8. BLOWOUT RELIEF DISK
9. ASHCROFT PRESSURE GAUGE
10. BRISTOL PRESSURE RECORDER
11. NONREGENERATIVE HEAT EXCHANGER
12. BACK PRESSURE REGULATOR
13. FLOW METER
14. REGENERATIVE HEAT EXCHANGER

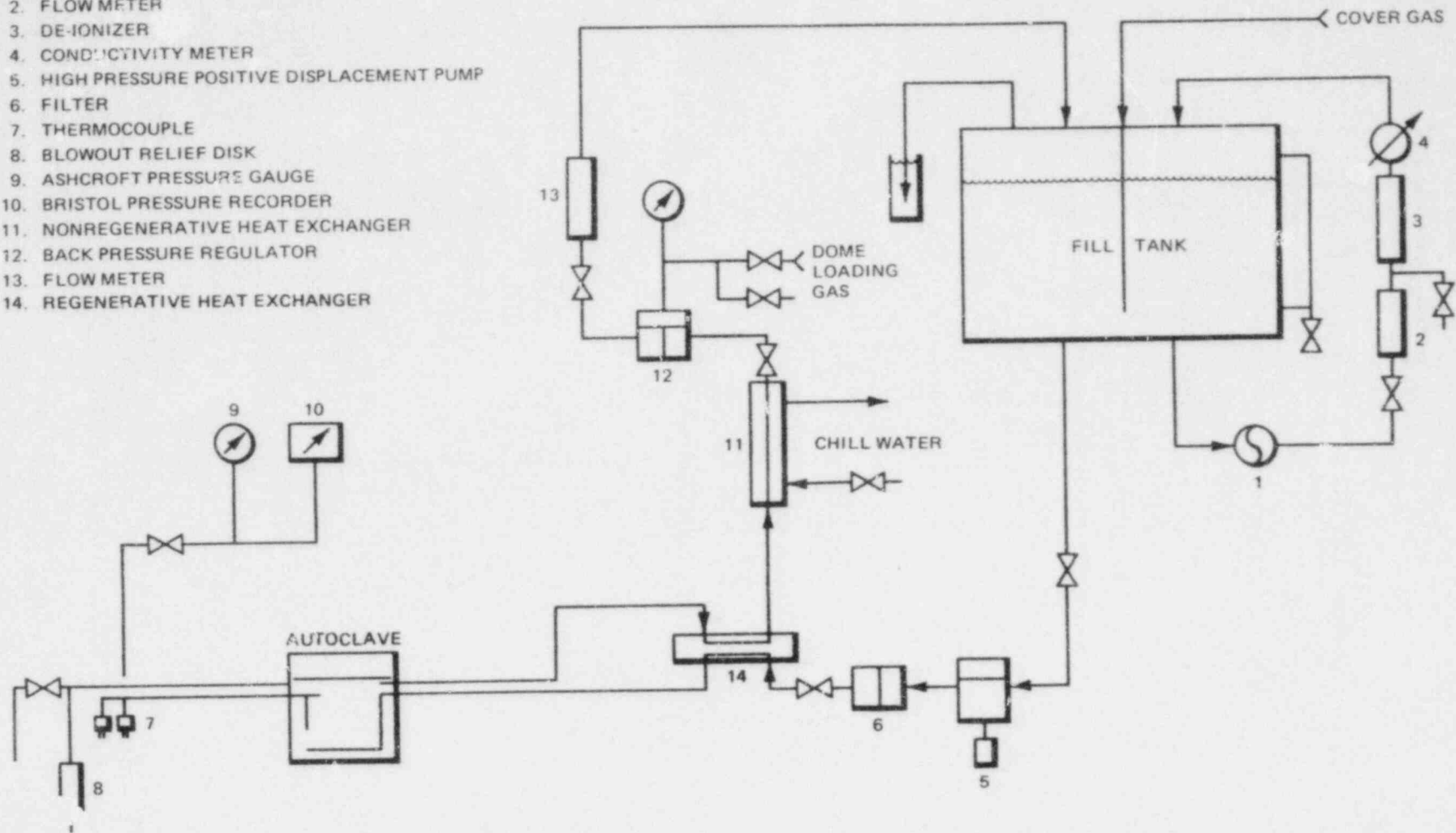
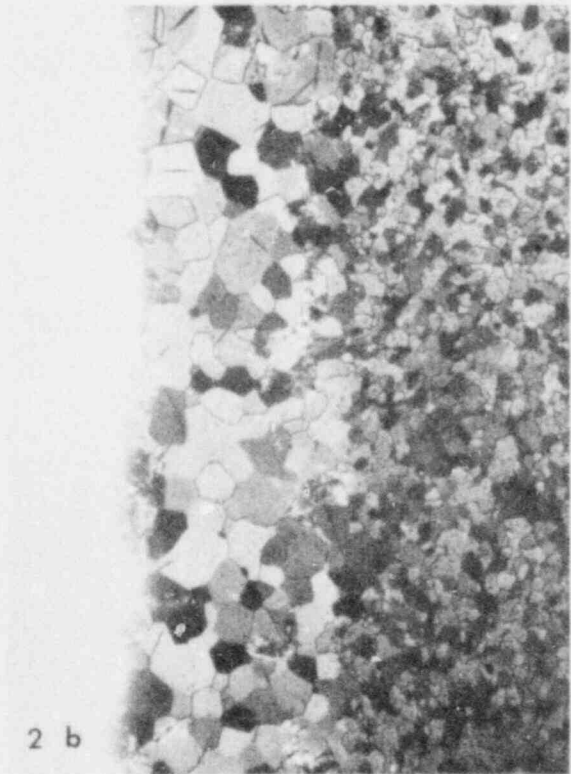
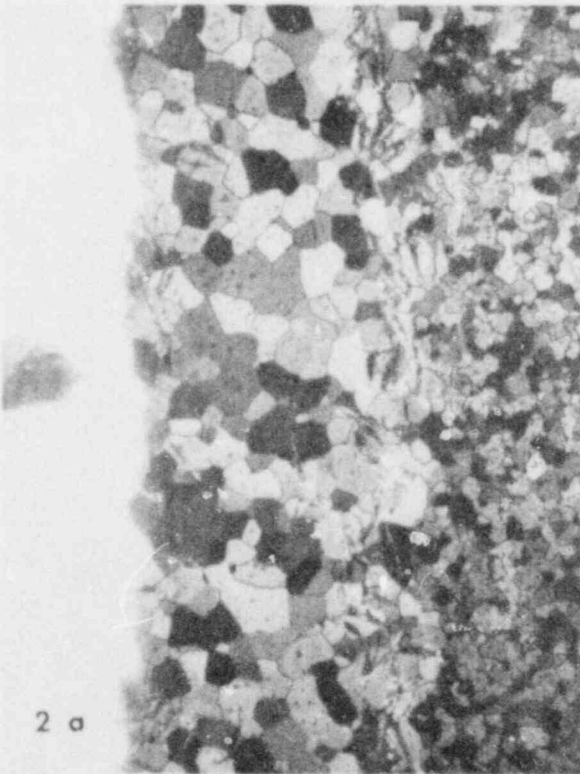
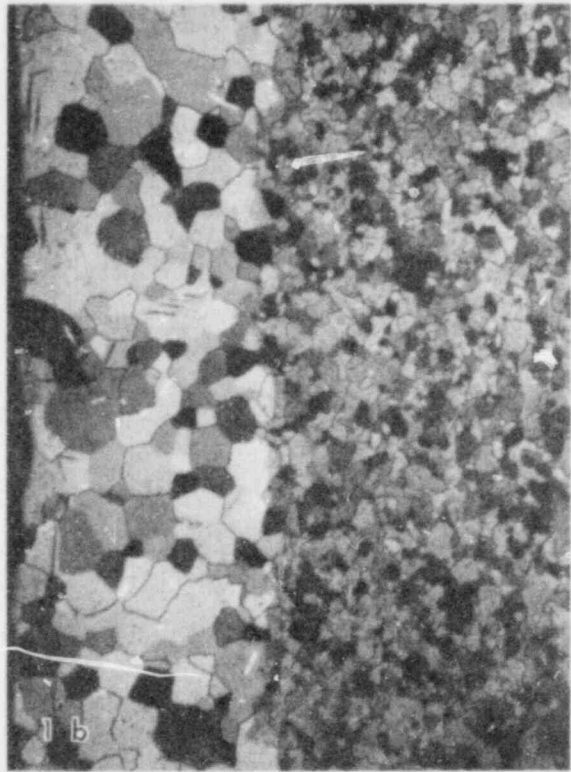
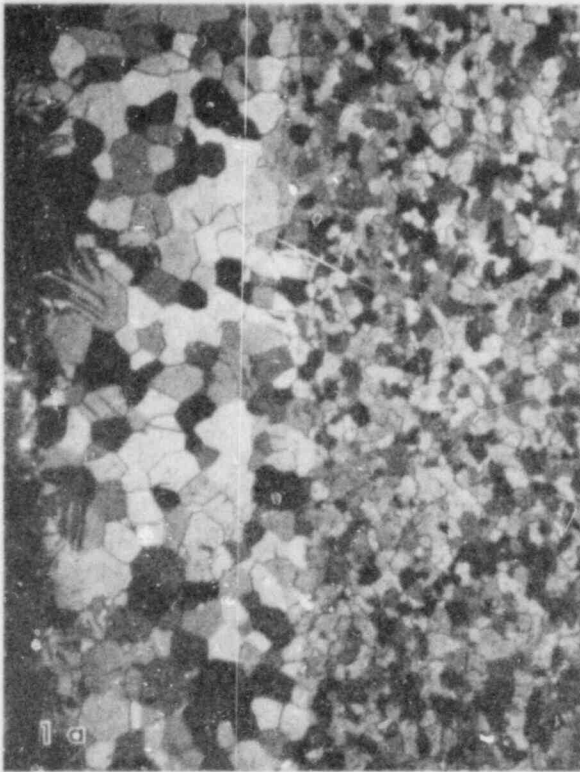


Figure 3.2-2. The Refreshed Autoclave System Shown Schematically



500X

Figure 3.2-3. Photomicrographs of (a) Low Oxygen Sponge and (b) Crystal Bar Zirconium-Lined Tubing Before Testing, (1), and After Being Tested in the Simulator at 350°C in 7.0 MPa (1000 psig) Steam for 3 days (2).

Table 3.2-1
WEIGHT GAIN DATA OF SAMPLES TESTED IN THE SIMULATOR AT 350 AND 400 °C.

Temperature °C	Duration, days	Weight Gain, mg/dm ²		
		Zircaloy-2	Crystal bar Only*	Low Oxygen Sponge Only*
352 ± 3	3	7.9	276 ± 20	192 ± 56
356 ± 6	12	14.7	963 ± 48	750 ± 89
354 ± 4	36	19.3	1451 ± 2	1486 ± 54
407 ± 7	3	—	894 ± 57	877 ± 3
403 ± 2	12	26.1	1443 ± 93	1556 ± 0

*Average of two specimens with range indicated.

The weight gain data obtained at 400 °C are shown in Table 3.2-1 and in Figure 3.2-5. Assuming that linear reaction kinetics exist also at 400 °C, it is shown in Figure 3.2-5 that both liner types will be completely oxidized in ~ 5 days. In other words, the corrosion reaction at 400 °C has also been stopped at the zirconium-Zircaloy interface and no significant reaction occurs for 7 days after the complete oxidation of the liners.

The reaction rates are obtained from the slopes of the lines shown in Figure 3.2-5 and are tabulated as follows:

Material	350 °C, μm/day	400 °C, μm/day
Zircaloy-2 cladding	0.05	not measured
Crystal bar zirconium	5.14	19.90
Low oxygen sponge zirconium	4.05	18.96

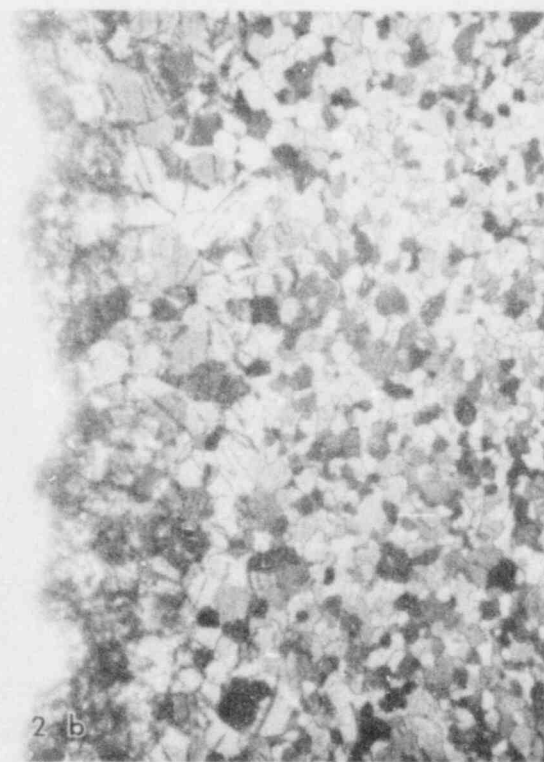
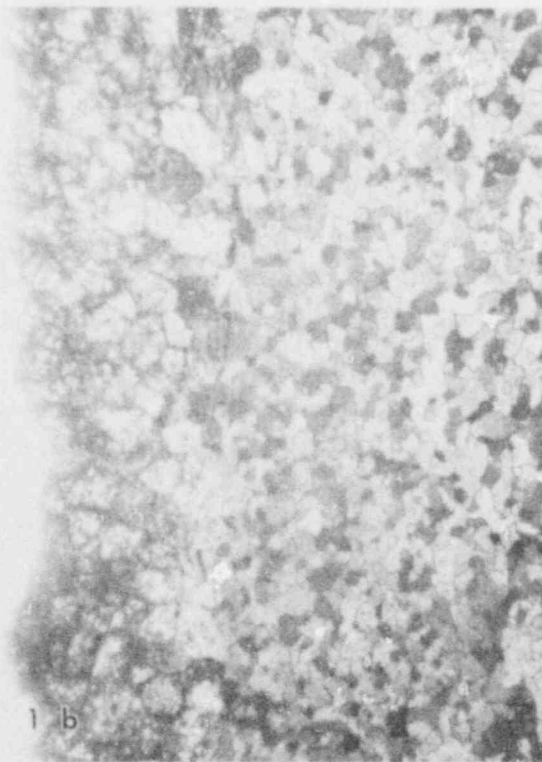
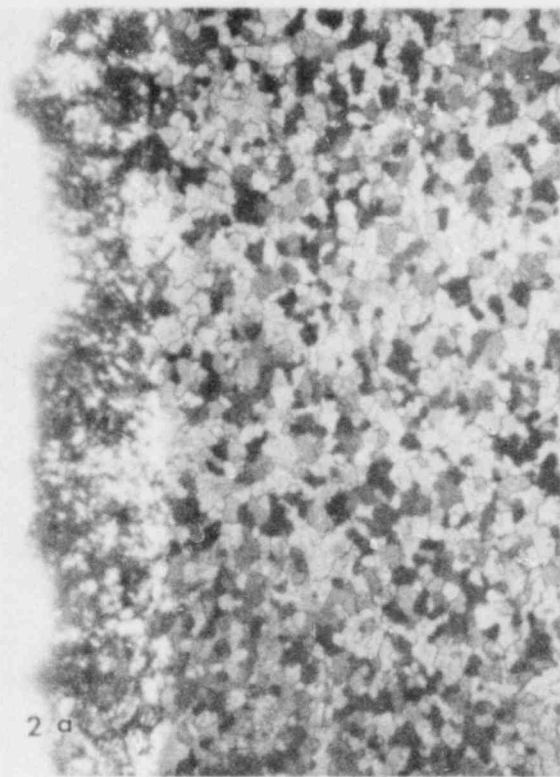
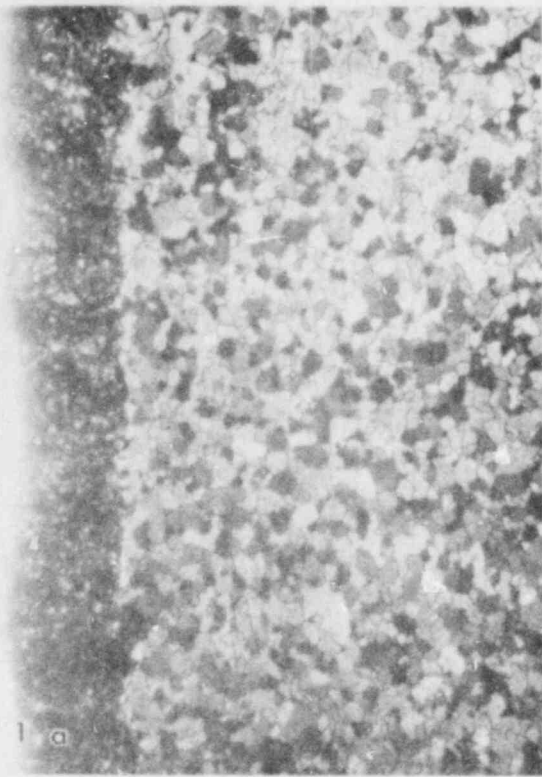
(B) Autoclave Test

Corrosion tests in the refreshed autoclave system were carried out at 350 and 400 °C in steam at a pressure of 7.0 MPa (1000 psig).

The corrosion weight gains for both types of barriers in 350 °C steam for 3 days were only ~ 1/3 of those obtained in the simulation tests, Tables 3.2-2 and 3.2-3. Metallographic examinations showed no evidence of hydrogen up in the first three days at 350 °C, Figure 3.2-6.

A 13 day test at 350 °C showed that the crystal bar liner formed a white powdery oxide layer, while the low oxygen sponge liner remained essentially black, L-1 and X-1 in Figure 3.2-7(a). The weight gain data showed only slight increases from the 3 day test. Also at 400 °C the corrosion rate of both liner types are significantly lower than those obtained from the simulation tests. A weight loss of 370 mg/dm² was obtained for the crystal bar liner in the 400 °C test because of the powdery nature of the oxide (samples hung vertically). The photomicrographs of the samples are shown in Figure 3.2-6.

A test was conducted at 350 °C for 13 days to compare the effect of surface finish, e.g., as-grit blasted and light etched, one minute etched, and hand polished with SiC paper (grade 600 grit). It was found that the one minute etching resulted in a corrosion rate of 18-30% less than the other two types of surface treatments. The effect of surface finish is, however, only secondary as compared to the difference between the liner types, Figure 3.2-7.



500X

Figure 3.2-4. Photomicrographs of (1) Low Oxygen Sponge and (2) Crystal Bar Zirconium Lined Tubing After Being Tested in the Simulator at 350°C in 7.0 MPa (1000 psig) Steam for 12 days. (a) and (b) Represent Different Locations of the Same Samples.

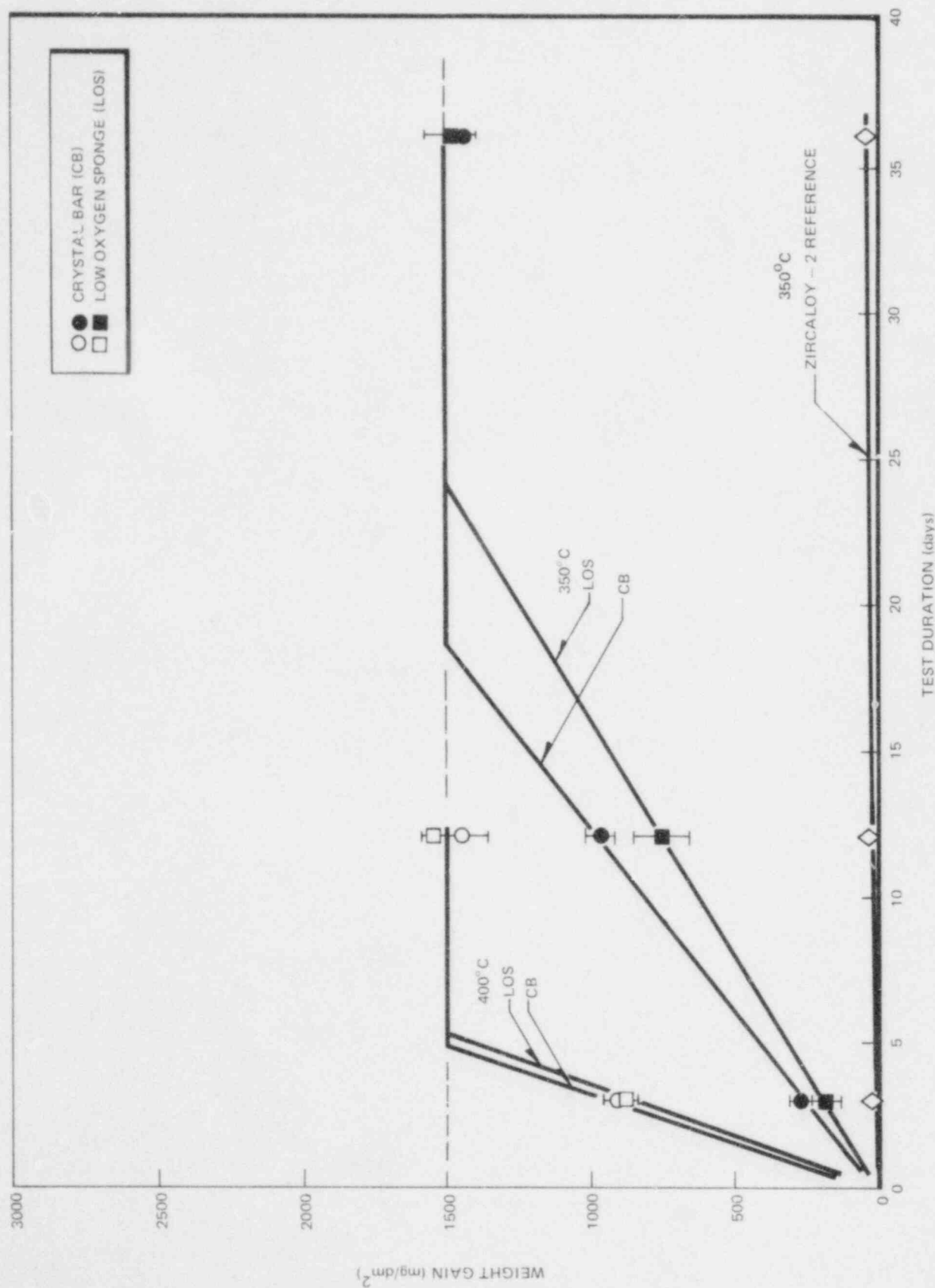


Figure 3.2-5. Corrosion Weight Gains for Zr-Liner Cladding and Reference Zircaloy-2 as a Function of Time at 350°C and 400°C in 7.0 MPa (1000 psig) Steam in the Simulator

Table 3.2-2
THE WEIGHT GAIN (mg/dm²) OF CLADDING SAMPLES TESTED IN THE
RECIRCULATING AUTOCLAVE AT 350 AND 400°C

Temperature °C	Duration, days	Reference	Crystal Bar	Low Oxygen Sponge
350	3	3.4	97 ± 4	65 ± 0
350	13	11.3	150 ± 4	65 ± 1
400	3	4.5	370 ± 12	180 ± 4

Table 3.2-3
WEIGHT GAIN (mg/dm²) OF SAMPLES TESTED IN THE RE-CIRCULATING AUTOCLAVE
TEST CONDITIONS: 350°C, 7.0 MPa (1000 psig), 13 DAYS

	As-received	1 Min Etched	Hand Polished (#600 SiC)
Crystal Bar	150 ± 4	103 ± 6	142 ± 3
Low oxygen sponge	65 ± 1	52 ± 5	61 ± 1
Reference		11.3	

The difference in corrosion performance of the zirconium liners in the simulator and the refreshed autoclave is believed to be due to the presence of hydrogen in the simulator. Tests of zirconium-based alloys in various laboratories have shown that higher corrosion rates can be expected if the tests are conducted in a small closed autoclave in which corrosion produced hydrogen can accumulate.⁶

3.2.1.1.4 Conclusions

1. The corrosion rates of zirconium liners in simulated defected rod conditions are significantly higher than those obtained in the refreshed autoclave. The accelerated reaction is attributed to the presence of significant amounts of hydrogen produced by the corrosion reaction.
2. The reaction rates obtained from the simulation tests at 350°C are 0.05 μm/d for Zircaloy-2, 5.14 μm/d for the crystal bar liner, and 4.75 μm/d for the low oxygen sponge liner.
3. The corrosion reaction in the simulator at 350 and 400°C appears to have stopped at the zirconium-Zircaloy interface. No significant corrosion of the underlying Zircaloy have occurred for up to 36 days at 350°C and 12 days at 400°C.

3.2.1.2 Characterization of Irradiated Zirconium Liners — (R. P. Tucker and R. B. Adamson, NFSED)

To characterize the zirconium liner materials, work is in progress to measure the relative microhardness of irradiated and unirradiated zirconium liners and Zircaloy cladding. A microhardness measurement plan has been carried out that provides a self-consistent and reliable data base for evaluating the effect of neutron fluence on the relative microhardness of Zircaloy-2, crystal bar zirconium and low-oxygen sponge zirconium. The testing was conducted primarily on one instrument by a single operator. Based on preliminary data using Knoop and diamond pyramid indenters and loads from 50 to 500 grams, the Knoop indenter and a 100 gram load were selected for generating reliable and directly comparable microhardness measurements for Zircaloy-2 tubing specimens with 0.076-mm thick zirconium liners.

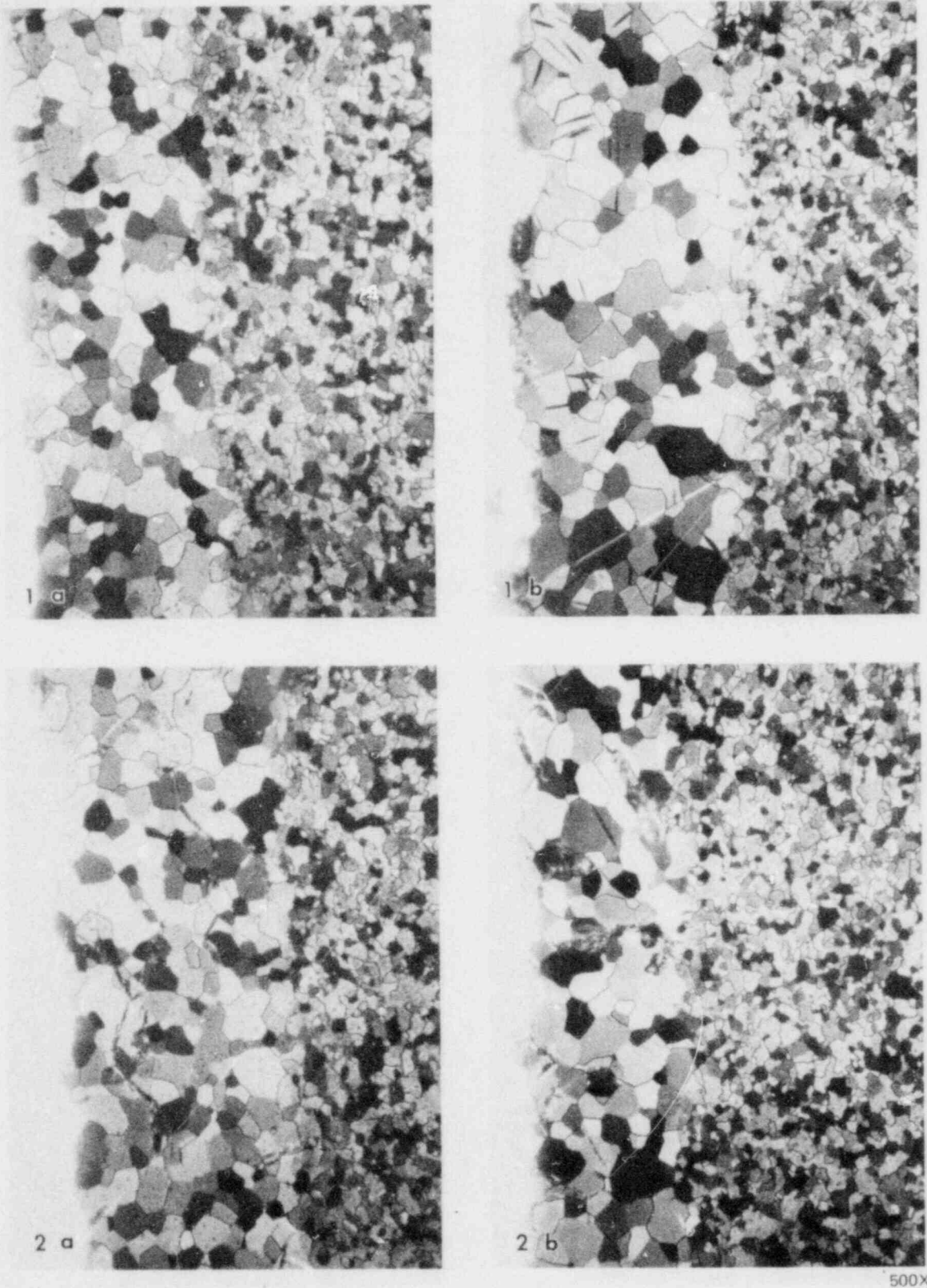
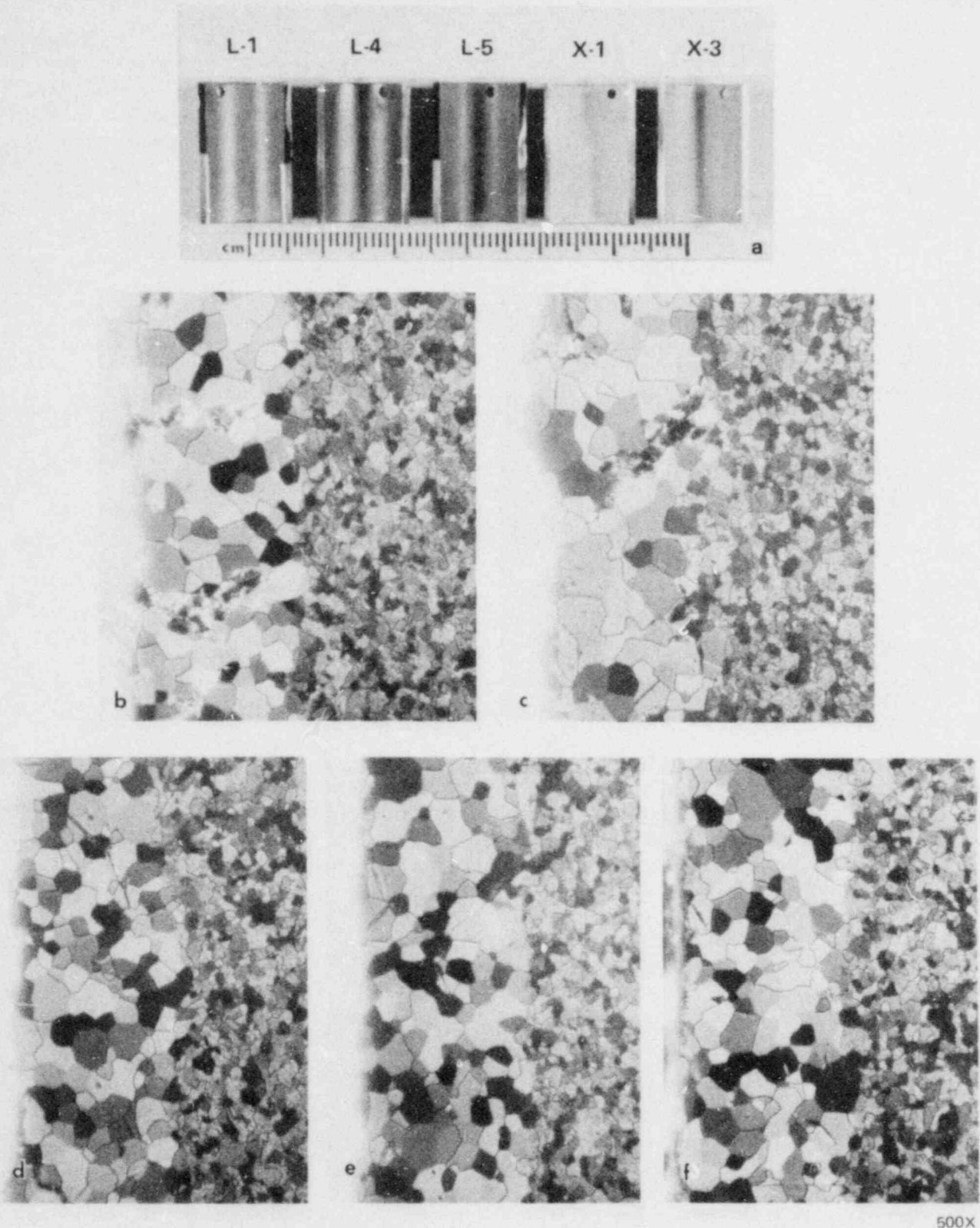


Figure 3.2-6. Photomicrographs of (a) Low Oxygen Sponge and (b) Crystal Bar Zirconium Lined Tubing After Being Tested in the Refreshed Autoclave at (1) 350°C and (2) 400°C in 7.0 MPa (1000 psig) Steam for 3 Days



500X

Figure 3.2-7. Photomacrographs and Photomicrographs of Specimens After Being Tested in the Refreshed Autoclave in Steam at 350°C, 7.0 MPa (1000 psig) for 13 days: (a) Inner Surface Visual Appearance; Specimens Labeled L have the Low Oxygen Sponge Zr-Liner While Those Labeled X Have the Crystal Bar Zr-Liner; (b) Crystal Bar Liner in the As-Received Condition; (c) Crystal Bar Liner in the Belt Ground Condition; Low Oxygen Sponge in (d) As Received; (e) 1 min Etched; (f) Belt Ground Conditions.

The Knoop hardness numbers (KHN) reported here are the average values from a minimum of three hardness impressions made at a load of 100 grams. The tests were conducted at room temperature. As anticipated, the microhardness values for annealed, unirradiated materials were lowest for high-purity crystal bar zirconium (KHN = 56-71), higher for low-oxygen sponge zirconium (KHN = 118), and were highest for Zircaloy-2 (KHN = 173-185). Following neutron irradiation to fluences in the range $1.3\text{-}2.0 \times 10^{21}$ n/cm² ($E > 1$ MeV), the microhardness measurements indicated hardening had occurred in all three materials, with Zircaloy-2 showing the greatest increase. The relative hardness of these materials remained in the same order as existed prior to irradiation. For Zircaloy-2 irradiated in the Segmented Rod Program (SRP), where the irradiation temperature was $\sim 288^\circ\text{C}$, the hardness was in the range of 232-255 KHN. At higher irradiation temperatures of 343°C (IMC-5 isothermal materials capsule irradiated in the GE Test Reactor) and 375°C (EBR-II-1), the Knoop hardness numbers for Zircaloy-2 were 191-201 and 220, respectively. The results indicate that irradiation hardening is somewhat reduced at the higher irradiation temperatures.

The crystal bar zirconium from irradiated SRP rods exhibited Knoop hardness values in the range 81-107, whereas the low-oxygen sponge zirconium irradiated in EBR-II-1 at $\sim 375^\circ\text{C}$ measured 126 KHN. Figure 3.2-8 presents a visual comparison between the Knoop impression size for crystal bar zirconium liner and Zircaloy cladding in an irradiated sample. The results on crystal bar zirconium indicate that although neutron irradiation results in hardening, the microhardness remains well below that of unirradiated Zircaloy-2 for fluences up to $\sim 2 \times 10^{21}$ n/cm². Currently, the only microhardness measurements on irradiated low-oxygen sponge zirconium are on material irradiated in the EBR-II at temperatures of 371°C and above. Since the effect of irradiation temperature on microhardness in this material remains to be documented, an inference regarding the amount of hardening to be expected in sponge zirconium under BWR conditions cannot be drawn yet. However, the data show that sponge zirconium at a fluence of $\sim 1.5 \times 10^{21}$ n/cm² remains softer than unirradiated Zircaloy-2 and suggest that even at high fluence the sponge liner probably will not exceed the hardness of unirradiated Zircaloy-2. Figure 3.2-9 summarizes the Knoop microhardness results for Zircaloy-2 and zirconium liner materials as a function of fast neutron fluence.

3.2.1.3 Irradiation Hardening of Zirconium — (R. B. Adamson and G. H. Henderson, NFSED)

Tensile tests have been conducted on irradiated zirconium sheets of two different purities. Crystal bar (200 ppm O) and sponge (800 ppm O) materials were irradiated at 327°C to a fluence of 6.8×10^{20} n/cm² ($E > 1$ MeV) and tensile tested at 310°C . The sheet thickness was 1.27 mm (0.050 inches) and the specimen geometry was that previously described⁴ for miniature uniaxial tensile specimens. Table 3.2-4 presents the data. It is seen that uniform elongation for both materials is low and the reduction in area is high. It is seen that the sponge material is significantly stronger than crystal bar material. Transmission electron microscopic characterization and optical metallography of these materials is in progress.

3.2.2 Subtask II.1.2 PCI Simulation Tests

3.2.2.1 Irradiations in the EBR-II — (R. P. Tucker and R. B. Adamson, NFSED)

Irradiation experiments are being conducted in the Experimental Breeder Reactor (EBR-II) to provide candidate barrier Zircaloy-2 cladding with high fluence exposures for post-irradiation evaluations of these materials including their resistance to stress corrosion cracking under simulated PCI conditions, i.e., expanding mandrel tests. Irradiation has been completed on two series, each with four nonfueled tubing rods. These rods have been received at the Vallecitos Nuclear Center for measurement, sectioning, characterization and testing.

The materials in the first experiment (EBR-II-1) were: (1) reference (bright-etched) Zircaloy-2, (2) copper on etched Zircaloy-2, (3) copper on autoclave-oxidized Zircaloy-2 and (4) 0.076-mm low-oxygen sponge zirconium-lined Zircaloy-2. The experimentally evaluated neutron fluences ($E > 1$ MeV) for rods (1) and (2) were 2.1×10^{21} n/cm² at core midplane ($T \approx 410^\circ\text{C}$) and 1.9×10^{21} n/cm² near the bottom of the core ($T \approx 371^\circ\text{C}$) and for rods (3) and (4) the corresponding fluences were 1.8×10^{21} n/cm² and 1.4×10^{21} n/cm², respectively. The four rods have been sectioned and mandrel samples prepared for testing. Microhardness measurements have been obtained on selected sections from the sponge zirconium liner and Zircaloy-2, with additional measurements required to evaluate the effect of irradiation temperature on microhardness.

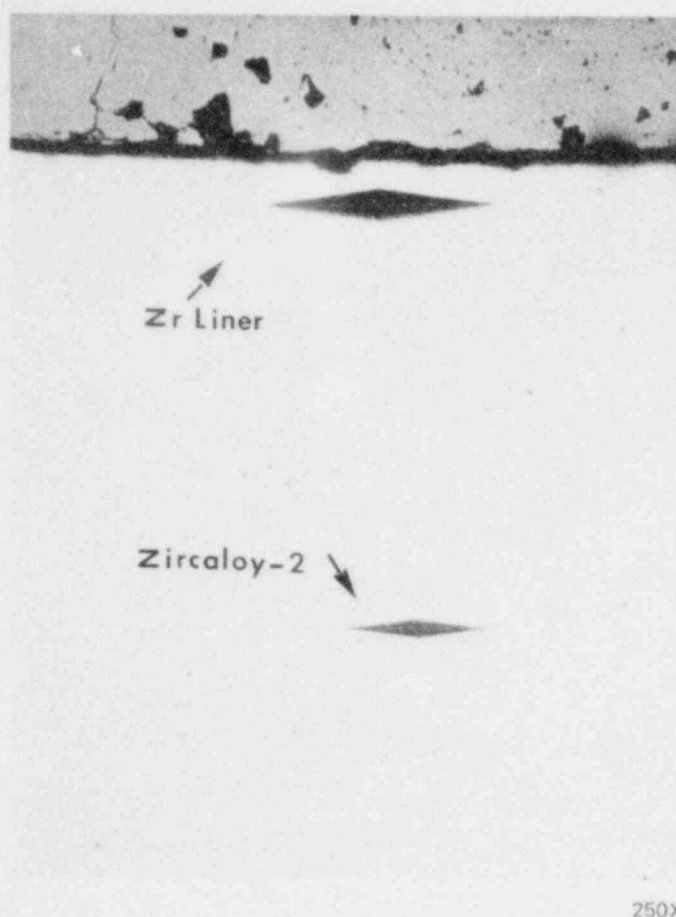


Figure 3.2-8. Comparison of Knoop Microhardness Impressions for Irradiated Crystal Bar Zirconium Liner and Zircaloy-2 Cladding. (Fluence = 1.5×10^{21} n/cm² ($E > 1$ MeV), Irradiation Temperature $\approx 288^\circ\text{C}$).

Metallographic evaluations of the EBR-II-1 materials indicate:

1. Blistering and delamination of the copper liner on the autoclave-oxidized rod.
2. Corrosion and/or porosity of the copper liner on both the oxidized and etched rods.
3. Interdiffusion of copper with Zircaloy in the copper on etched rod with the diffusion layer increasing in thickness with increasing irradiation temperature.
4. No macroscopic visual evidence of radiation effects on the sponge zirconium liner.
5. Hydrides, indicative of ~ 100 ppm hydrogen in all rods with no evidence of increased hydrides at the zirconium liner/cladding interface. (The hydrogen concentration was determined by comparison with metallographic standards.)

Metallographic evaluations of unirradiated control specimens which simulate the thermal history of the EBR-II-1 experiment are consistent with the results on the companion irradiated specimens.

The second series of rods (EBR-II-2) included the following materials: (1) reference (bright-etched) Zircaloy-2, (2) 0.076-mm low-oxygen sponge zirconium-lined Zircaloy-2, (3) 0.076-mm crystal bar zirconium-lined Zircaloy-2 and (4) copper on autoclave-oxidized Zircaloy-2. Irradiation to an estimated fluence ($E > 1$ MeV) of $\sim 8 \times 10^{21}$ n/cm² at core midplane and $\sim 4.5 \times 10^{21}$ n/cm² near the bottom of the core was completed in October 1979.

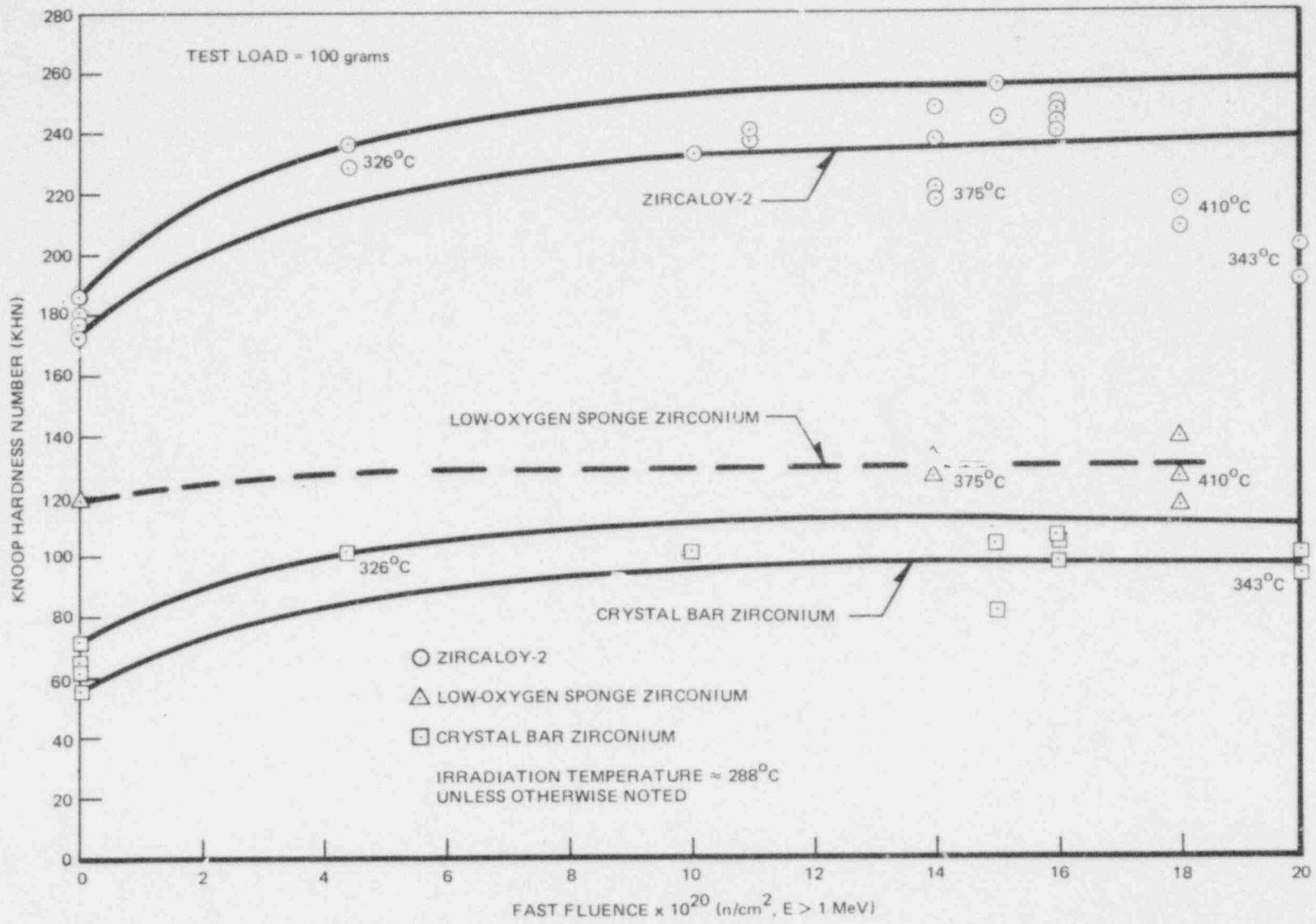


Figure 3.2-9. Knoop Microhardness vs. Fast Neutron Fluence for Zirconium and Zircaloy-2

Table 3.2-4
TENSILE TESTS OF ZIRCONIUM IRRADIATED AT 327°C TO
FLUENCE 6.8×10^{20} n/cm² (E > 1 MeV)

Specimen	0.2% Offset Yield Strength MPa (ksi)	Ultimate Strength MPa (ksi)	Total Elongation (%)	Uniform Elongation From Chart (%)	Reduction in Area (%) (.)
Annealed Zirconium Sponge	362.8 (52.6)	364.8 (52.9)	24.7	0.43	64.1
Annealed Crystal Bar Zirconium	375.9 (54.5)	378.6 (54.9)	31.3	0.53	73.0
	257.9 (37.4)	257.9 (37.4)	25.3	0.20	76.4
	216.6 (31.4)	233.1 (33.8)	22.3	0.89	71.0
	261.4 (37.9)	261.4 (37.9)	24.0	0.20	65.7

*Final thickness measurement is accurate. Final width was hard to measure accurately because the fracture tapered to a knife-edge. The "reduction in area" values reported are minimum values.

These rods are currently being sectioned to obtain expanding mandrel specimens, flux monitors and metallographic/microhardness specimens.

Irradiation of a third series of rods (EBR-II-3) began in December 1979 and is scheduled for completion in August 1980. The projected fluence (E > 1 MeV) is $\sim 4.2 \times 10^{21}$ n/cm² at core midplane and $\sim 3.8 \times 10^{21}$ n/cm² at the bottom of the core. The materials in EBR-II-3 are: (1) reference (bright-etched) Zircaloy-2, (2) 0.076-mm low-oxygen sponge zirconium-lined Zircaloy-2, (3) 0.076-mm low-oxygen sponge zirconium-lined Zircaloy-2 heat treated to recrystallize the liner and to stress relieve the cladding and (4) thin (~ 0.03 -mm) low-oxygen sponge zirconium-lined Zircaloy-2. The special heat treatment of material with 60-70% cold work (item 3) was a four hour isothermal anneal at 480°C. The thin zirconium liner (item 4) was prepared by coating the outside and end surfaces of the tube with lacquer to prevent chemical attack and then immersing the tube for short times in a bath of 45% HNO₃ (conc), 2% HF and 53% H₂O to reduce the liner thickness. This rod will provide irradiated material for the evaluation of the effect of liner thickness on the resistance to failure under simulated PCI conditions.

3.2.2.2 Expanding Mandrel Tests — (S. B. Wisner, G. H. Henderson and R. B. Adamson, NFFSD)

To simulate the behavior of high fluence and high activity (> 100 R/hr) Zircaloy cladding under PCI stress conditions and environment, a fully remote expanding mandrel loading system (REMLS) has been designed and installed in a remote handling cell at General Electric's Vallecitos Nuclear Center.

The in-cell expanding mandrel test is similar to the out-of-cell test except for some special equipment that was redesigned or modified for remote use. Figure 3.2-10 is a photograph of the REMLS and shows the special equipment. In the left foreground is a spotwelder which positions and welds a chromel-alumel thermocouple onto the outer surface at the midline of the specimen. This thermocouple is used to monitor the specimen temperature and for thermal control. The extensometer positioner is a vehicle that moves on tracks and precisely positions an extensometer around the specimen midplane diameter. The extensometer gives the average diametral extension during a test. Also seen in the figure at the right side is the remote handling "slave." There are two slaves, left and right, with extensive x-y-z linear motion and 360° rotary capability at the gripping jaws. The REMLS is now fully operational, and simulated PCI tests on specimens irradiated in the EBR-II-1 and EBR-II-2 experiments are now in progress.

POOR ORIGINAL

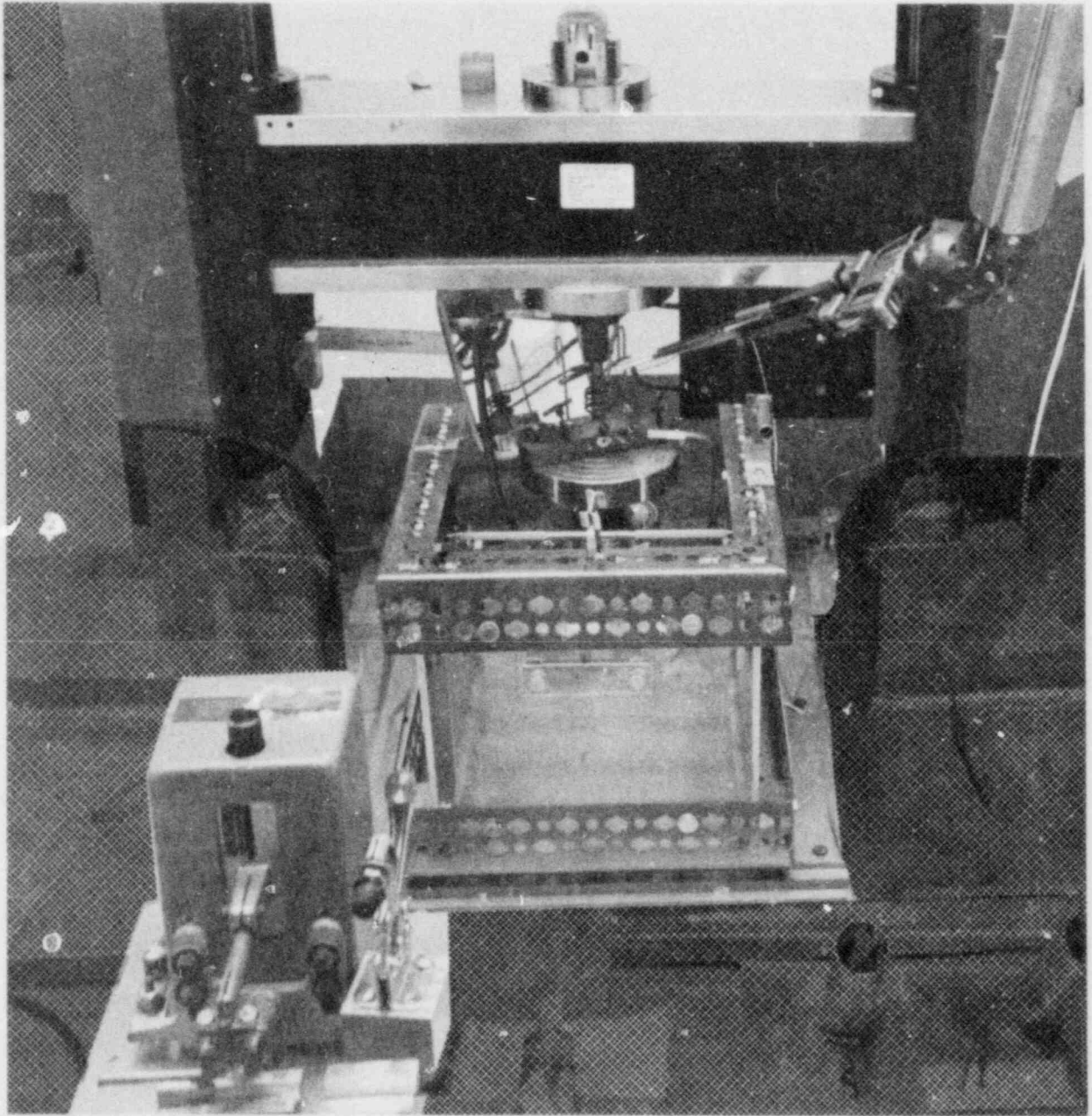


Figure 3.2-10. Remote Expanding Mandrel Loading System (REMLS)

ACKNOWLEDGEMENTS

The contributing authors of Subsection 3.2 gratefully acknowledge the invaluable assistance of:

R. E. Blood and R. D. Jones of NFSED in the preparation and shipping of rods for the EBR-II experiments.

R. E. Smith, D. L. Orton and R. D. Sanchez of the Irradiation Processing Operation for hot cell metallography and microhardness measurements.

G. C. Martin, R. D. Reager and D. H. Simpson of NFSED for fluence determinations on rods irradiated at the EBR-II.

G. P. Lundeen and D. Pereyra of NFSED for metallographic support.

W. L. Denison, M. A. Bell, G. E. Dunning and W. E. Maki of Nuclear Power Systems Engineering Department for fabrication and characterization of rods for the EBR-II experiments.

3.3 SUBTASK II.2 LICENSING TESTS

3.3.1 Loss-of-Coolant-Accident Simulation — (M. B. Reynolds, R. E. Blood, R. D. Jones, NFSED)

3.3.1.1 Introduction

An experimental program designed to compare, under simulated loss of coolant accident (LOCA) conditions, the behavior of reference Zircaloy cladding and various types of barrier cladding has been carried out and reported earlier.² In those experiments a segment of cladding tubing containing depleted UO_2 pellets was surrounded by saturated steam at atmospheric pressure and heated electrically at rates postulated for a LOCA event. Fission gas pressure loading on the tube test segment was simulated by pressurizing with argon. Tests were carried out at fixed argon pressures corresponding to hoop stresses of 3.45, 5.17 and 6.90 MPa. Tube failures were not observed at the lowest (3.45 MPa) hoop stress level within the heating times used (6.2 minutes). The present series of experiments was carried out to supplement the earlier work.

3.3.1.2 Experimental Details

A. Test Material

The following materials were used in these tests:

- 1) Bright reference Zircaloy-2 (unlined) tubing
- 2) Low oxygen sponge Zirconium-lined tubing
- 3) Crystal bar, Zirconium-lined tubing

Each of these materials were in the fully recrystallized (annealed) condition.

B. Test Procedures

The test specimens, filled with pellets of depleted uranium oxide, were electrically heated in saturated steam at atmospheric pressure in a Vycor chamber. Details of test configuration, including thermocouple placement between the pellets were described previously.² The UO_2 pellets are distributed approximately symmetrically about the thermocouple junctions at the specimen midplane although the thermocouple leads and insulation in the upper half of the specimen somewhat alter this symmetry with respect to thermal capacity.

The test specimen was resistively heated by passing current from a phase controlled ignitron low-voltage power supply through it. The "control thermocouple" in the center of the specimen was connected to a closed loop temperature controller driving the firing control network of the ignitron power supply. The specimen heating schedule was determined by a temperature programmer. The temperature-time program used in this series of tests was that used in the previously reported test and is illustrated in Figure 3.3-1.

Specimen rupture was indicated by an abrupt drop in pressure in the specimen. Pressure within the specimen was indicated by a strain gage type transducer.

Data from the specimen thermocouple, optical pyrometer and pressure transducer were collected and stored during the course of a test by a computer system, converted to temperature or pressure and plotted as functions of time by an X-Y plotter. Two of the four input channels of the computer preamplifier were connected to the chromel-alumel thermocouple between the pellets at the midplane of the specimen, a third channel was connected to the pressure transducer, and the

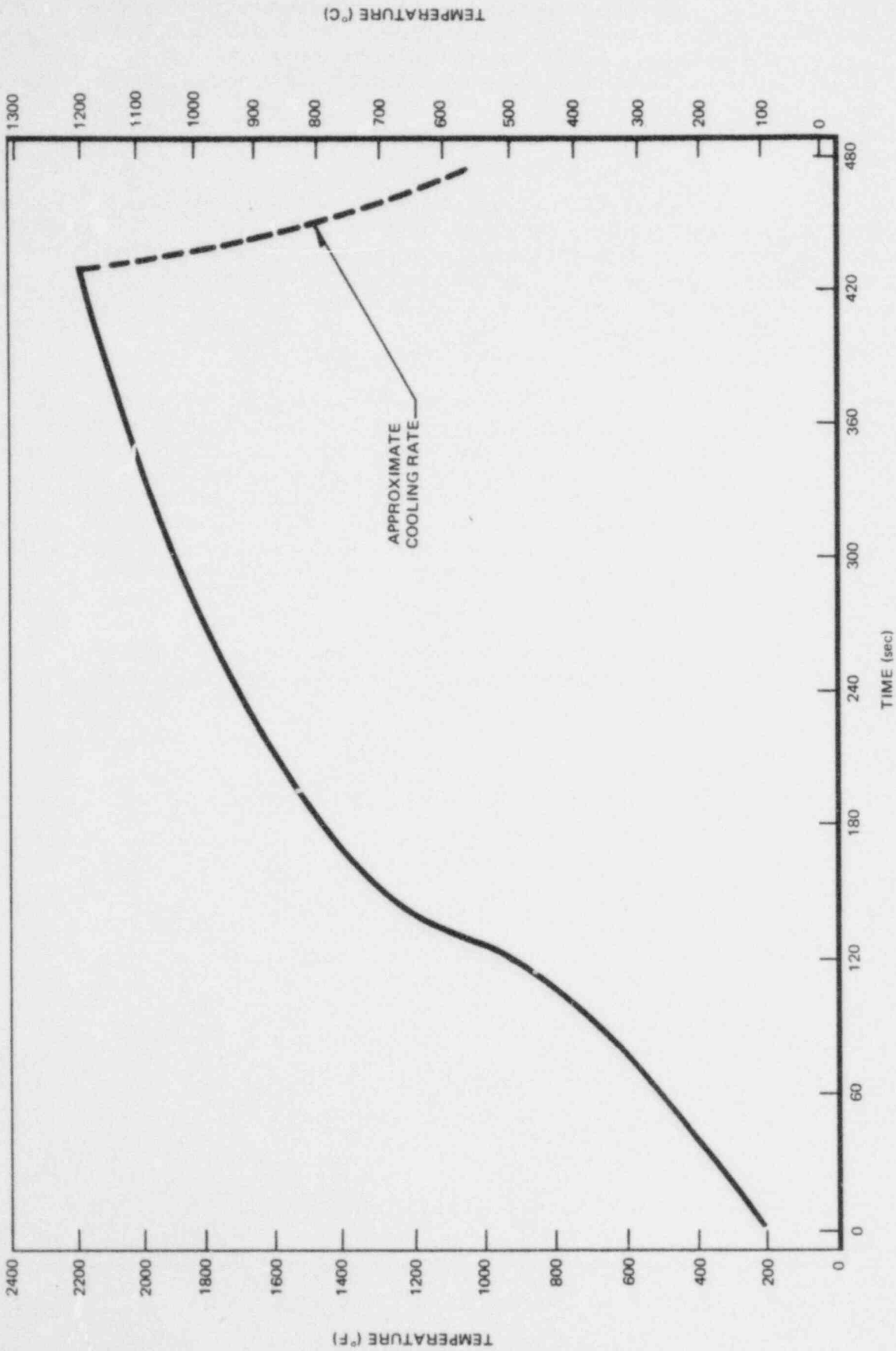


Figure 3.3-1. Temperature as a Function of Time for Simulated LOCA Testing

fourth channel to the optical pyrometer. The computer was programmed to sweep all four channels every two seconds until a total of 1200 readings (300 per channel) were collected. The total sample collection time of 600 seconds was chosen to match the program drum rotation rate of the temperature programmer. A temperature/pressure versus time plot from a typical test is shown in Figure 3.3-2.

3.3.1.3 Test Results

A series of specimens were tested — two or three from each of three tubing types at each of two hoop stress levels. The temperature and strain data from these tests are summarized in Table 3.3-1. The barrier tubes and the reference tubes did not differ significantly in behavior under the simulated LOCA conditions of this test series so far as rupture temperature and time to rupture were concerned. Circumferential fracture strain was somewhat higher for the zirconium-lined tubes than for the unlined Zircaloy tubes. Photographs of ruptured tubes are shown in Figures 3.3-3 and 3.3-4. Without measured values of surface temperature at the point of rupture it is not possible to relate rupture strains accurately to temperature.

It is a characteristic of the test apparatus for the temperature of the lower end of the specimen to lead the temperature at the specimen midplane by as much as one hundred degrees Celsius* during the heating phase of the test. Consequently, failures occur in the lower, hotter portion of the specimen. In order that present test results be consistent with previously reported results, no effort was made to change this behavior by modification of the test configuration or test procedure used earlier². All reported rupture temperatures obtained with this apparatus are low by about $\sim 100^\circ\text{C}$. Previously reported rupture temperatures are the average of midplane pellet and cladding surface temperatures — neither of which represents the visually obviously higher temperatures at the point of rupture. In Table 3.3-1 pellet temperature and the midplane cladding surface temperature are reported.

Strain values are based on mean of major and minor diameter measured at point of rupture and at specimen midplane where surface temperature was measured. Results of these measurements are given in Table 3.3-1.

*Visual estimate based on color differences. The optical pyrometer focuses on the specimen at midplane.

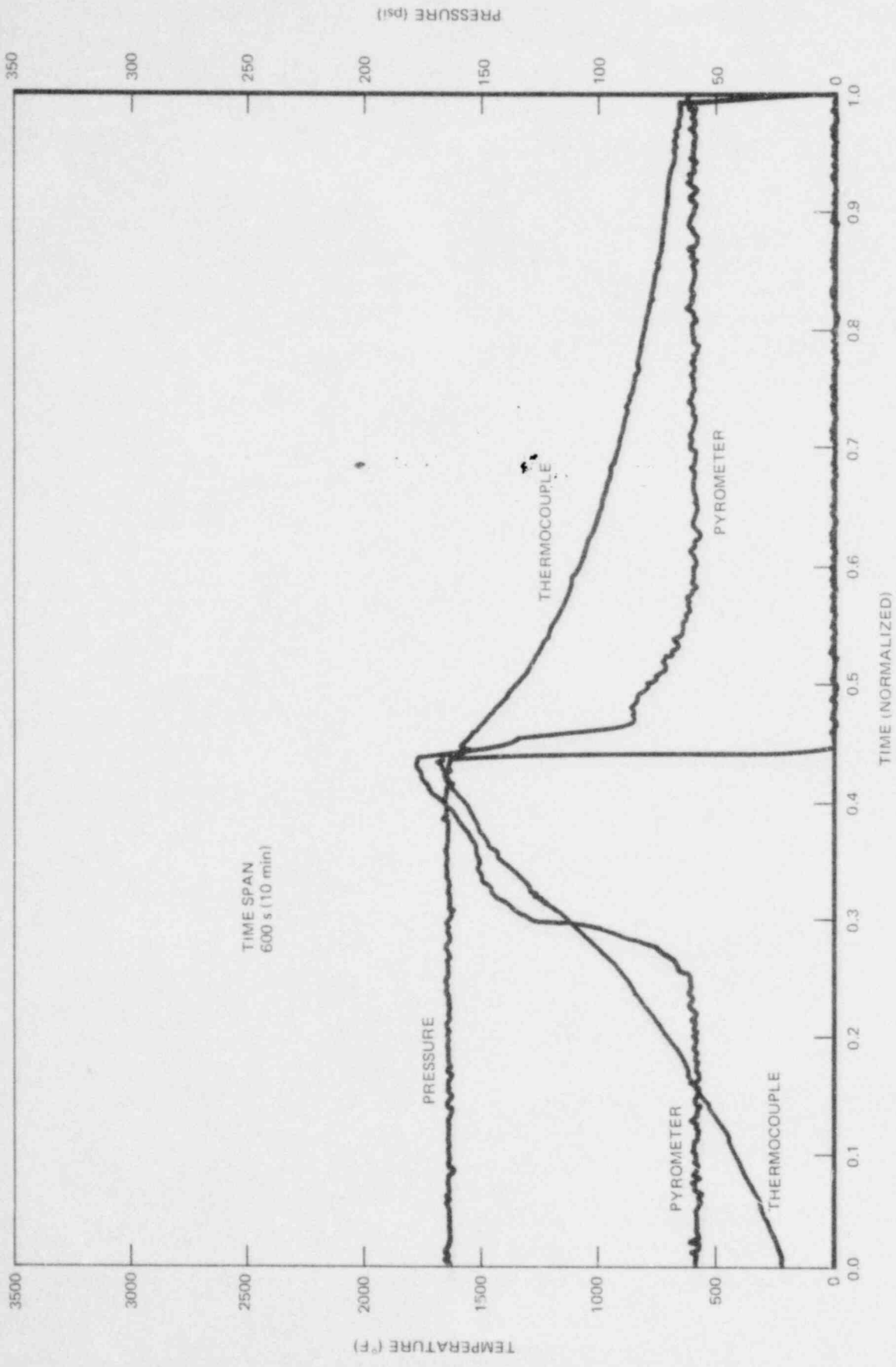
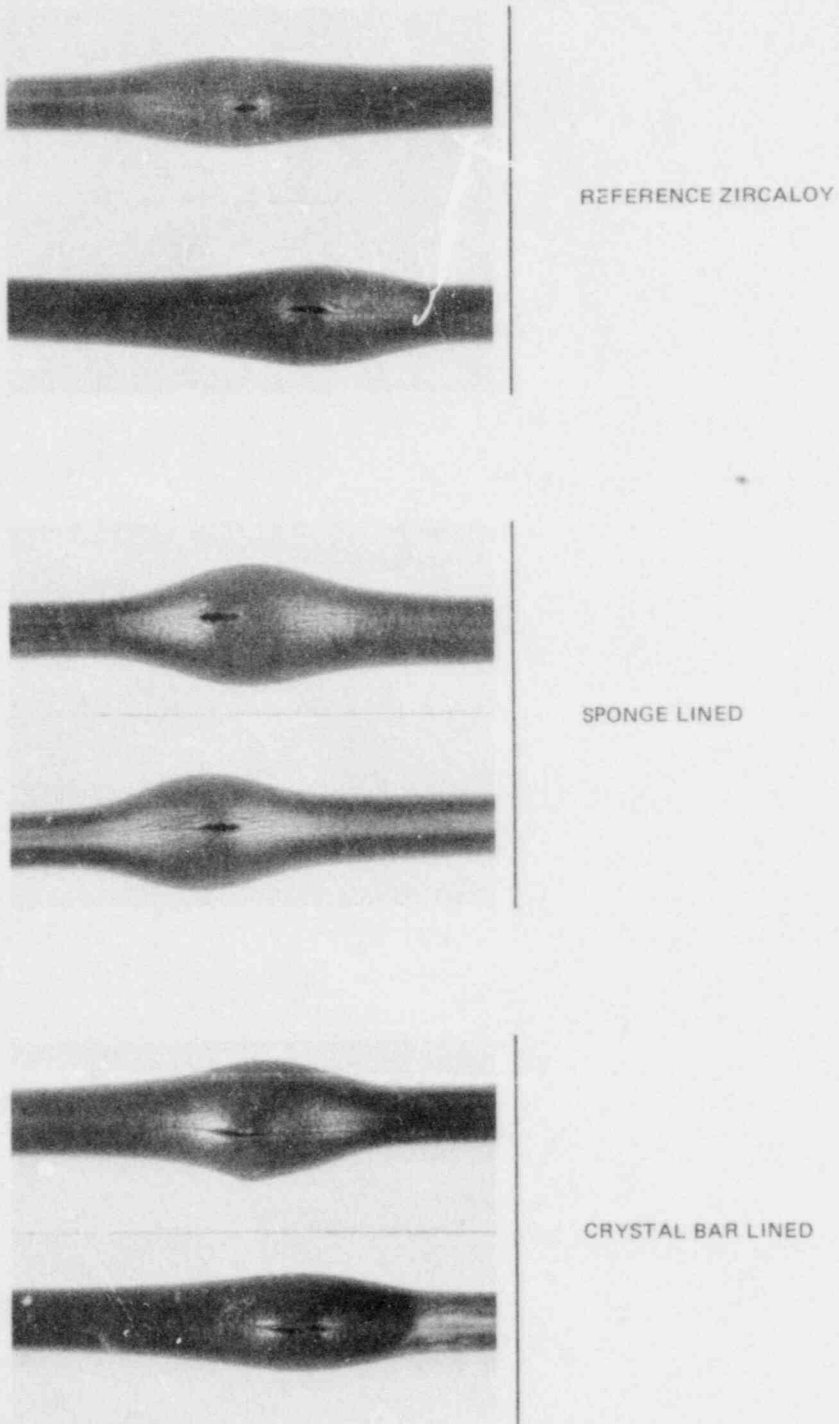


Figure 3.3-2. Typical Computer Output for LOCA Test



1 cm
|-----|

Figure 3.3-3. LOCA Specimens Tested at 5.2 MPa Hoop Stress Original Tubing Outer Diameter = 12.3 mm

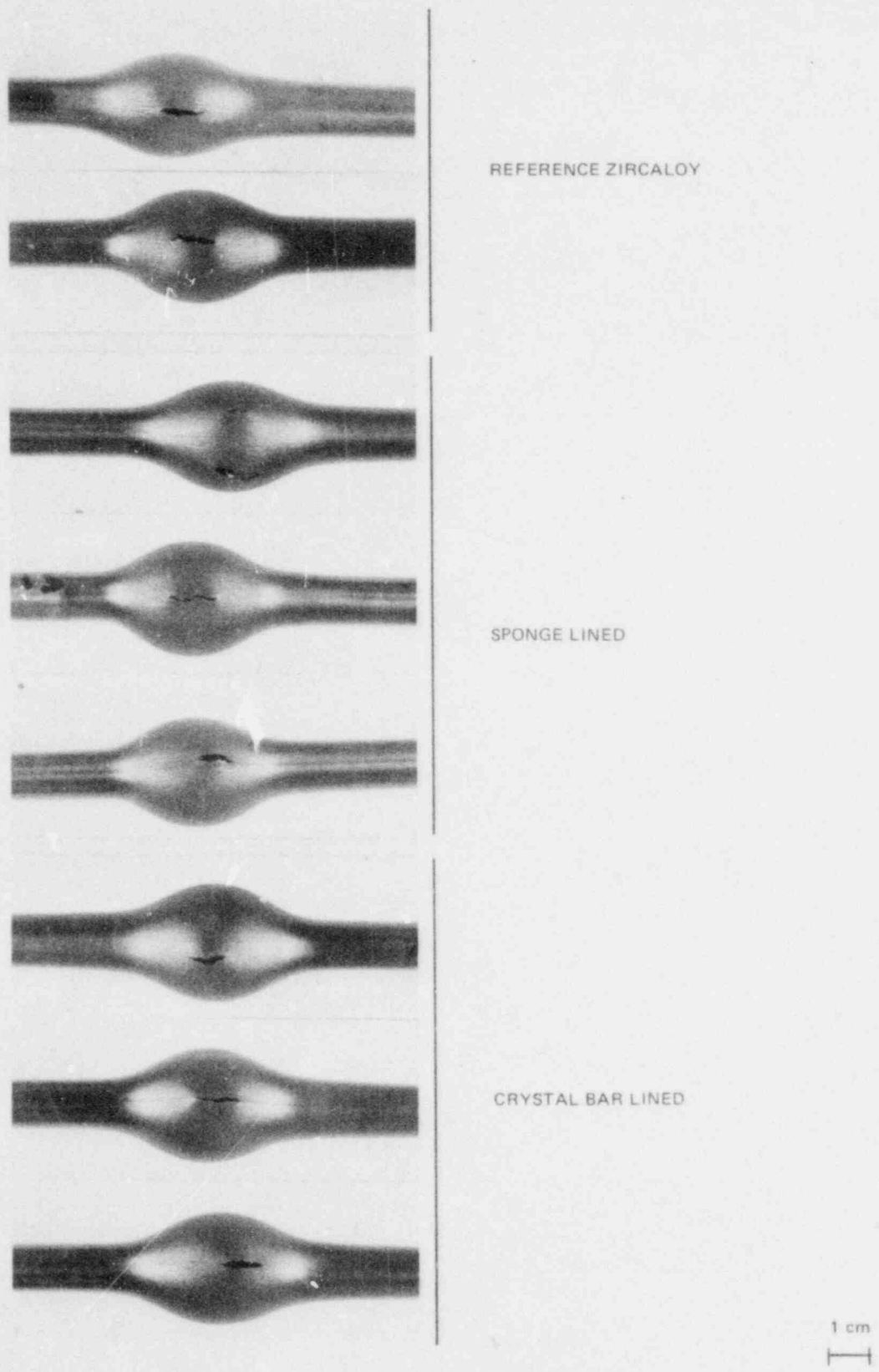


Figure 3.3-4. LOCA Specimens Tested at 6.9 MPa Hoop Stress

Table 3.3-1
LOCA TEST SUMMARY

Specimen Type	Rupture Temperature, °C (°F)		Hoop Stress MPa (PSI)	CFE, %	CUE,* %	Failure Time, Minutes
	Center	Surface*				
A-1	922 (1817)	1008 (1846)	5.17 (750)	55	8.3	4.75
A-1	978 (1792)	1008 (1846)	5.17 (750)	71	8.3	4.9
A-2	918 (1685)	971 (1779)	6.90 (1000)	112	7.5	4.5
A-2	907 (1665)	981 (1798)	6.90 (1000)	130	5.1	4.3
S-1	971 (1780)	1016 (1860)	5.17 (750)	107	13.9	4.7
S-1	984 (1803)	1006 (1842)	5.17 (750)	98	8.0	5.3
S-2	777 (1430)	916 (1680)	6.90 (1000)	132	1.74	3.45
S-2	919 (1687)	967 (1773)	6.90 (1000)	124	4.0	4.3
S-2	907 (1664)	—	6.90 (1000)	126	4.7	4.0
X-1	967 (1772)	996 (1825)	5.17 (750)	99	9.4	4.5
X-1	971 (1780)	1049 (1920)	5.17 (750)	67	6.5	4.6
X-2	921 (1690)	1199 (2190)	6.90 (1000)	129	6.4	4.3
X-2	909 (1668)	964 (1767)	6.90 (1000)	127	4.7	4.0
X-2	926 (1699)	962 (1764)	6.90 (1000)	136	5.6	4.2

A — Bright etched, annealed
S — Low oxygen sponge zirconium lined
X — Crystal bar zirconium lined
1 — 5.17 MPa

2 — 6.90 MPa
CFE — Circumferential fracture elongation
CUE — Circumferential uniform elongation
* — Measured at specimen midplane

3.4 SUBTASK II.3 FUEL IRRADIATION TESTS

3.4.1 Segmented Rod Irradiation Tests (J. H. Davies, E. Rosicky, D. K. Dennison and E. L. Esch, NFFSD)

3.4.1.1 Bundle Status

The irradiation status of the three segmented test rod (STR) assemblies in the segmented rod program (SRP) is updated in Table 3.4-1. No bundle reconstitutions were performed during the current reporting period.

3.4.1.2 Power Ramp Tests

3.4.1.2.1 Introduction

Following the successful ramp testing of 12 GE fuel rods performed in 1978 in the R2 Reactor at Studsvik^{2,3}, a larger program was defined for testing in 1979. Thirty-six fuel rods segments were selected from segmented rod assemblies in both the Monticello (SRP-2) and the Millstone (SRP-3) power reactors and carefully characterized in the Hotcells of the GE Vallecitos Nuclear Center. This included visual examination, profilometry, gamma scanning, neutron radiography and pulsed eddy current testing. The rods were shipped to Studsvik in July and ramp tested during the Fall. They included 14 reference fuel rods, 6 Zr-liner and 16 Cu-barrier fuel rods. The test program had four main objectives:

1. Investigation of the need for an extended low power standardization period prior to ramp testing.

The 300-hour standardization irradiation, which was used in the 1978 R2 test series, was a somewhat arbitrary requirement, included to preserve test parity with earlier tests at the GE Test Reactor (GETR). This phase of the test was time-consuming and expensive and perhaps unnecessary.

2. Testing the PCI resistance of Cu-barrier fuel at lead exposures.
3. Testing the ability of Zr-liner and Cu-barrier fuel to survive a large power step at low to medium exposures.

This test was a closer simulation of a control blade withdrawal than the standard "staircase" ramp test.

4. Investigation of performance limits of Cu-barrier fuel.

Failure of two Cu-barrier rods with a thin (5 μm) layer of copper in the 1978 test series, after universally good performance at lower exposures, indicated a possible exposure-dependent loss of protectiveness of the Cu-barrier. A small test matrix was set up to explore the effects of residual copper layer thickness and exposure.

3.4.1.2.2 Test Description

The R2 Test Reactor facilities have been described previously². The 36 fuel rods selected for ramp testing are described in detail in Table 3.4-2. As before, reference rods were defined broadly as those rods with unmodified Zircaloy cladding, although there were differences among references in conventional design features (cladding wall thickness, diametral gap, helium pressure).

**Table 3.4-1
SRP IRRADIATION STATUS**

STR Bundle	Segment Tier	Average Exposure (MWt/kg U)	Highest SRP Segment Average Exposure (MWd/kg U)	Date
SRP-1 (Quad Cities-1)	Top	12.5	14.7	November 30, 1979
	Mid-Top	18.2	21.5	
	Mid-Bottom	18.2	22.3	
	Bottom	14.7	18.5	
	Bundle Average	15.9		
SRP-2 (Monticello)	Top	13.8	18.2	December 31, 1979
	Mid-Top	21.4	27.8	
	Mid-Bottom	23.9	30.9	
	Bottom	20.8	27.0	
	Bundle Average	20.0		
SRP-3 (Millstone)	Top	12.9	17.4	December 31, 1979
	Mid-Top	19.5	23.7	
	Mid-Bottom	22.1	25.3	
	Bottom	19.8	22.5	
	Bundle Average	18.6		

Table 3.4-2
DESCRIPTION OF FUEL RODS RAMP TESTED IN 1979

Segment Identification	Design Feature ^{(a)(b)}	Cladding Wall (mm)	Diametral Gap (mm)	He Pressure (MPa)	Ave. Burnup ^(c) (MWd/kg U)	Test Objective ^(d)
SRP-2/7	Reference	0.86	0.18	0.1	15.9	1
SRP-2/8	Reference	0.86	0.18	0.1	14.9	
SRP-2/9	Reference	0.86	0.23	0.1	13.8	
SRP-2/16	Reference	0.86	0.23	0.1	15.8	
SRP-2/25	Reference	0.71	0.18	2.2	18.1	
SRP-2/26	Reference	0.86	0.23	0.1	20.4	
SRP-2/27	Reference	0.86	0.23	0.1	19.2	
SRP-2/28	10 μ m Cu-barrier (nonbonded)	0.86	0.23	0.1	13.1	2
SRP-2/29	10 μ m Cu-barrier (nonbonded)	0.86	0.23	0.1	15.2	
SRP-2/30	10 μ m Cu-barrier (nonbonded)	0.86	0.23	0.1	13.0	
SRP-3/40	10 μ m Cu-barrier (electroless)	0.86	0.23	0.3	6.3	
SRP-2/12	Reference	0.86	0.23	0.1	12.4	3
SRP-2/15	Reference	0.86	0.23	0.1	16.4	
SRP-2/21	Reference	0.86	0.23	0.1	10.4	
SRP-2/22	Reference	0.86	0.23	0.1	15.9	
SRP-2/24	Reference	0.71	0.18	2.2	19.4	
SRP-3/7	Reference	0.71	0.23	1.7	3.6	
SRP-3/29	High O/U Fuel ^(e)	0.71	0.23	1.7	9.0	
SRP-2/2	10 μ m Cu-barrier (nonbonded)	0.86	0.23	0.1	10.5	
SRP-2/31	10 μ m Cu-barrier (nonbonded)	0.86	0.23	0.1	8.1	
SRP-2/32	10 μ m Cu-barrier (on-oxide)	0.86	0.23	0.3	4.8	
SRP-3/16	5 μ m Cu-barrier (nonbonded)	0.71	0.23	1.7	5.0	
SRP-3/41	10 μ m Cu-barrier (electroless)	0.86	0.23	0.3	6.2	
SRP-3/42	5 μ m Cu-barrier (electroless)	0.86	0.23	0.3	5.7	
SRP-2/34	76 μ m Zr-liner (sponge)	0.86	0.23	0.3	4.8	
SRP-3/20	76 μ m Zr-liner (crystal bar)	0.71	0.23	1.7	5.6	
SRP-3/44	76 μ m Zr-liner (crystal bar)	0.71	0.23	1.7	5.9	
SRP-3/45	76 μ m Zr-liner (crystal bar)	0.71	0.23	1.7	5.7	
SRP-3/46	76 μ m Zr-liner (crystal bar)	0.71	0.23	1.7	7.4	
SRP-3/47	76 μ m Zr-liner (crystal bar)	0.71	0.23	1.7	7.0	
SRP-3/24	10 μ m Cu-barrier (bonded)	0.71	0.23	1.7	9.6	4
SRP-3/25	10 μ m Cu-barrier (bonded)	0.71	0.23	1.7	9.3	
SRP-3/31	5 μ m Cu-barrier (bonded)	0.71	0.23	1.7	10.9	
SRP-3/32	5 μ m Cu-barrier (bonded)	0.71	0.23	1.7	10.5	
SRP-3/38	10 μ m Cu-barrier (bonded)	0.71	0.23	1.7	15.5	
SRP-3/39	10 μ m Cu-barrier (bonded)	0.71	0.23	1.7	15.0	

NOTES

- a) All cladding is Zircaloy-2 (recrystallization anneal); fuel density, 95.5%.
 b) Cu-barriers are all electroplated except for Cu (on-oxide) and where stated to the contrary. Bonded barrier means plated tubes subjected to a diffusion anneal during fabrication to form Cu-Zr intermetallic layer.
 c) Burnups calculated from ¹³⁷Cs gamma scans by comparison to known standards.
 d) See Introduction for definition of Objectives. Objective 1, 2, 4 rods — Ramp Sequence A. Objective 3 — Ramp Sequence B.
 e) Fuel O/U ratio in range 2.02 - 2.07.

Table 3.4-2 also indicates the Test Objective for each rod. For Objectives 1, 2 and 4, a "staircase" ramp sequence was employed similar to that used previously. This was labeled Ramp Sequence A and is depicted in Figure 3.4-1. The big step ramp to meet Objective 3 was labeled Ramp Sequence B and is shown in Figure 3.4-2. Note that Sequence A standardization is at 9 kW/ft (29.5 kW/m), slightly higher than the nominal level, 8 kW/ft (26.2 kW/m), employed previously. This change was necessary, because the six-hour standardization had to be performed in the ramp test rig in R2 with the reactor at full power, and it was not possible to guarantee the specified maximum peak power of 18 kW/ft (59.0 kW/m) using the ^3He coil alone, if the standardization power was less than half the maximum. In Ramp Sequence B the specified power shock was from 8 to 16 kW/ft (26.2 to 52.5 kW/m) the factor of 2 power increase being within the capacity of the ^3He device. If a rod survived this test, it was given an additional small power shock, not exceeding 2 kW/ft (6.6 kW/m), using any residual capacity still available in the ^3He coil (see Figure 3.4-2).

Rod failures were recognized by steep increases in the loop activity level, but additional evidence was collected to show that this burst of activity often lags considerably behind actual rod deflection. In several tests the activity burst was preceded by the small "power" spike noted previously.^{2,3} In one case (Figure 3.4-3) the spike coincided (allowing for the appropriate delay time) with a small, but discernible activity increase, supporting the hypothesis that the spikes are early (probably virtually instantaneous) indications of rod deflection and large activity releases are delayed until pressure equilibrium has been established across the defect and/or small pressure transients or power ripples promote an aspiration effect. Forsyth et al.⁷ have reported that pressure changes of about 1 bar will produce such bursts of activity and they have also shown that small PCI defects may virtually reseal themselves. The "power" spikes are not a general observation and the phenomenology of the effect remains to be defined.

Following a certified rod failure, power was rapidly reduced by pressurizing the ^3He coil. Shortly thereafter the rod was raised from the core and, after an appropriate cooling period, it was removed from the rig.

All the rods will be visually examined in the Studsvik hotcells and neutron radiographed prior to shipment back to the GE Vallecitos Nuclear Center for a more detailed examination.

3.4.1.2.3 Results and Discussion

Preliminary results of the ramp tests are summarized in Table 3.4-3. The results of the first seven tests, addressing Objective 1, are compared with prior Reference J rod results in Figure 3.4-4. The premature failure of SRP-2/26 during the standardization period at 9 kW/ft (29.8 kW/m) was inconsistent with other Test Reactor Ramp test results reported in the literature, but not inconsistent with the low probability failure threshold observed in some power reactor experience⁸. This rod will be examined closely in the post-irradiation examination phase of the work. Because SRP-2/26 failed during the low power standardization step, the results could not be included in the evaluation of the effect of standardization time on ramp test failure power. From the remaining results in Figure 3.4-4 it was judged that there was not a significant difference in failure propensity between rods standardized for six hours and 300 hours respectively. All subsequent tests were performed using the six-hour period.

Three of the four Cu-barrier rods, ramped to test the PCI resistance of Cu-barrier fuel at lead exposures, survived. However, the highest burnup rod, SRP-2/29, failed, albeit at the maximum peak power of 58 kW/m (17.7 kW/ft). This result was consistent with prior experience, which indicated that the effectiveness of the Cu-barrier as a PCI remedy appears to decrease at burnups around 15 MWd/kg U. The total ramp test experience with Cu-barrier fuel is shown in Figure 3.4-5. A literature representation of power reactor fuel performance⁹ is included for comparison. It is believed that the "wear-out" effect is due to the slow interdiffusion of copper and zirconium forming a brittle intermetallic layer. This problem, which was anticipated, led to the development of a process for plating copper on autoclave oxidized cladding, where the oxide film acts as a diffusion barrier to prevent copper-zirconium interdiffusion. Rods of this design, to be tested at the appropriate burnups, are being irradiated in the SRP bundles.

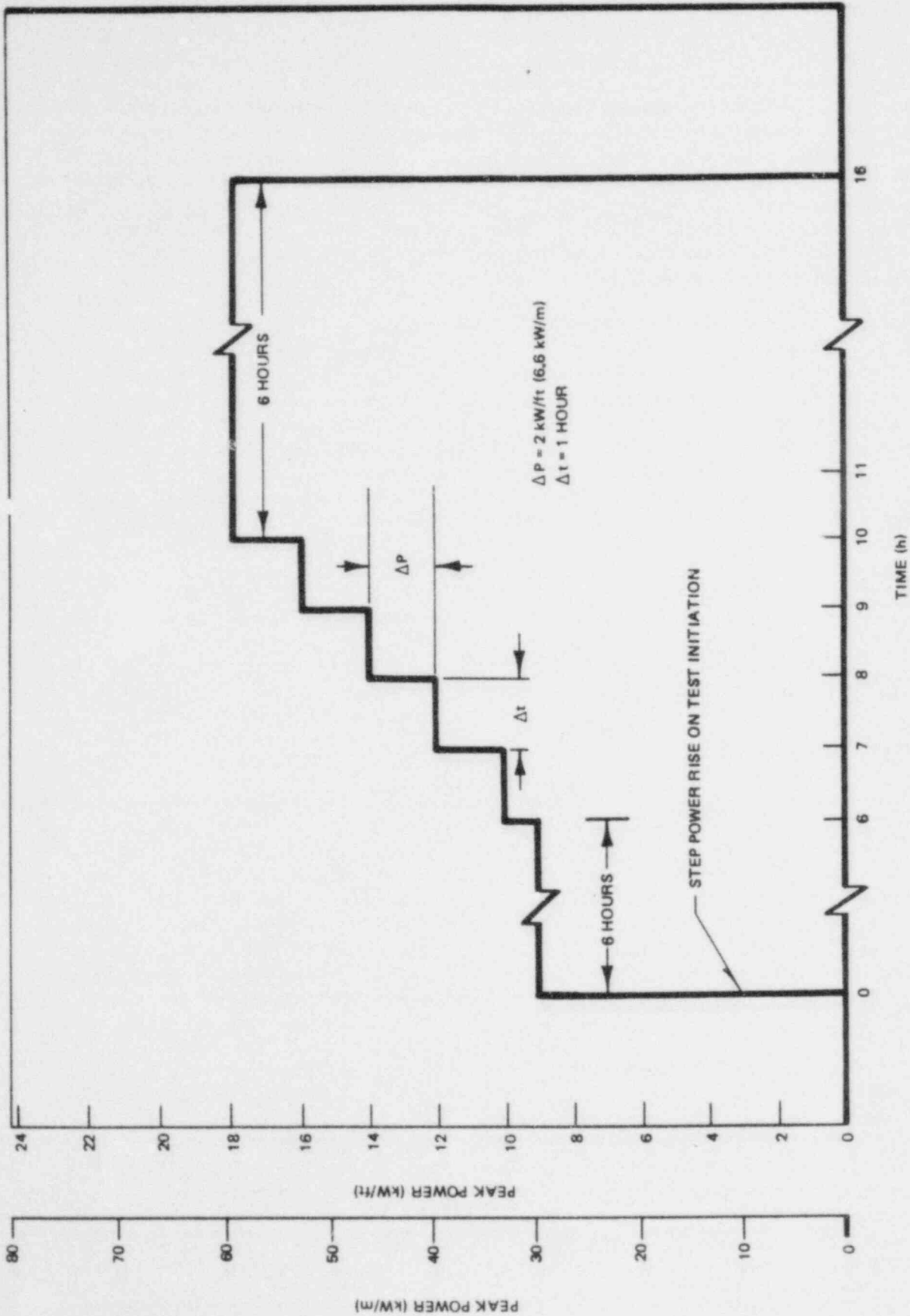


Figure 3.4-1. Ramp Test Sequence to Investigate Effect of Short (6 Hours) Standardization Phase. Ramp Test Sequence A

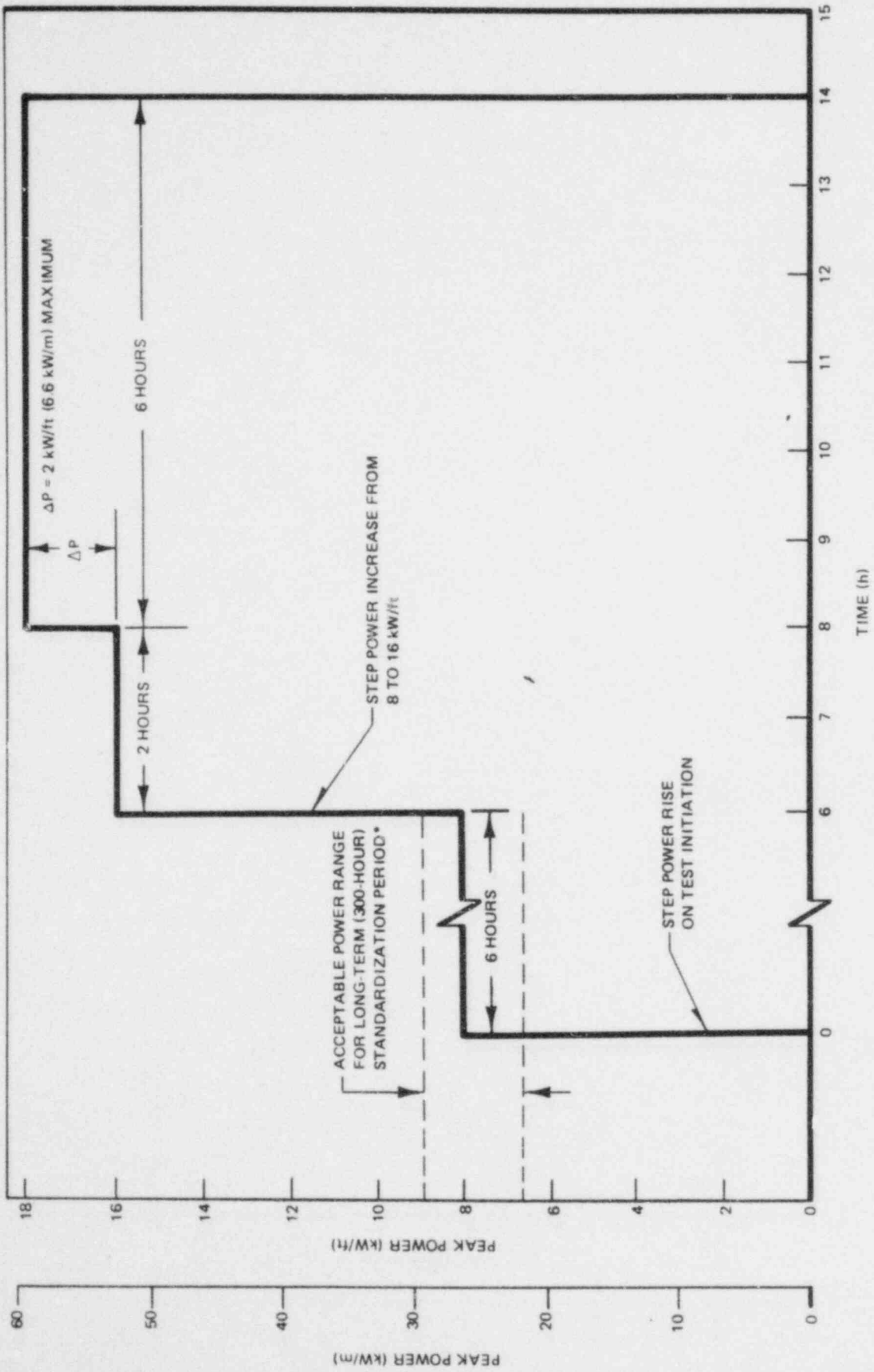


Figure 3.4-2. Ramp Test Sequence B

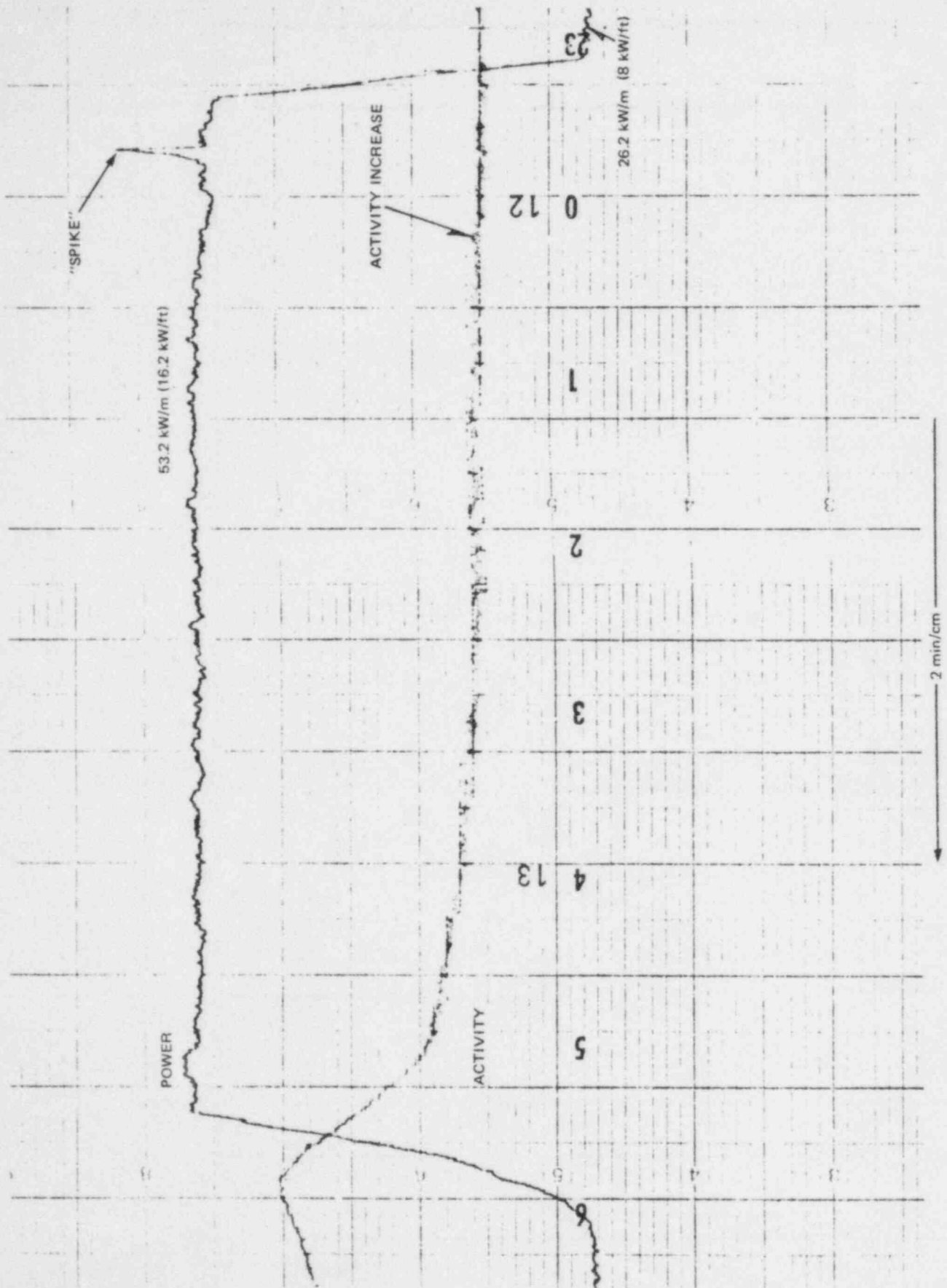


Figure 3.4-3. Recorder Chart Output, SRP-2/21

Table 3.4-3
1979 SRP RAMP TEST, PROGRAM RESULT SUMMARY

Rod Identification	Rod Design	Average Exposure MWd/kg U	Maximum Peak Power		Time to Failure ^(a) (minutes)	Result	Remarks
			kW/m	kW/ft			
SRP-2/7	Reference	15.9	46.2	14.1	45	Failed	
SRP-2/8	Reference	14.9	46.5	14.2	50	Failed	
SRP-2/9	Reference	13.8	46.0	14.0	15	Failed	
SRP-2/16	Reference	15.8	52.6	16.0	0.5	Failed	
SRP-2/25	Reference	18.1	52.3	16.0	6.5	Failed	
SRP-2/26	Reference	20.4	29.8	9.1	26	Failed	
SRP-2/27	Reference	19.2	39.4	12.0	41	Failed	Power Spike (11 min) ^(b)
SRP-2/28	Cu-barrier	13.1	58.8	17.9	—	Sound	
SRP-2/29	Cu-barrier	15.2	58.0	17.7	147	Failed	Power Spike (44 min) ^(b)
SRP-2/30	Cu-barrier	13.0	59.0	18.0	—	Sound	
SRP-3/40	Cu-barrier	6.3	58.7	17.9	—	Sound	
SRP-2/12	Reference	12.4	53.2	16.2	50	Failed	
SRP-2/15	Reference	16.4	50.5	15.4	23 (75) ^(c)	Failed	Power Spike (15 min) ^(b)
SRP-2/21	Reference	10.4	53.2	16.2	2.5 ^(d)	Failed	Power Spike (2 min) ^(b)
SRP-2/22	Reference	15.9	52.1	15.9	40	Failed	
SRP-2/24	Reference	19.4	52.1	15.9	4.5	Failed	
SRP-3/7	Reference	3.6	59.1	18.0	—	Sound	
SRP-3.29	High O/U Fuel	9.0	58.7	17.9	—	Sound	
SRP-2/2	Cu-barrier	10.5	58.6	17.9	—	Sound	
SRP-2/31	Cu-barrier	8.1	59.0	18.0	—	Sound	
SRP-2/32	Cu-barrier	4.8	59.0	18.0	—	Sound	
SRP-3/16	Cu-barrier	5.6	59.3	18.1	—	Sound	
SRP-3/41	Cu-barrier	6.2	59.0	18.0	—	Sound	
SRP-3/42	Cu-barrier	5.7	58.8	17.9	—	Sound	
SRP-2/34	Zr-liner	4.8	59.0	18.0	—	Sound	
SRP-3/20	Zr-liner	5.6	59.4	18.1	—	Sound	
SRP-3/44	Zr-liner	5.9	59.3	18.1	—	Sound	
SRP-3/45	Zr-liner	5.7	58.5	17.8	—	Sound	
SRP-3/46	Zr-liner	7.4	58.8	17.9	—	Sound	
SRP-3/47	Zr-liner	7.0	59.1	18.0	—	Sound	
SRP-3/24	Bonded Cu-barrier	9.6	52.5	16.0	28	Failed	
SRP-3/25	Bonded Cu-barrier	9.3	58.2	17.8	30	Failed	
SRP-3/31	Bonded Cu-barrier	10.9	52.2	15.9	55	Failed	
SRP-3/32	Bonded Cu-barrier	10.5	52.7	16.1	34	Failed	
SRP-3/38	Bonded Cu-barrier	15.5	52.3	16.0	21	Failed	
SRP-3/39	Bonded Cu-barrier	15.0	52.6	16.0	9	Failed	

(a) Failure times based on loop activity level. Minutes to failure from end of last ramp step.

(b) See discussion in text and Figure 3.4-3. Time in parenthesis is the time from end of last ramp step to the spike.

(c) Small activity increase noted on chart 23 mins after ramp. Large increase after 75 min ended test.

(d) See Figure 3.4-3.

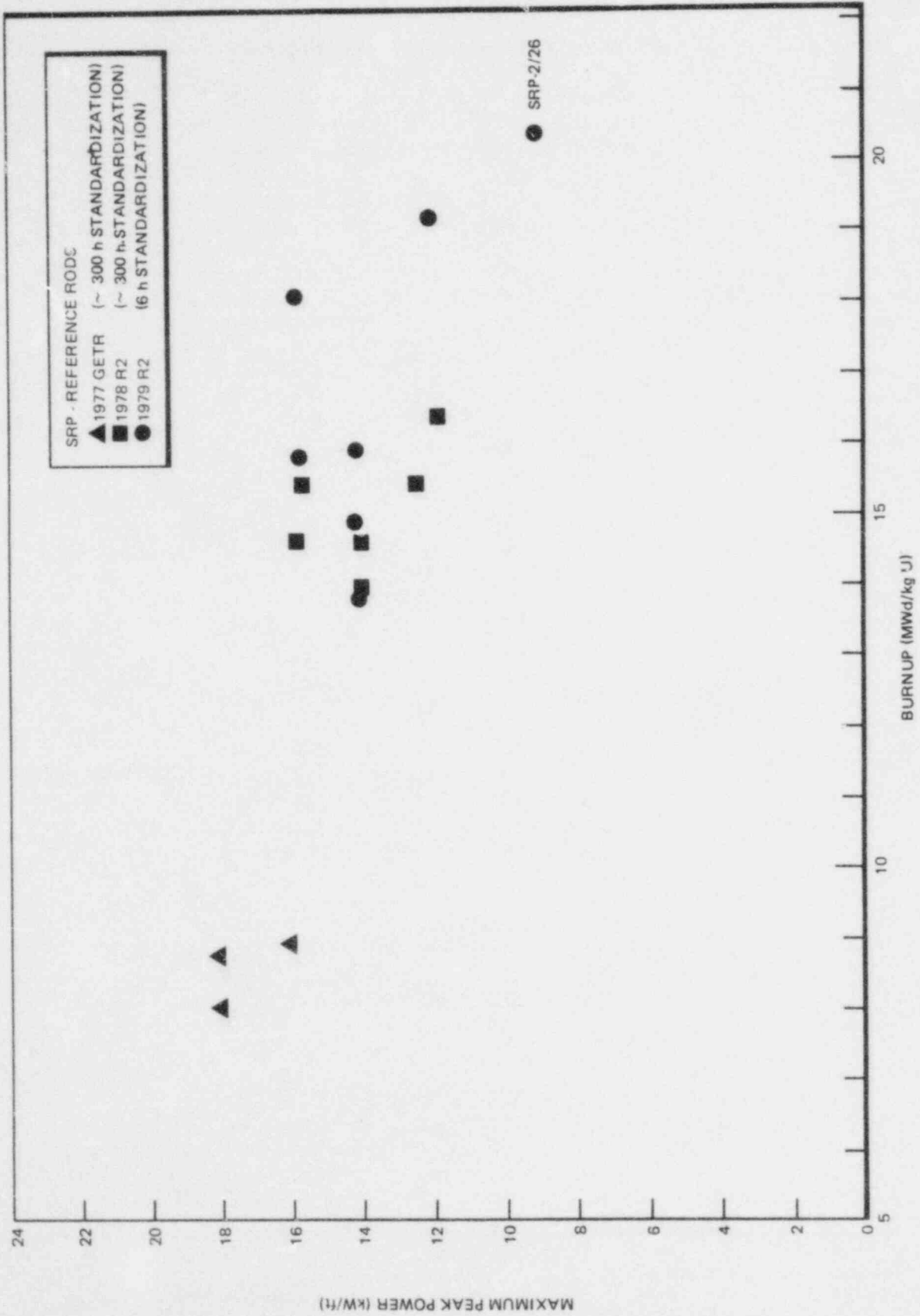


Figure 3.4-4. Ramp Sequence A — Effect of Standardization Time

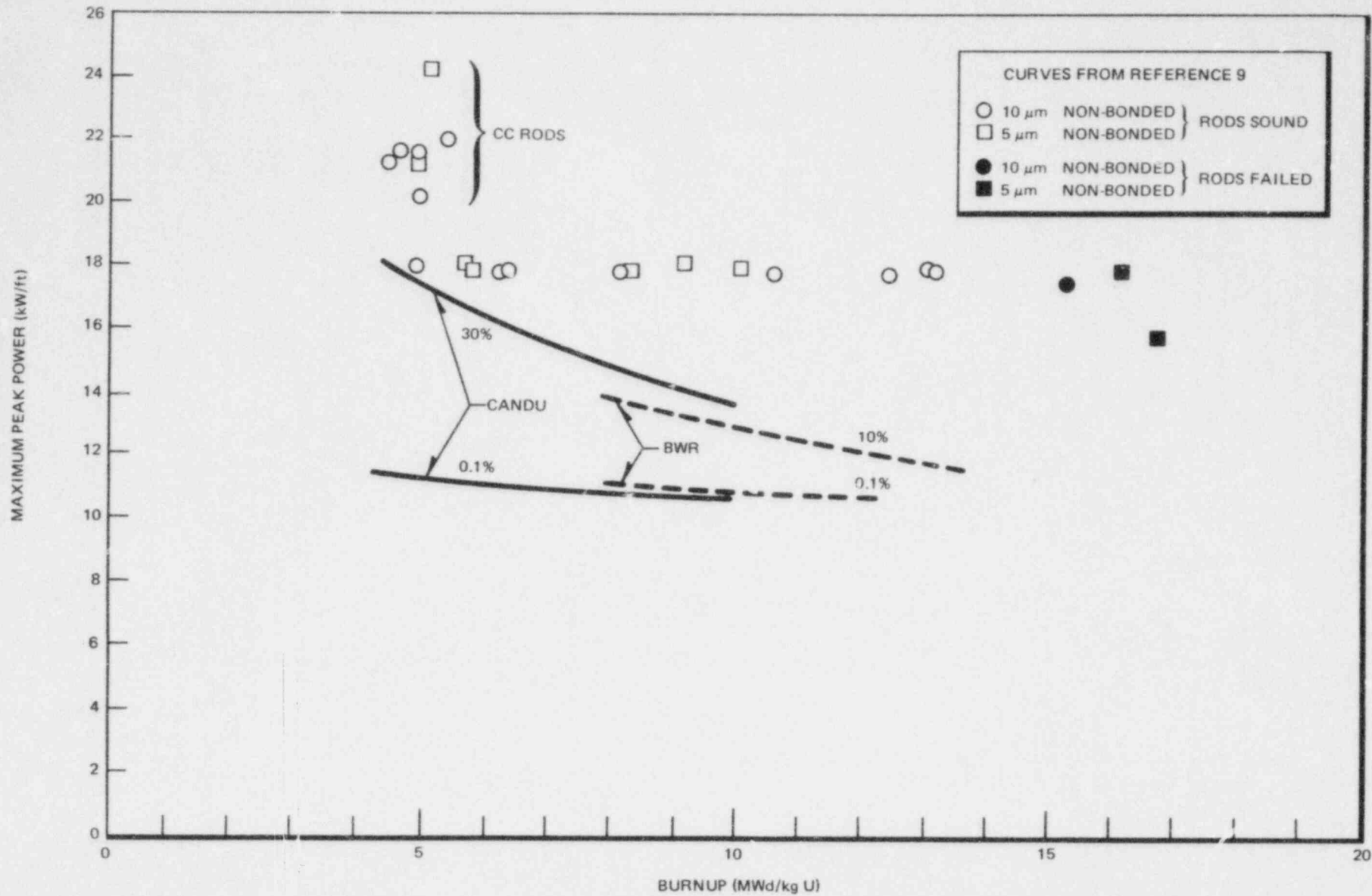


Figure 3.4-5. Copper Barrier (Nonbonded) — Total Experience

All of the reference rods, except the very low exposure rod, SRP-3/7, failed following the step ramp (Sequence B) from 8 to 16 kW/ft (26.2 to 52.5 kW/m). All of the barrier rods plus a rod, SRP-3/29, containing fuel with a high O/U ratio survived this test. The results are presented in Figure 3.4-6. Although the burnup disparity between References and Barriers detracts from the impact of this result, the hundred percent success rate on the latter is significant. The literature representation of power reactor fuel performance⁹ is included to emphasize this conclusion. The reference rod results in this range suggest that the B Sequence ramp is at least as severe as A Sequence ramps. Sequence B ramps to progressively lower terminal powers are needed to define the threshold failure power in this type of test.

All of the bonded Cu-barrier rods (i.e., barrier diffusion bonded to cladding during fabrication) failed with little improvement over references. Clearly the Cu-Zr intermetallic layer degrades the performance Cu-barrier fuel and must be avoided. Preliminary evaluation of the data suggests that the thickness of the intermetallic layer is more important than that of the residual copper layer in determining performance.

Note in Tables 3.4-2 and 3.4-3 that the test matrix included low burnup rods containing electroless copper (SRP-3/40, -3/41, 3/42), copper-on-oxide (SRP-2/32) and sponge zirconium (SRP-2/34). These newer barrier designs all performed successfully.

3.4.1.2.4 Conclusions

Reducing the pre-ramp standardization time from 300 hours to six hours did not significantly effect ramp test performance.

Although Cu-barrier fuel (nonbonded) out-performs Reference fuel, it is not immune to failure at high burnups.

All barrier fuel subjected to a single large power step ramp test at low to medium exposures survived.

The development of a Cu-Zr intermetallic layer between barrier and cladding clearly degrades the performance of Cu-barrier fuel.

3.4.1.3 Nondestructive Post-Irradiation Examination

The non-destructive post-irradiation examination (PIE) of the twelve rods ramp tested^{2,3} at Studsvik in 1978 has been completed at the GE Vallecitos Nuclear Center. The visual examination and neutron radiography were performed at Studsvik shortly after testing, and the results were reported previously². The additional characterization steps included profilometry and pulsed eddy current (PEC) traces. A summary of these results is given in Table 3.4-4. The PIE results have confirmed the ramp test results with respect to the condition of the rods (i.e., sound versus failed).

Post-irradiation characterization results summaries for three rods are shown in a convenient pictorial format in Figures 3.4-7, 3.4-8 and 3.4-9. The rods, SRP-2/1, SRP-3/35 and SRP-2/14, are a sound Cu barrier rod, a sound Zr-liner rod and a failed reference rod respectively. The main points to note are the high permanent cladding strains suffered by the sound barrier rods compared to the almost zero failure strain in the reference, and the PEC signals from the inner surfaces of the two sound rods. The high cladding strains in SRP-2/1 and SRP-3/35 testify to the severity of the test, particularly to the effect of the power increment above 14 kW/ft (46 kW/m), the maximum peak power of the failed Reference (SRP-2/14). It is also noteworthy (Table 3.4-5) that the Zr-liner cladding strains in this test series were much higher than in similar, but lower burnup, rods ramp tested earlier³ in the General Electric Test Reactor (GETR). Possible causes of this difference are being evaluated.

The remarkable plastic strains in the sound barrier rods, compared with those in the failed reference rods, are shown in Figure 3.4-10. The strain values shown here and in Tables 3.4-5 and 3.4-6 do not include the strain due to rigging.

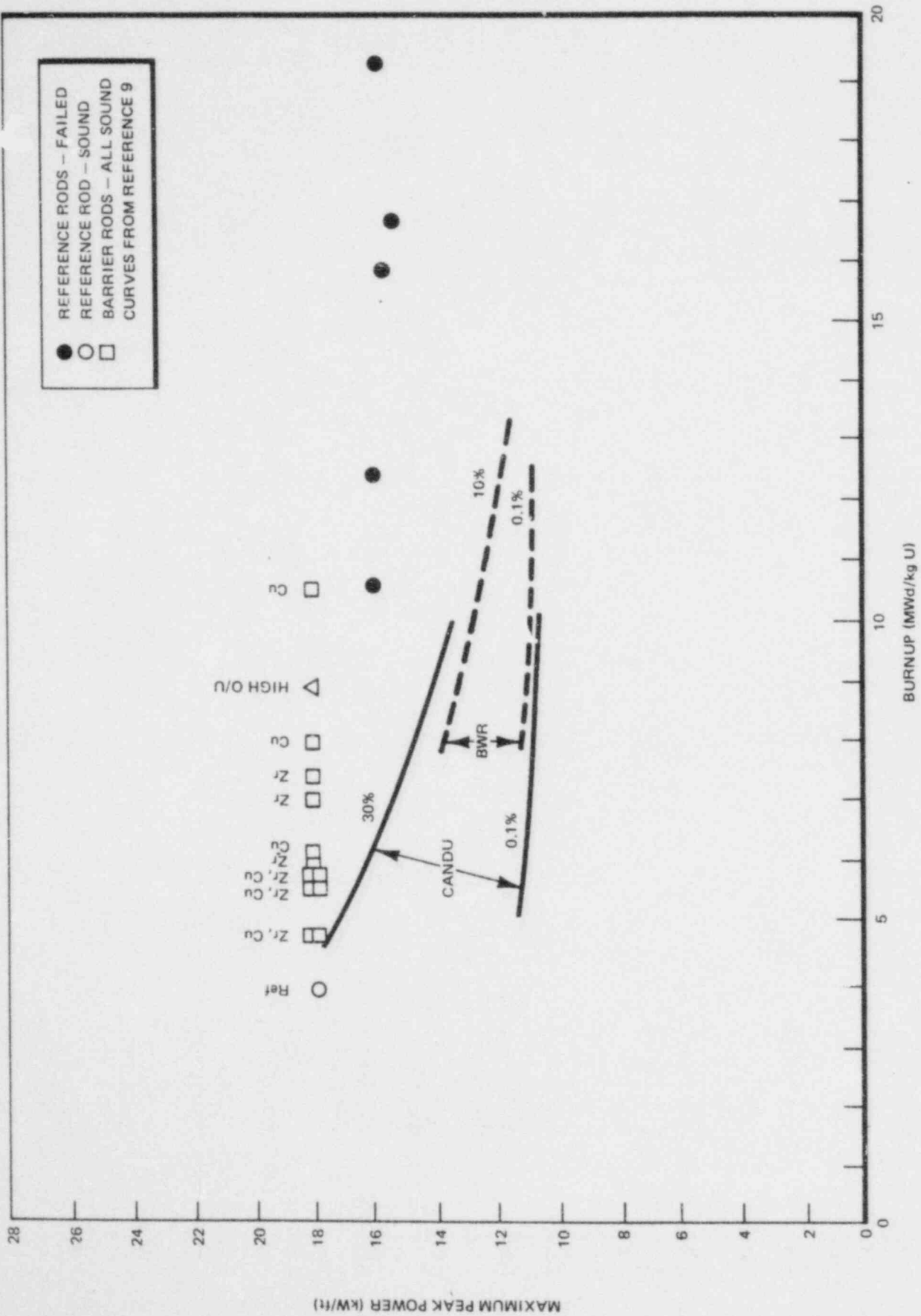


Figure 3.4-6. Ramp Sequence B Results

Table 3.4-4
1978 RAMP TESTS — NONDESTRUCTIVE PIE RESULTS SUMMARY

Fuel Rod Identification	Design Feature	Ave. Burnup (MWd/kg U)	Max. Peak Power (kW/m)	Rod Condition	Max. Cladding Strain % ^(a)	No. of Cladding Ridges	No. of PEC Through Wall Indications
SRP-2/10	Reference	16.5	39.2	Failed	None	None	2-4 ^(b)
SRP-2/11	Reference	15.4	46.2	Failed	None	None	1-2 ^(b)
SRP-2/13	Reference	15.4	51.8	Failed	0.08	None	2-4 ^(b)
SRP-2/14	Reference	14.6	46.0	Failed	None	1	2-5 ^(b)
SRP-2/19	Reference	14.6	52.2	Failed	0.08	2	1
SRP-2/20	Reference	13.8	52.0	Failed	0.08	3	1
SRP-2/1	10 μ m Cu-Barrier (non-bonded)	12.4	58.2	Sound	0.4	19	None
SRP-2/4	10 μ m Cu-Barrier (bonded)	14.4	58.5	Failed	0.3	20	1
SRP-3/33	5 μ m Cu-Barrier (non-bonded)	16.7	52.1	Failed	0.16	8	1-3 ^(b)
SRP-3/34	5 μ m Cu-Barrier (non-bonded)	16.1	59.0	Failed	0.2	7	3-5 ^(b)
SRP-3/35	Zr-Liner (crystal bar)	16.6	58.6	Sound	0.5	24	None
SRP-3/36	Zr-Liner (crystal bar)	15.3	58.6	Sound	0.5	20	None

^(a)Does not include ridging strain.

^(b)Includes possible through-wall signals.

P.E.C. TESTING:
I.D. SIGNALS ≥ 10
O.D. SIGNALS ≥ 30 } @ 20 MV/DIV

1.28"
MONTICELLO SPACER #2

12.30"

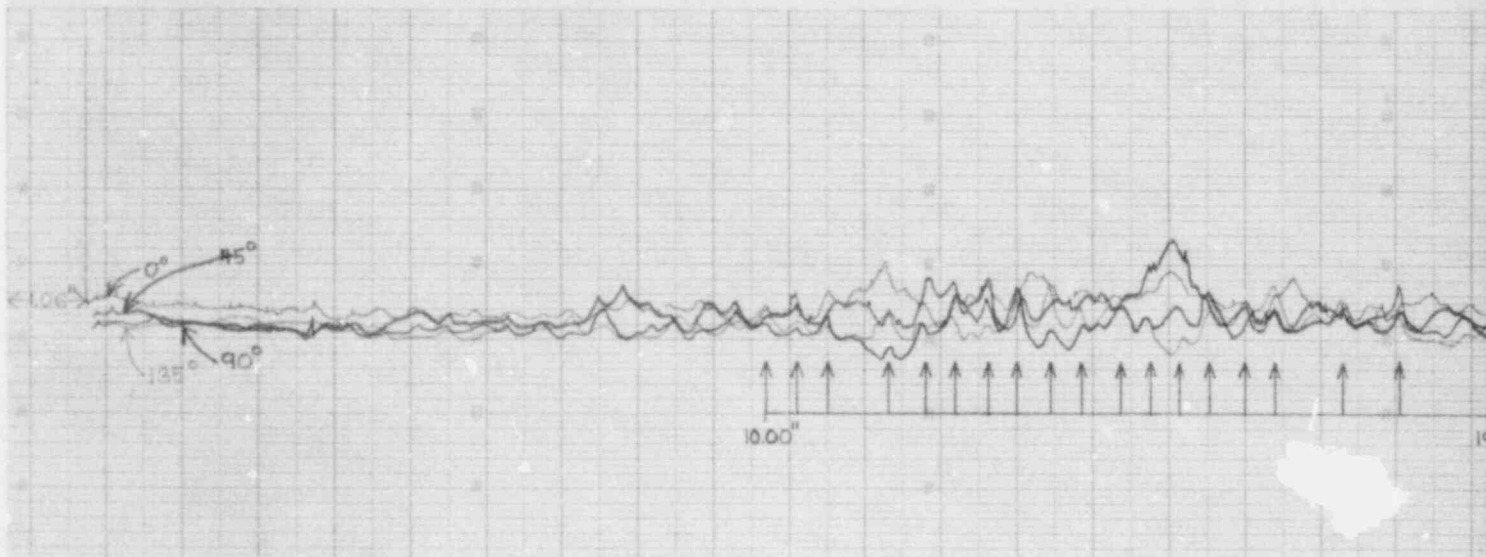
PEAK POWER
18.0 KW/FT
13.66"

~20 P.E.C. SIGNALS
TYPICAL

I.D./10-58
0°-360°
18.55"

VISUAL EXAM: NO DEFECTS OR ANOMALIES.

12.55"
12.05" 13.05" 13.75" 14.00" 18.35" 19.0"
BU BU MET B TAPERED-GRIND MET C MET E



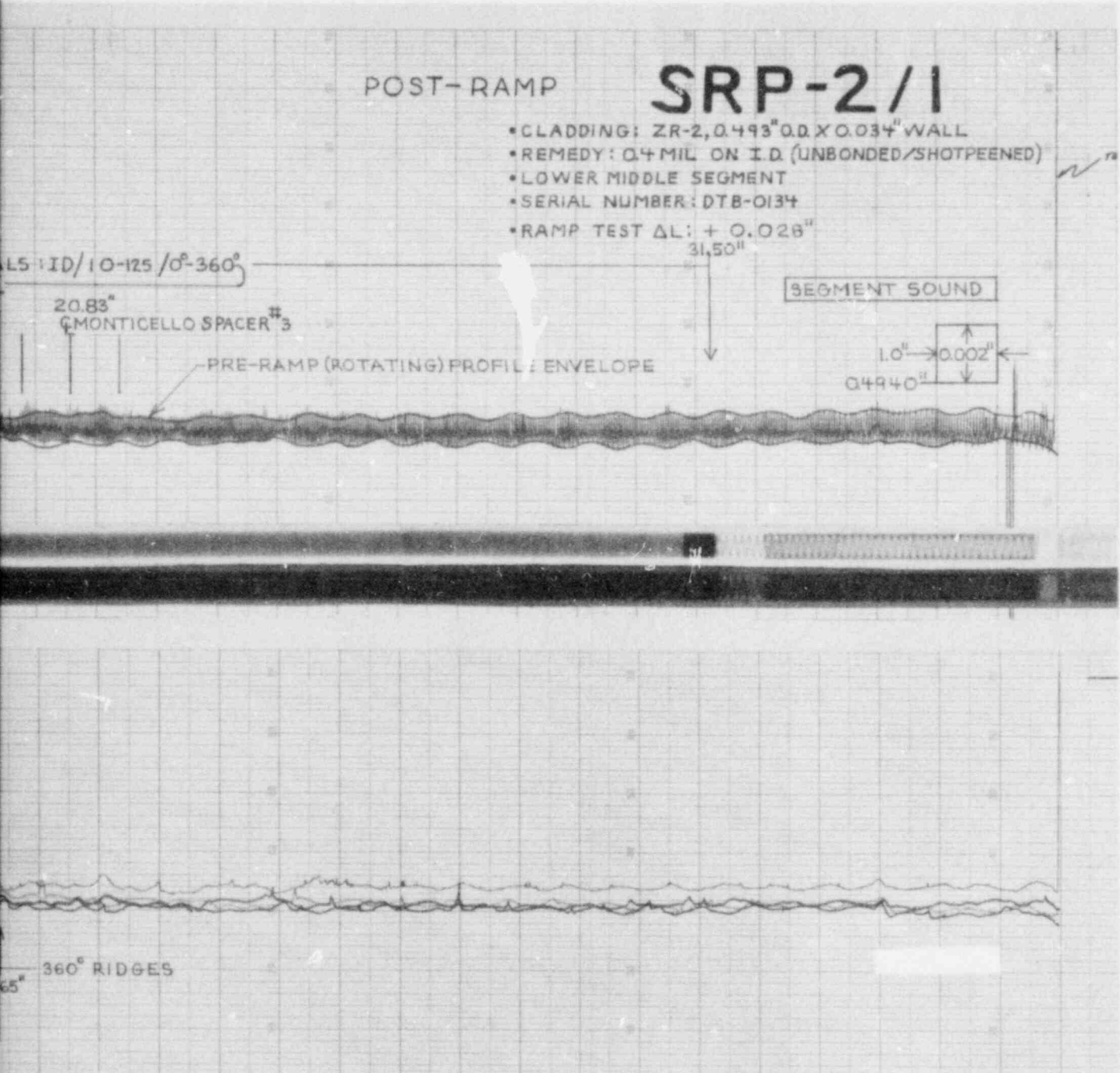
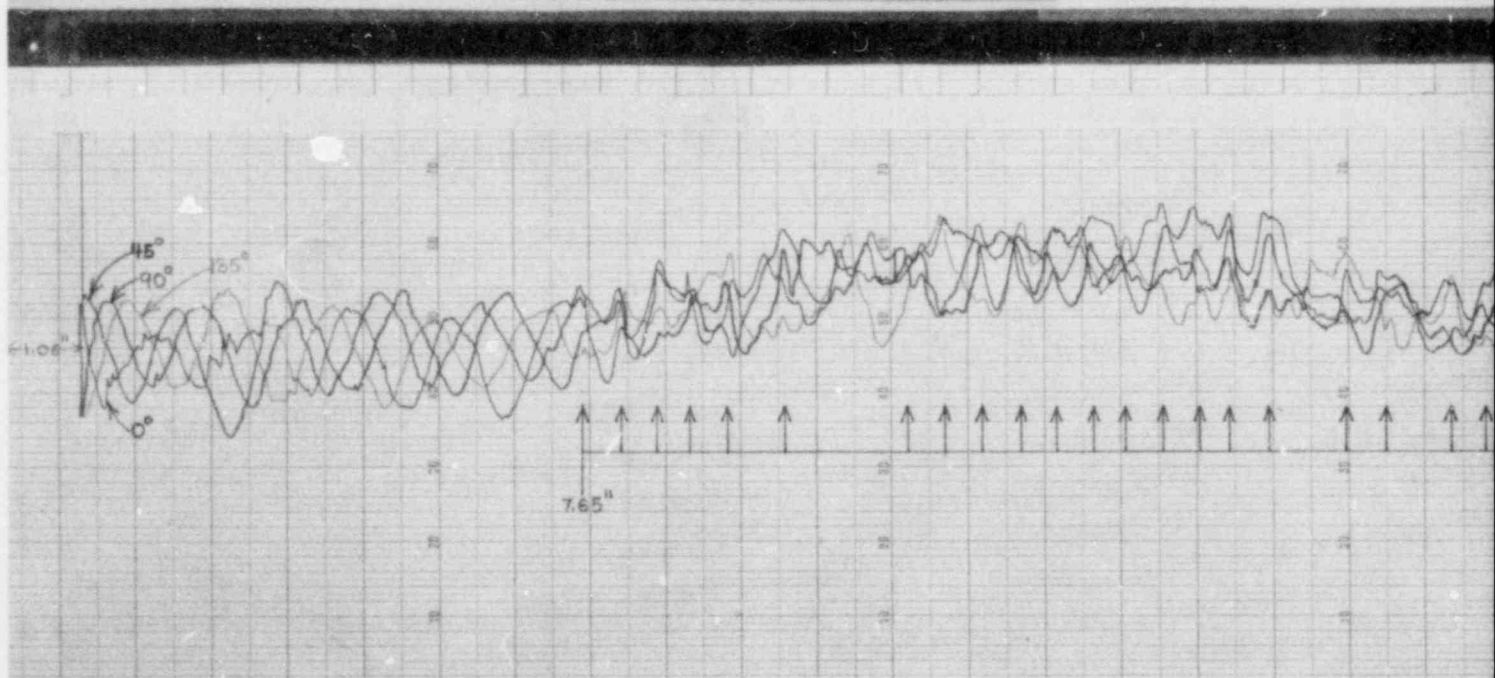
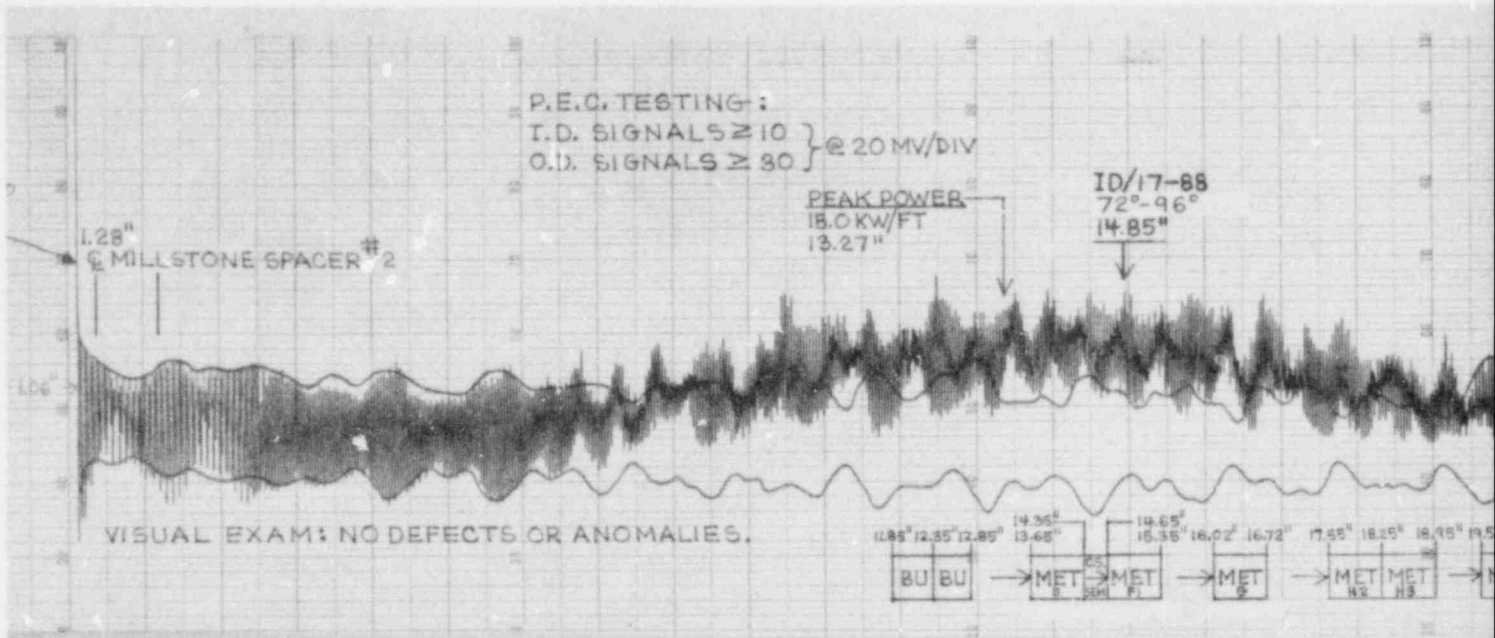


Figure 3.4.7. Nondestructive Test Results — Cu-barrier Rod SRP-2/1



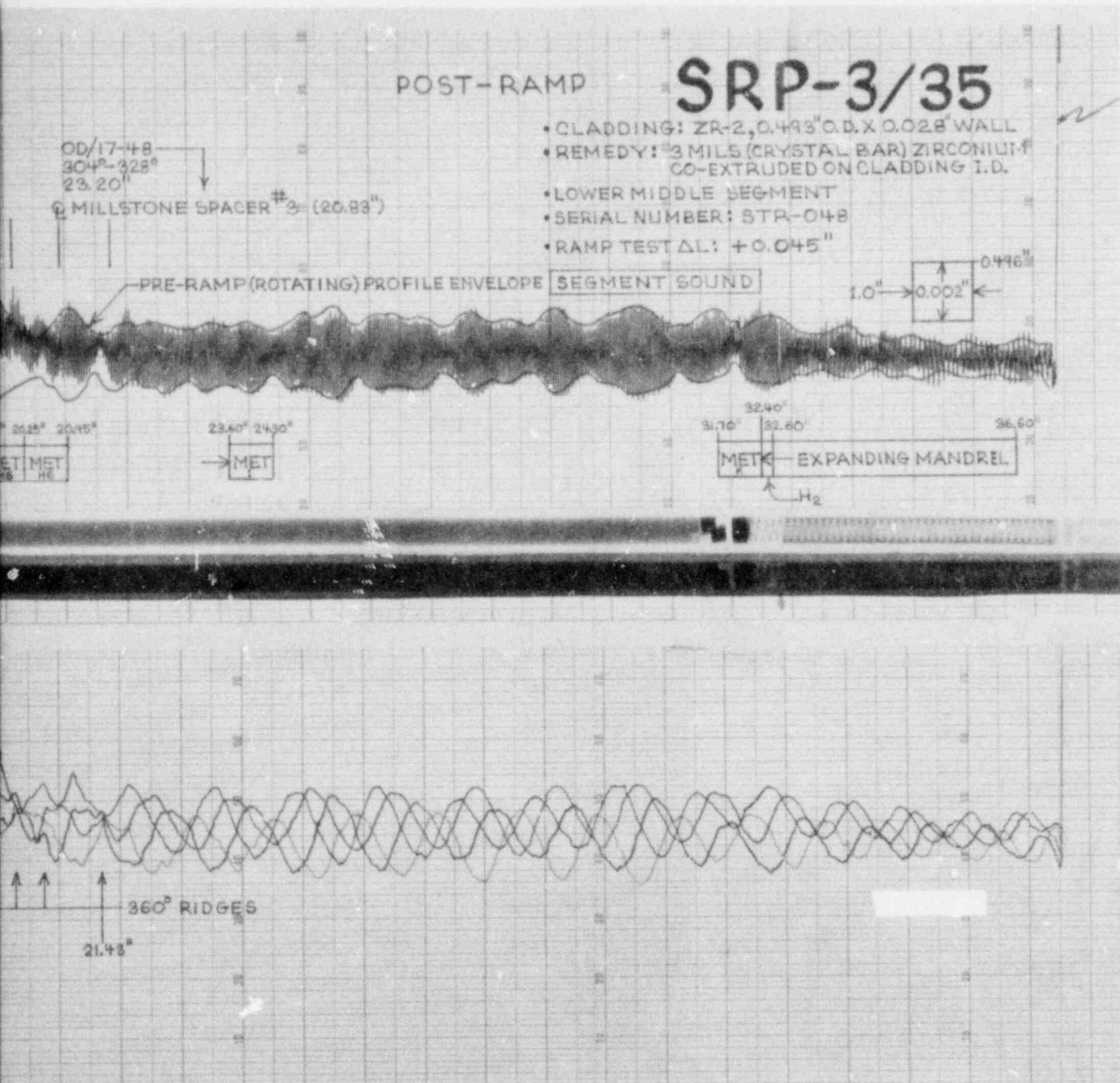
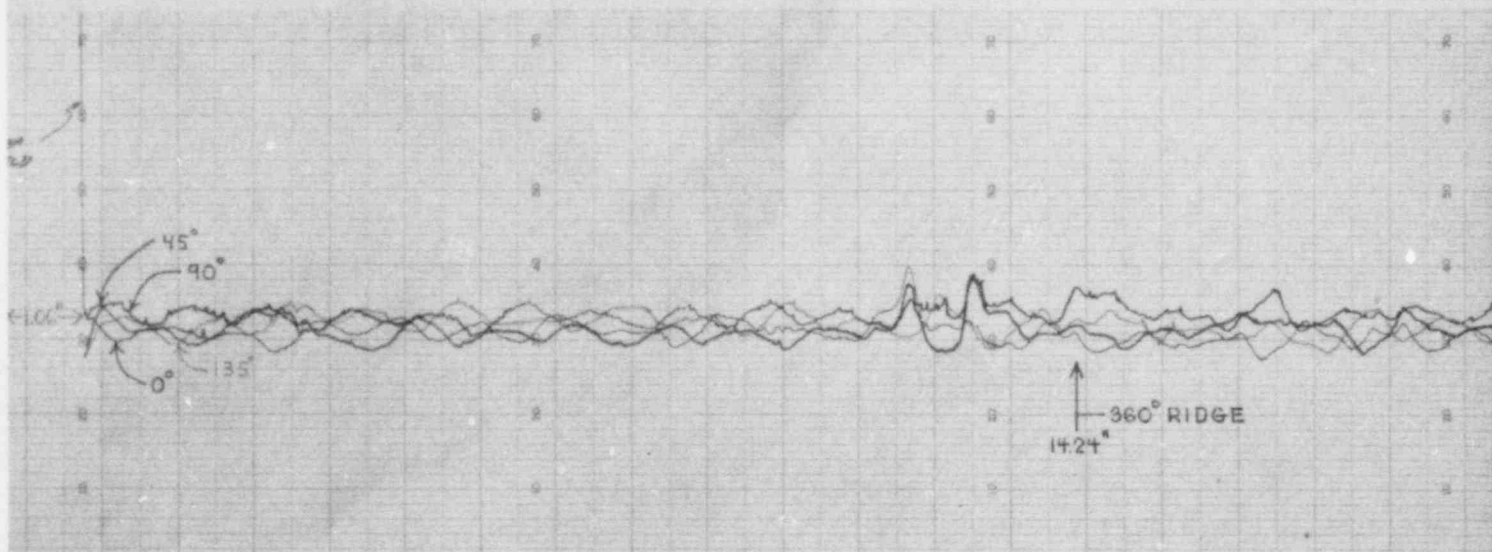
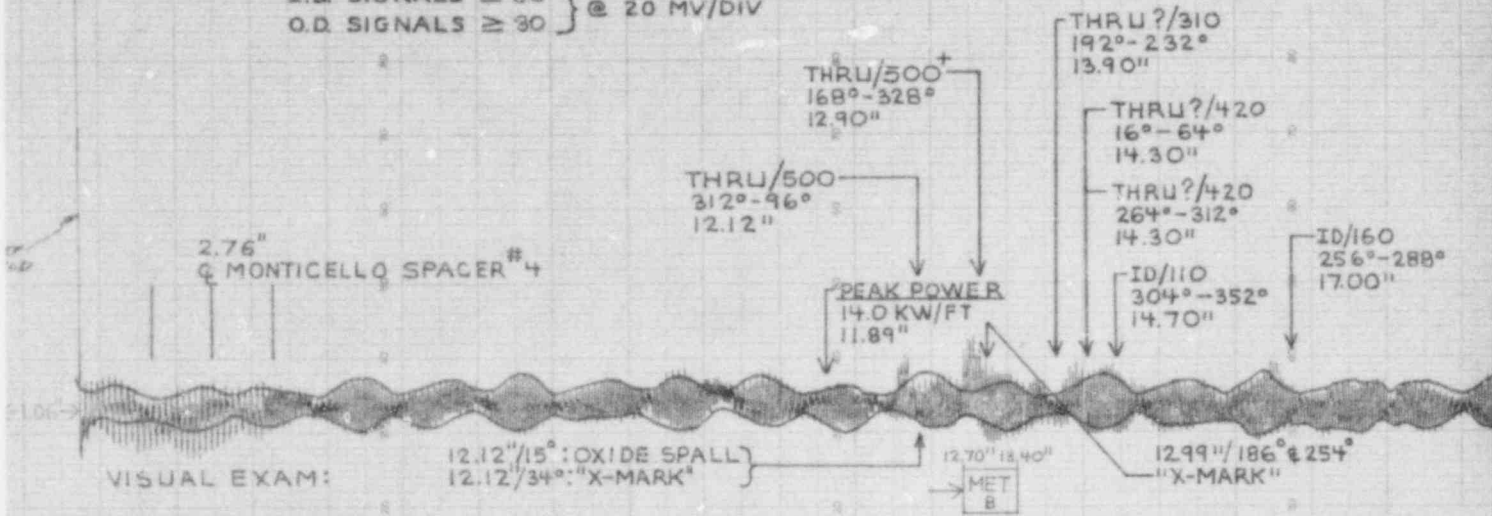


Figure 3.4-3. Nondestructive Test Results — Zr-liner Rod SRP-3/35

RE.C. TESTING:
 I.D. SIGNALS ≈ 30
 O.D. SIGNALS ≈ 30 } @ 20 MV/DIV



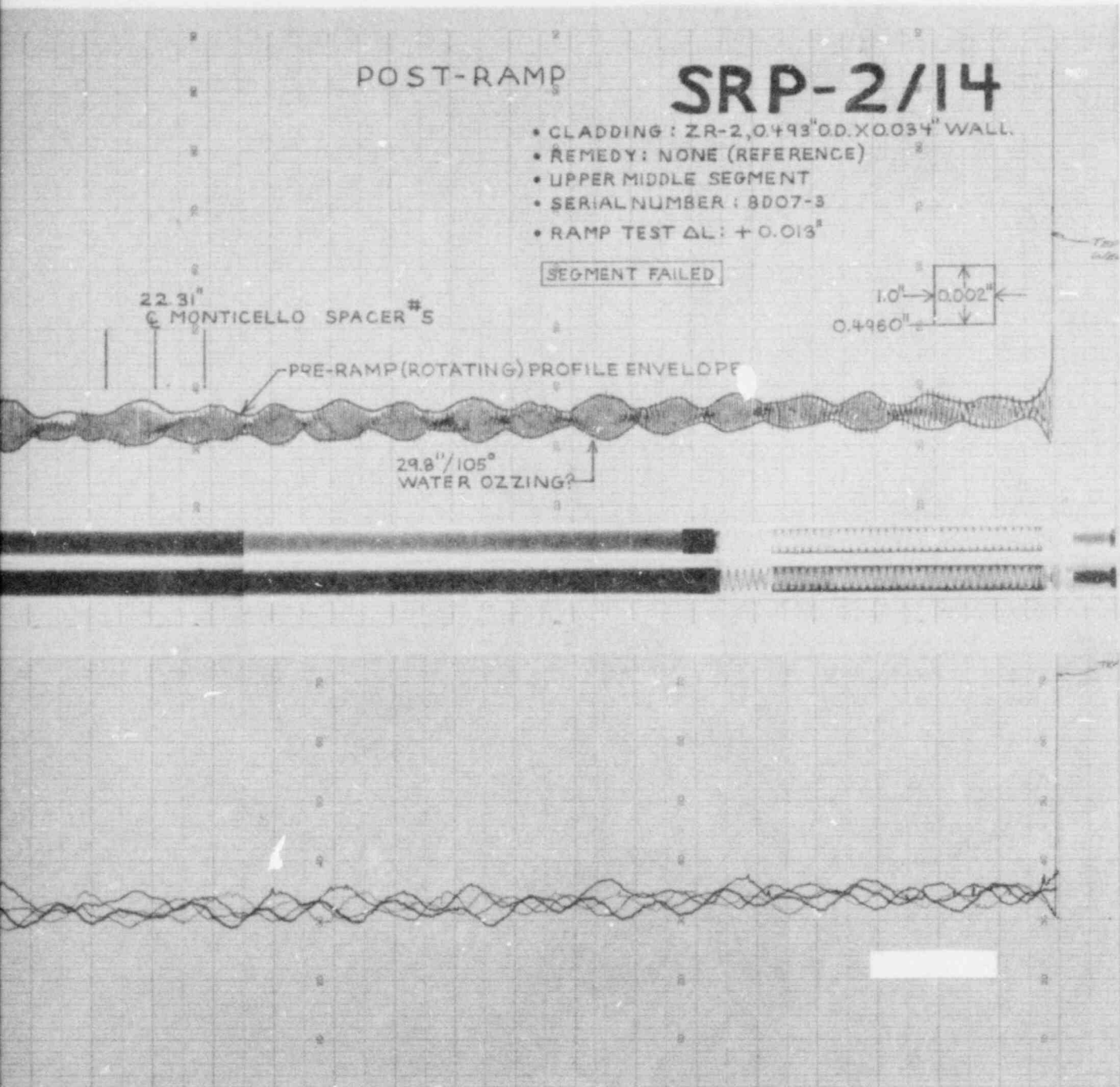


Figure 3.4-9. Nondestructive Test Data — Reference Rod SRP-2/14

Table 3.4-5
CLADDING STRAINS — Zr-LINER RODS

Test Reactor	Rod I.D.	Average Burnup (MWd/kg U)	Maximum Peak Power		Peak Circumferential Plastic Strain (%)
			(kW/ft)	(kW/m)	
GETR	SRP-3/17	7.9	18.0	59.0	0.1
GETR	SRP-3/18	10.1	18.0	59.0	0.2
GETR	SRP-3/19	8.8	18.1	59.4	0.2
R2	SRP-3/35	16.6	17.9	58.6	0.5
R2	SRP-3/36	15.3	17.9	58.6	0.5

The PEC signals in SRP-2/1 and SRP-3/35 were a consequence of ramp testing, *i.e.*, the signals were not recorded during pre-ramp characterization tests. As shown in Figures 3.4-7 and 3.4-8 respectively, metallography samples were selected at PEC signal locations to try and determine the cause of the signals. The SRP-2/1 samples have not yet been examined. The metallographic examination of the SRP-3/35 sample has been initiated, and preliminary results are described below; but no obvious cladding feature on the inner surface was located to account for the PEC signal in this rod.

3.4.1.4 Destructive Examination — Metallography

Five of the 12 rods ramp tested in R2 in 1978 were selected for destructive examination. Among the objectives were:

- Investigate the cause of the PEC signals in the sound rods, SRP-2/1 (Cu-barrier) and SRP-3/35 (Zr-liner)
- Determine the thickness of any Zr-Cu intermetallic layer in SRP-2/1 and generally characterize the Cu barrier
- Characterize the state of the Cu barrier and the Cu-Zr interface in the failed barrier rod SRP-3/33

Work was initiated on the sound Zr-liner rod, SRP-3/35, during this period and preliminary results are reported below.

A transverse section was taken in the vicinity of the PEC signal (Figure 3.4-8) and ground through several planes bracketing the signal location. The sample was polished and examined at each plane, and a small fabrication flaw (Figure 3.4-11) was noted. More important features were the many micro-cracks around the cladding inner surface. Examples are shown in Figure 3.4-12, and the distribution of the cracks around the liner inner circumference is represented in Figure 3.4-13. The depth of the microcracks was about 10 to 12 μm , and there were more than 200 in some planes, apparently depending on the local cladding circumferential strain. Additional metallographic sections were selected from SRP-3/35 (see Figure 3.4-8) and the number of microcracks were related to local cladding strain and maximum nodal power. These data are tabulated in Table 3.4-6. Further evaluation to determine the nature of the microcracks is in progress.

From the depth of these cracks and from their uniform depth of penetration, it appears that the zirconium next to the fuel (within 12 μm of the inner surface) has changed its properties to allow nucleation of microcracks. However, beyond that depth the properties of the zirconium remain such that PCI cracks cannot propagate, even when the strain is high. The observed crack depth corresponds approximately to both the range of fission fragments and, based on Kleykamp's work,¹⁰ to the expected diffusion depth for a significant concentration of oxygen from the fuel.

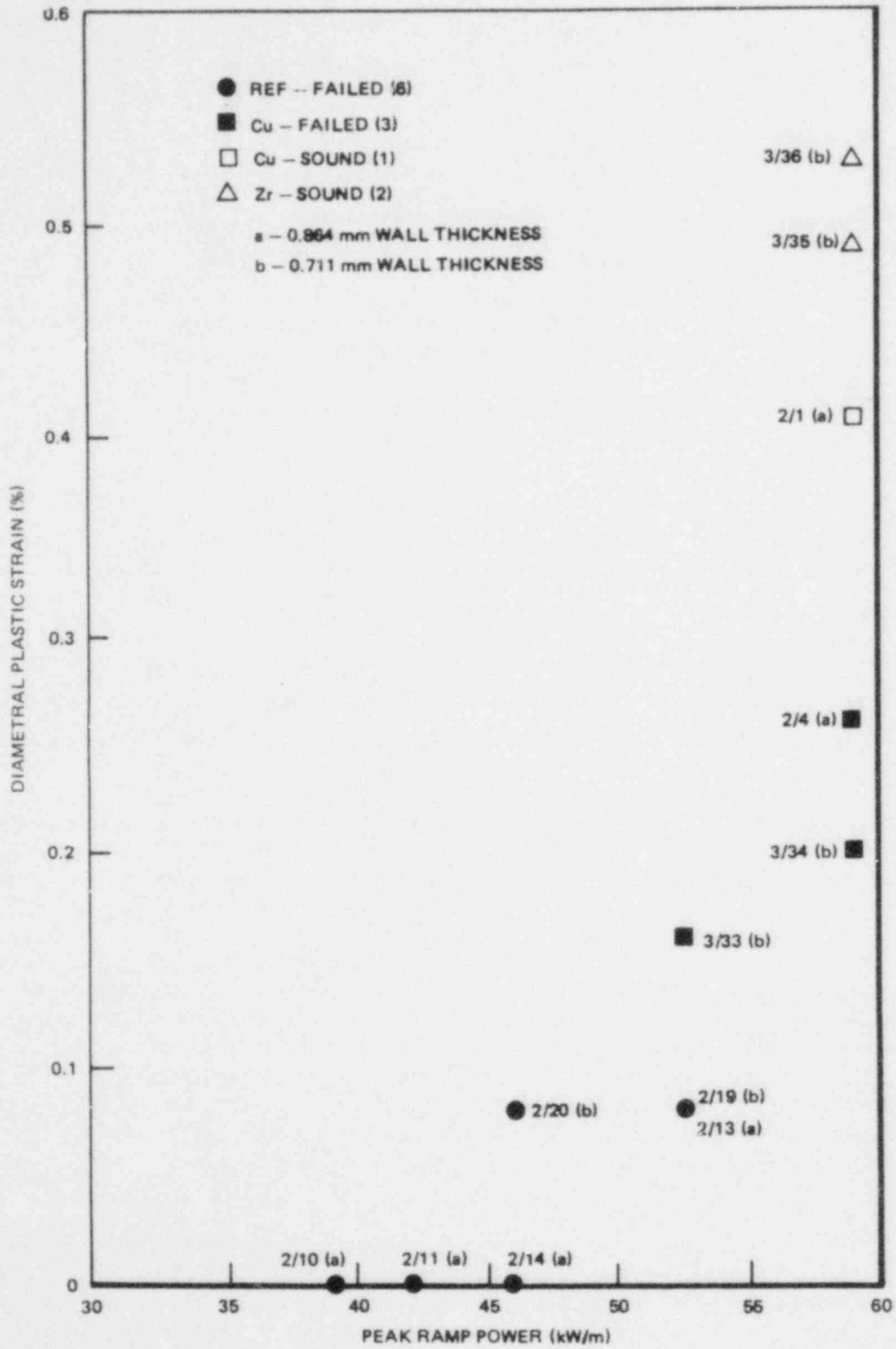


Figure 3.4-10. SRP Segment Cladding Strain Due to Power Ramp Testing

Table 3.4-6
CORRELATION BETWEEN MICROCRACKS AND CLADDING DUTY
IN SRP-3/35

(cm)	Axial Location ^a	Local Cladding Plastic Strain (%)	Local Peak Power		Number of Microcracks in Cross Section
	(in.)		(kW/m)	(kW/ft)	
35.18	13.85	0.5	58.4	17.8	110-148 ^b
37.72	14.85	0.5	57.4	17.5	115-293 ^b
41.20	16.22	0.5	55.4	16.9	110
44.5	17.5	0.4	51.5	15.7	170
46.2	18.2	0.3	49.5	15.1	83
49.5	19.5	0.2	45.3	13.8	41
51.3	20.2	0.1	42.7	13.0	9
60.5	23.8	0	29.9	9.1	0
82.0	32.3 (plenum)	0	0	0	0

^aDistance from tip of bottom end plug

^bSeveral planes examined

The thickness of oxide patches on the liner inner surface were about $2.5 \mu\text{m}$. The oxide thickness on the outer surface was in the range $11\text{-}17 \mu\text{m}$ with some circumferential variation. This may be compared with the mean oxide thickness of $9.4 \mu\text{m}$ reported³ for SRP-3/17, -3/18 and -3/19 with one less cycle of exposure. A substantial fraction of the corrosion hydrogen has been picked up by the cladding; in the plenum section, but not in fueled sections, this hydrogen is concentrated in the Zr-liner.

3.4.2 Fuel with Cladding Perforation (J. H. Davies)

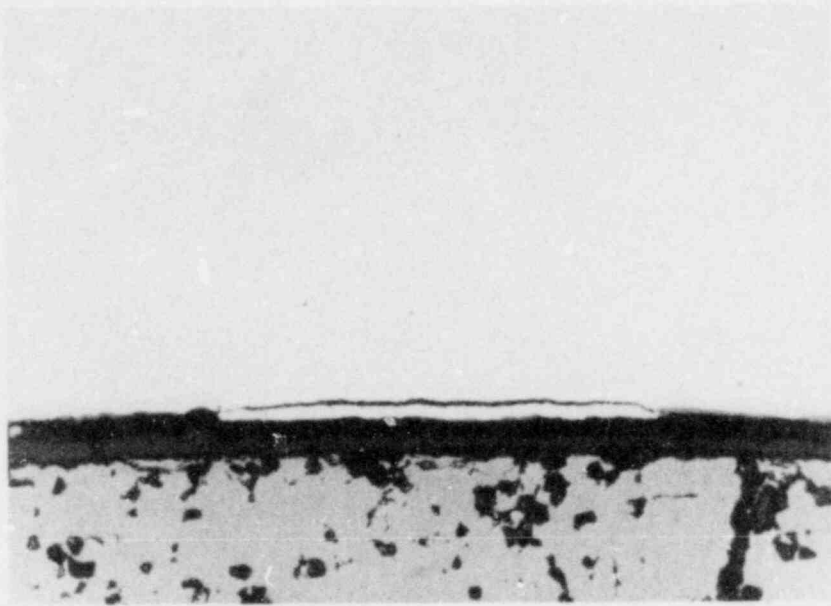
3.4.2.1 Introduction

There is a need to evaluate the post-defect performance of barrier fuel relative to that of conventional fuel. An experiment has been designed to compare the irradiation performance of Zr-liner fuel rods, each having a hole drilled to perforate the cladding, to a similarly defected reference rod. As described previously¹, defected standard fuel rods can be operated successfully for long periods without severe degradation or secondary damage, provided heat fluxes do not exceed some critical value. An empirical relationship between this critical heat flux and the time to failure (severe secondary damage) has been established by Locke¹¹ and this relationship has been used to design the experiment. Defected BWR 8×8 fuel rods operating around 10 kW/ft (32.8 kW/m) should operate successfully (*i.e.*, no major secondary damage) for up to a year. In the current test three Zr-liner rods and one reference, all artificially defected, have been required to operate for 1900 hours at a steady state power of $35 \pm 5 \text{ kW/m}$ (10.7 kW/ft). The relative performance of the Zr-liner and reference fuel rods is to be determined by post-irradiation examination.

3.4.2.2 Test Rod Design

The design of the test fuel rods is depicted in Figure 3.4-14 and additional design details are provided in Table 3.4-7. The length of the enriched fuel column is about 42 cm. The artificial defects are single small drilled holes at the location shown in Figure 3.4-14, which were mechanically drilled through the cladding prior to fuel loading. Hole diameters are given in Table 3.4-7. The defected rods were filled and welded in dry helium, but no precautions were taken to preserve the helium atmosphere during handling and shipping.

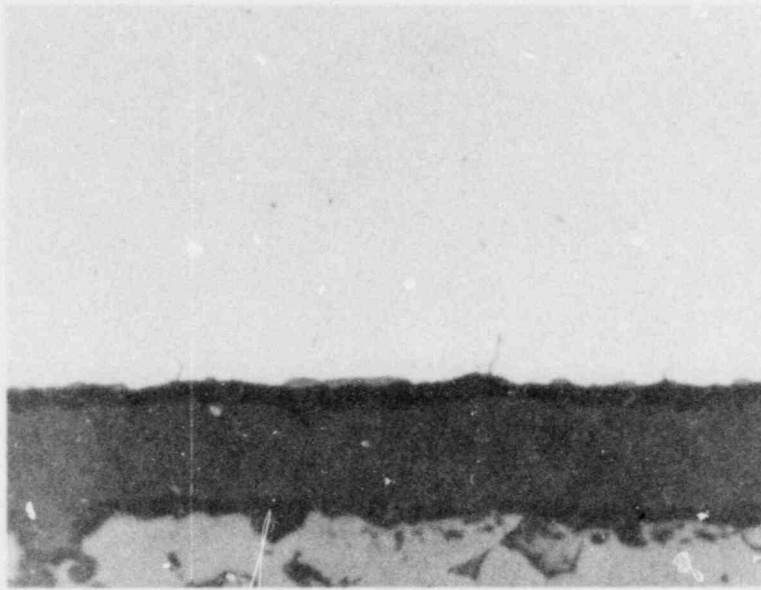
POOR ORIGINAL



MAG 250 X

Figure 3.4-11. Fabrication Flow in the High Power Region of Zr-liner Fuel Rod SRP-3/35

POOR ORIGINAL

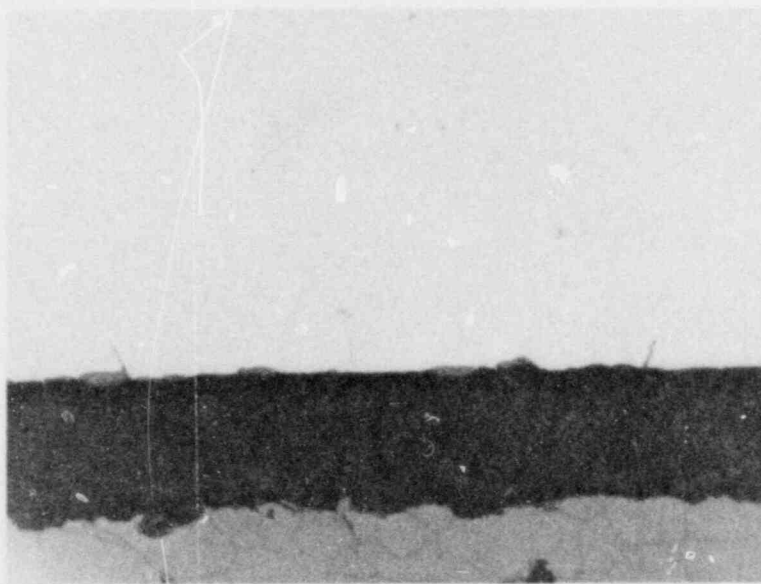


(a)

ZIRCALOY

ZIRCONIUM

C578-20
MAG 500X



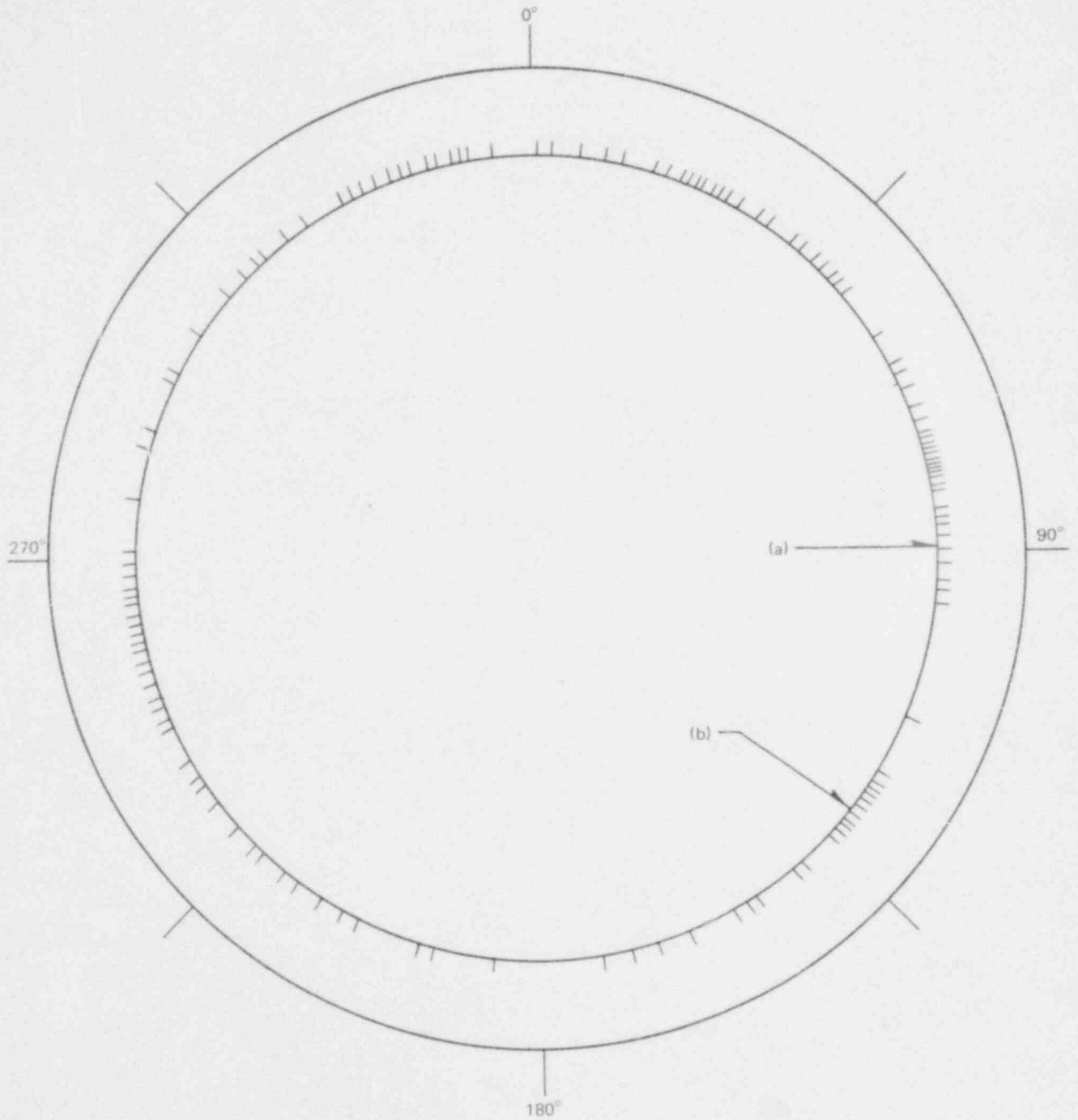
(b)

ZIRCALOY

ZIRCONIUM

C578-21
MAG 500X

Figure 3.4-12. Microcracks in the High Power and High Strain Region of Zr-liner Fuel Rod SRP-3/35



~ 148 MICROCRACKS

Figure 3.4-13. Locations of Microcracks on Inner Surface of Zr-liner Fuel Rod SRP-3/35. Crack Locations are Marked, but Are Not Drawn to Scale. Locations Marked (a) and (b) are the Areas Which Appeared in Figure 3.4-12(a) and (b) Respectively.

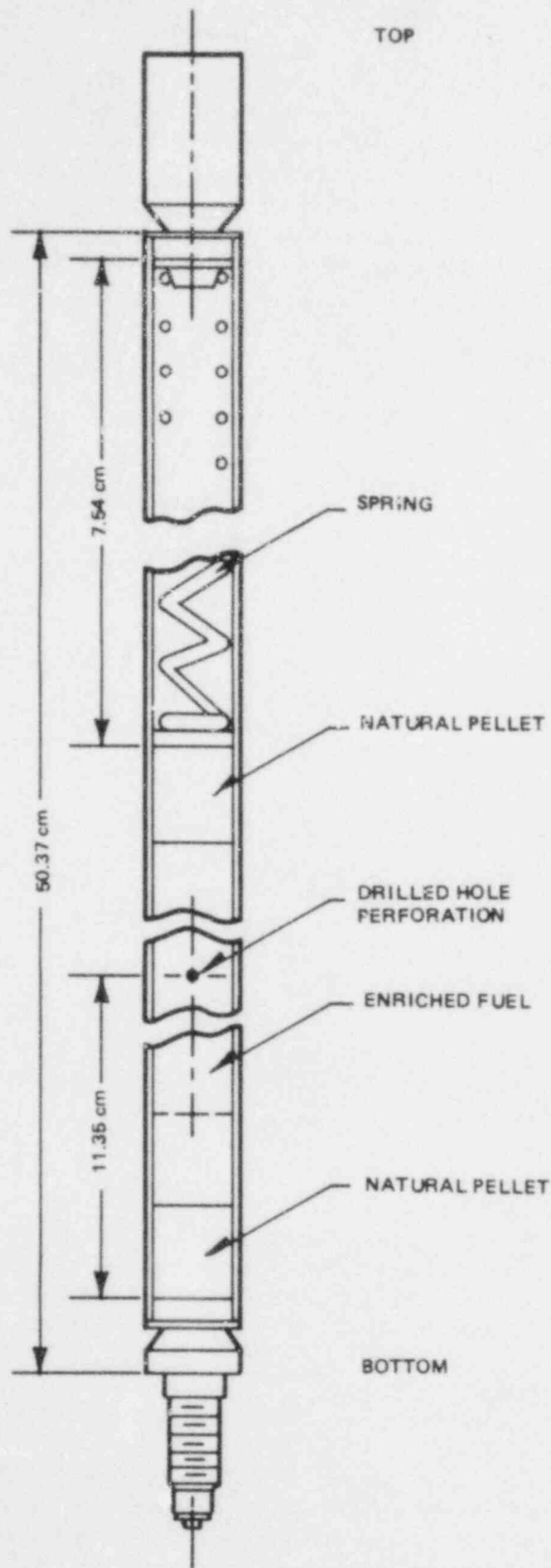


Figure 3.4-14. Perforated Fuel Test Rod

3.4.2.3 Irradiation

The rods are being irradiated in a test rig in Loop No. 2 of the Studsvik R2 reactor. Loop No. 2 is a pressurized light water loop used mainly for testing BWR fuel rods under operating conditions. The features of the reactor and the primary test loops have been described previously.² The power levels of the fuel experiments in R2 are controlled in three ways: composition of the reactor core loading, choice of reactor power level, control rod shimming. Power levels in the loop experiments are monitored calorimetrically using thermocouple and flow rate measurements. A special startup procedure (Table 3.4-8) has been established for the perforated fuel rod test to ensure that there is no buildup of destructive steam pressures inside the rods during startup. This procedure, which has been demonstrated to be effective, applies to all startups during the course of the experiment. The test is scheduled to run for six reactor cycles.

Table 3.4-7
PERFORATED ROD DESIGN DETAILS

Design Feature	Hole Size (mm)	Cladding Wall (mm)	Diametral Gap (mm)	Fuel Pellet Diam (mm)	Fuel Enrich. (w/o)
Reference	0.15	0.86	0.23	10.57	2.85
Crystal Bar Zr-Liner	0.15	0.86	0.23	10.57	2.85
Crystal Bar Zr-Liner	0.25	0.86	0.23	10.57	2.85
Sponge Zr-Liner	0.15	0.86	0.23	10.57	2.85

Table 3.4-8
SPECIAL REACTOR STARTUP PROCEDURE

R2 Power Range (MW)	Minimum Time to Complete Power Increase (minutes)
0.1- 1.0	10
1.0- 5.0	30
5.0-10.0	10
10.0-20.0	5
20.0-50.0	No restriction

Although all four fuel rods are operating within the specified peak power range of 35 ± 5 kW/m, there is a flux gradient across the test rig, and two rods are always at slightly higher powers than the other two. The reference and the crystal bar Zr-liner rod with the smaller hole were selected for the higher power locations. Typically, the other rods run at $\sim 13\%$ lower power. The peak-to-average power ratio along the fuel rods is ~ 1.16 and the power level at the axial location of the drilled holes is $\sim 90\%$ percent of peak. The test rig is in the B3 leg of Loop 2, where the direction of coolant flow is upwards. The coolant pressure is set at ~ 8.2 MPa and the calculated cladding surface temperature at the peak power location is 293 to 299 °C.

Although the relative performance of the Zr-liner and reference rods is to be determined by post-irradiation examination, a measure of the state of the fuel is provided by the level of fission product activity in the loop coolant. However, it has not been possible to use the normal loop activity monitoring system, because the activity level is too high and the Cerenkov detector becomes saturated. Therefore, test progress is being monitored by the radiation levels registered on area gamma monitors (plastic scintillation detectors) located in the loop machinery room, and by occasional removal and analysis of loop coolant aliquot samples.

During normal operations, when there are no fission products in the loop coolant, one gamma monitor ordinarily records radiation levels of 2 to 3 mR/hour. For radiological safety considerations, an arbitrary limit of 30 mR/hour has been set for the current experiment. If the time averaged reading over several days exceeds this limit, the test may be interrupted or prematurely terminated. Output from the area gamma monitors and from the appropriately decalibrated Cerenkov detector (raised discriminator setting) are continuously recorded on chart paper during the course of the test, as well as in the reactor process computer. Reactor power and coolant pressure levels are also recorded. Snapshots from the chart recording during the first cycle are shown in Figures 3.4-15 and 3.4-16.

The output of the controlling radiation monitor is on a pseudo-logarithmic scale so that small differences in signal height on the chart paper in Figures 3.4-15 and 3.4-16 represent substantial changes in activity level. The periodicity in the activity levels evident in Figures 3.4-15 and 3.4-16, and its correspondence with small periodic decreases in coolant pressure is therefore considered significant. The rapid regular decreases of the loop pressure from about 8.2 to 8.1 MPa correspond to those times in the duty cycle when the heater, associated with the loop pressurizer, was switched off. This effect of pressure on loop activity has been reported previously by Forsyth et al⁷. It appears to be more complex than simple aspiration, but it may be a primary mechanism for release of fission products from defected fuel. Figure 3.4-16 was recorded during reactor shutdown and the relatively large pulses of activity may be associated with the phenomenon of iodine "spiking," which is well known.

At least two loop coolant samples are collected and analysed for each reactor cycle. (One sample is taken during shutdown to establish background level and the second is taken at a convenient time close to the end of a reactor cycle to maximize equilibration of 5.3 day ¹³³Xe.) Sample size is about 20 ml (total coolant mass is ~200 kg), and the samples are transferred to the Hot Cell area for analysis by gamma spectrometry using a calibrated Ge (Li) detector. The main fission product species contributing to the sample spectra are ¹³³Xe, ^{133m}Xe, ¹³⁵Xe, ^{85m}Kr, ⁸⁸Kr and ⁸⁷Kr. Iodine and other fission product activity levels are maintained below detection limits by continuous operation of the loop ion-exchange purification circuit during both the irradiation and shutdown periods.

3.4.2.4 Results and Discussion

The test started on November 22, 1979 and two irradiation Cycles were satisfactorily completed by year-end. In Figure 3.4-17 the output of the controlling area gamma monitor and the rod peak power (averaged for the four rods) are plotted as a function of time. While rod power remained very constant throughout this period, loop coolant activity rose steadily throughout the first cycle to twice initial levels. A step increase in activity was noted following the second cycle startup and is attributed to the well-known "spiking" phenomenon. However, the activity level appeared to decrease during the remainder of the cycle and at the end it was comparable to that at the end of the first cycle. This is confirmed by the results of the water sample analyses, which are shown in Table 3.4-9. There is little difference between the two sets of analyses taken near the end of the first and second Cycles.

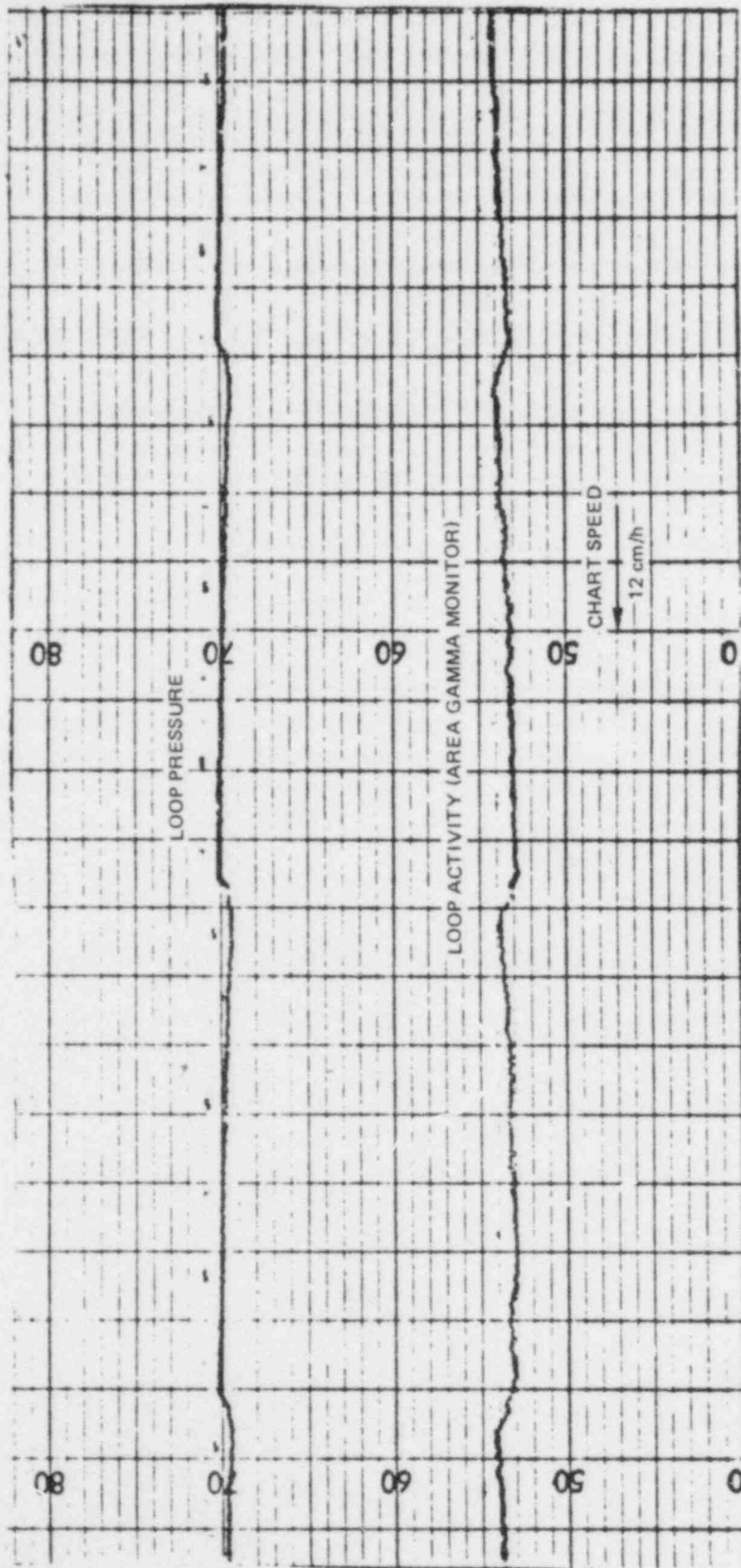


Figure 3.4-15. Correlation Between Loop Activity and Loop Pressure During Steady State Operation

POOR ORIGINAL

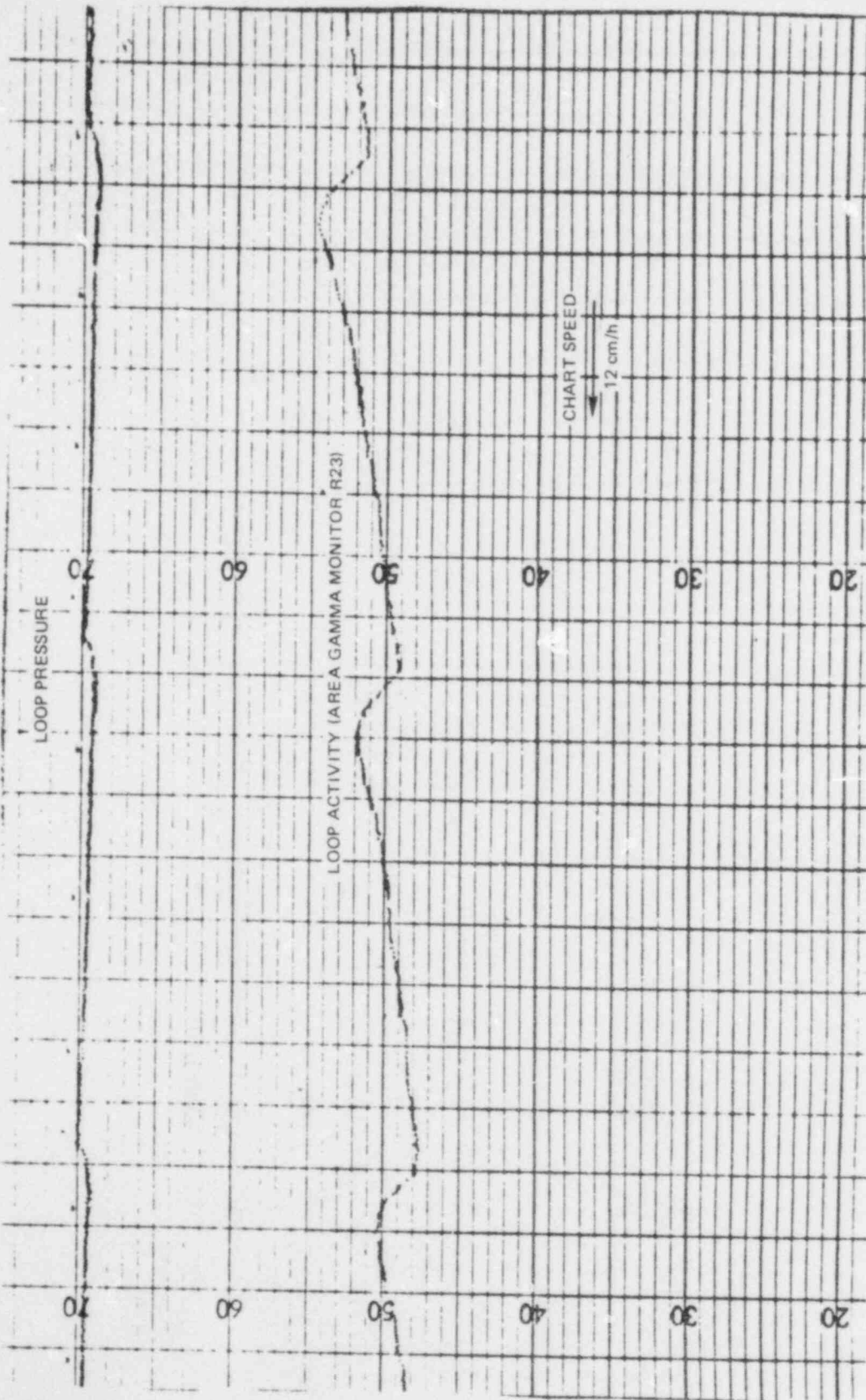


Figure 3.4-16. Correlation Between Loop Activity and Loop Pressure Shortly After Reactor Shutdown

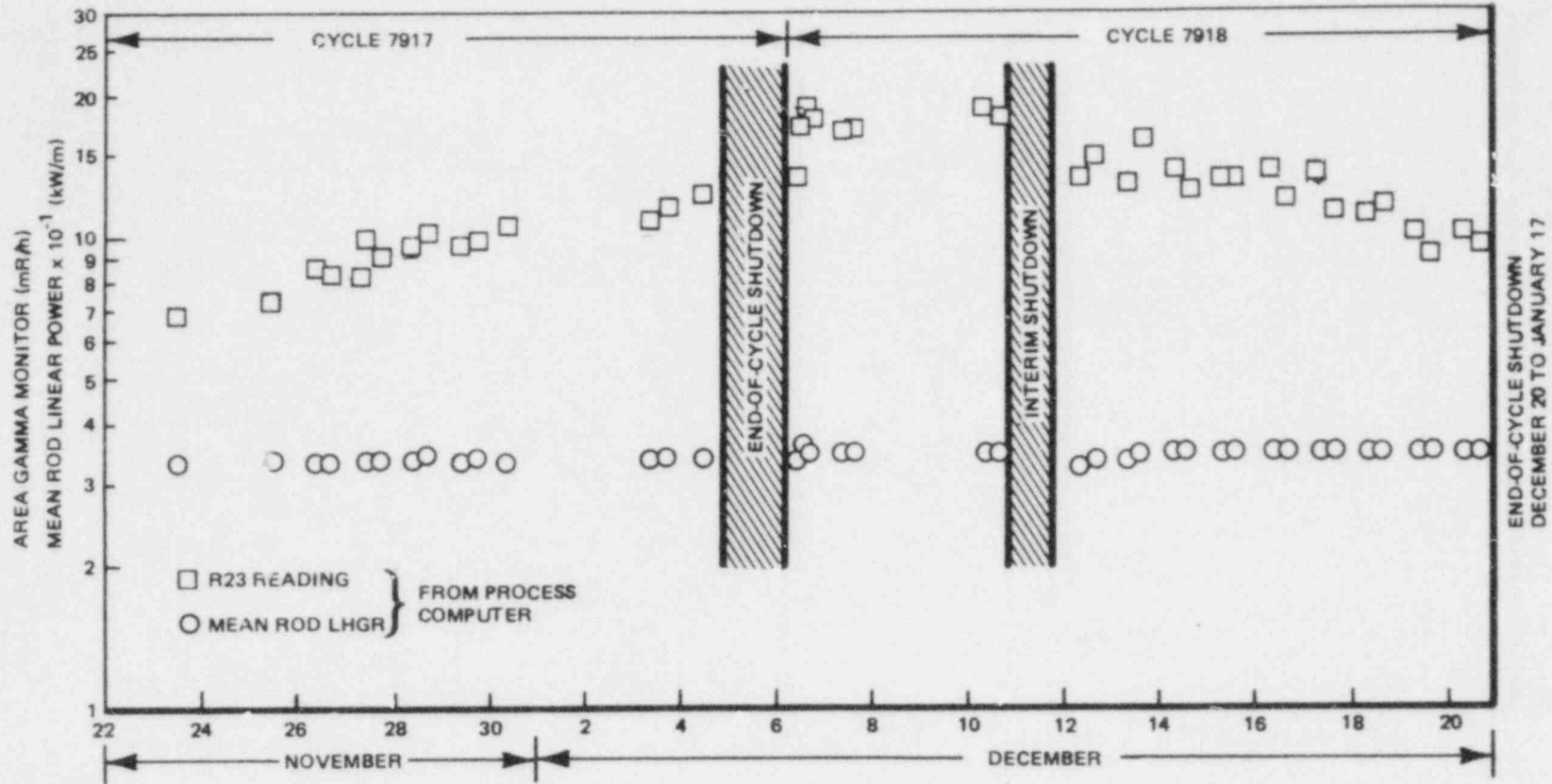


Figure 3.4-17. Trend of Loop 2 Coolant Activity Through First Two Cycles

Table 3.4-9
WATER SAMPLE ACTIVITY ANALYSIS — DATA SUMMARY

Nuclide	Half-Life	Sample Date Time	Activity ^(a) (Ci/ml)		
			December 3, 1979 07.04	December 5, 1979 ^(b) 10.06	December 19, 1979 07.00
¹³³ Xe	5.29 d		1.44×10^{-4}	2.25×10^{-6}	1.55×10^{-4}
^{133m} Xe	2.26 d		2.87×10^{-6}	—	2.86×10^{-6}
¹³⁵ Xe	9.2 h ^(c)		9.09×10^{-5}	—	8.42×10^{-5}
^{85m} Kr	4.48 h		1.46×10^{-5}	—	1.26×10^{-5}
⁸⁷ Kr	1.27 h		1.11×10^{-5}	—	0.96×10^{-5}
⁸⁸ Kr	2.80 h		1.28×10^{-5}	—	1.29×10^{-5}

NOTES:

- a) All activities corrected for decay back to sample time.
 b) Background sample taken during shutdown. (Note that the fission products are being stripped from the coolant. The time constant for this process must be established before quantitative release rates can be determined.)
 c) Effective half-life during irradiation much shorter (~ 1.8 h) due to neutron capture.

ACKNOWLEDGEMENTS

The authors of Subsection 3.4 gratefully acknowledge the help of:

K. Saltvedt and his staff at the R2 Test Reactor, Energiteknik AB, Studvik, for help with both the power ramp tests and the irradiation of fuel with a cladding perforation.

R. Forsyth and his staff at the Studsvik Hot Cells for their assistance with the defected fuel tests.

C. M. Berry of NFS&D directed the fabrication of fuel rods with cladding perforation.

C. C. Guitton of NFSE&D assisted with design of the perforated cladding test fuel rods.

R. E. Smith of the Irradiation processing Operation for hot cell metallography.

G. L. Holloway of NFSED for nuclear physics support.

4. TASK III. DEMONSTRATION

4.1 OBJECTIVES

1. Design and manufacture of PCI-resistant fuel for demonstration of PCI resistance under steady state and under power ramp conditions.
2. Irradiate, test, and evaluate the performance of the demonstration fuel in a commercial BWR power station.

4.2 SUBTASK III.1. DESIGN AND LICENSING OF DEMONSTRATION FUEL

(J. A. Baumgartner and C. C. Guitton, NFD)

As was mentioned in Section 2 of this report, the demonstration is planned for Quad Cities Unit 2 starting in Cycle 6. This will require delivery of the 132 bundles of barrier fuel in August of 1981. Specific design, manufacturing and licensing schedules are now being planned consistent with that delivery date.

4.3 SUBTASK III.2 FABRICATION OF DEMONSTRATION FUEL

4.3.1 Zr-liner (D. E. Allen, R. E. Donaghy, and R. J. Mack, WMD)

In PHASE 1 Zircaloy-2 tubeshells coextruded with zirconium liners were obtained from Teledyne Wah Chang Albany. Liners of two purity levels were used: crystal bar zirconium (oxygen content ≤ 200 ppr) and low-oxygen sponge zirconium (oxygen ≤ 600 ppm). In this current report period four tubeshells coextruded with liners of low oxygen sponge zirconium were received from Ugine Aciers, and these have been evaluated. Figure 4.3-1 is a photomicrograph from one of these low oxygen sponge zirconium-lined tubeshells after an anneal at $628 \pm 21^\circ\text{C}$ for $\sim 1\frac{1}{4}$ h. A portion of each tubeshell has been processed by GE to produce tubing, and evaluation of the tubing is now in progress.

4.3.2 Cu-barrier (W. T. Grubb, CRD; R. E. Donaghy, WMD, and R. J. Mack, WMD)

A microstructural comparison was made between: (a) electroless copper plated onto autoclave-oxidized Zircaloy and (b) electroless copper plated onto oxygen-oxidized Zircaloy. The former was prepared at the facilities of the GE Wilmington Manufacturing Department (WMD) in Wilmington, North Carolina, and the latter at the GE Corporate Research and Development Center (CRD) in Schenectady, New York. The evaluations were done at CRD. The salient difference between the two materials is the oxidation procedure. The material designated WMD was oxidized in steam at 400°C at a pressure slightly over one atmosphere (~ 0.17 MPa) for approximately 14 h, while that designated CRD was oxidized in gaseous oxygen at a pressure of 0.1 MPa (1 atm) at 400°C for 24 h. In both situations the oxidation step was done following the etch treatment in an ammonium bifluoride solution⁴. While the plating procedures were similar, the CRD specimen had a thicker copper plating ($13 \pm 0.7 \mu\text{m}$) than did the WMD specimen ($10.6 \pm 0.5 \mu\text{m}$); at CRD the plating time was extended for this specimen.

Metallographic examinations were done using a tapered section to enhance the apparent thickness of the oxide and the copper plating by approximately $10\times$. Results are shown in Figures 4.3-2 and 4.3-3.

The structures of the copper plating were compared by scanning electron microscopy directly on their surfaces (Figure 4.3-4) and in cross-section after etching in a mixture of nitric, acetic and phosphoric acids (Figure 4.3-5).

Finally, the copper was chemically removed from the tubing (using dilute aqueous nitric acid) and the underlying surfaces were compared by scanning electron microscopy as seen in Figure 4.3-6.

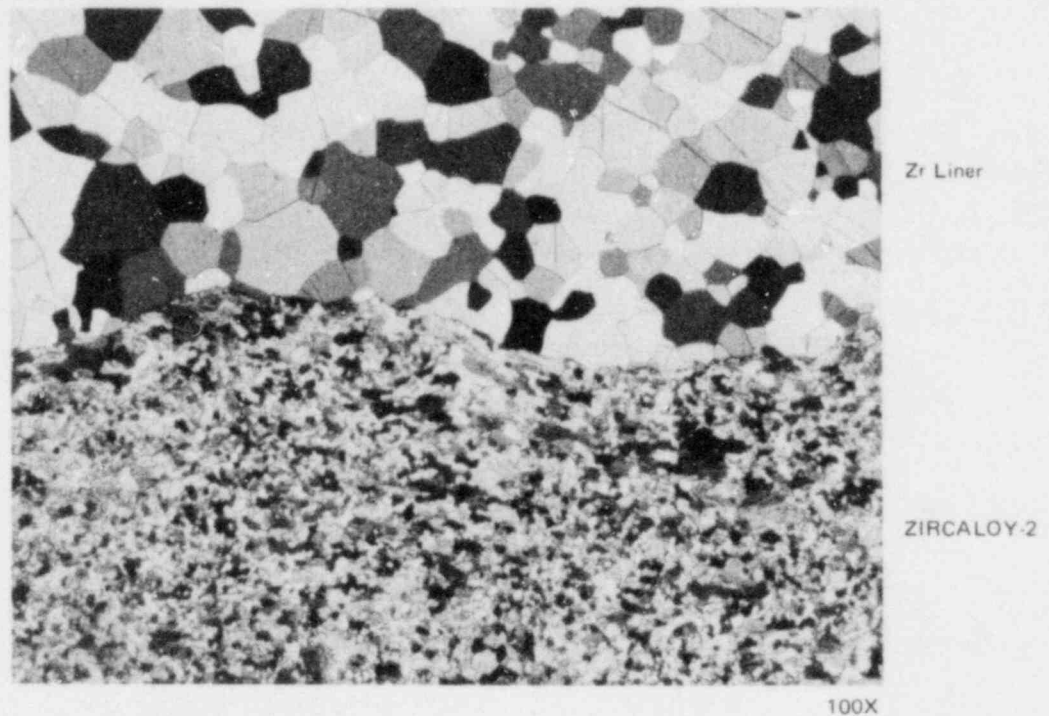
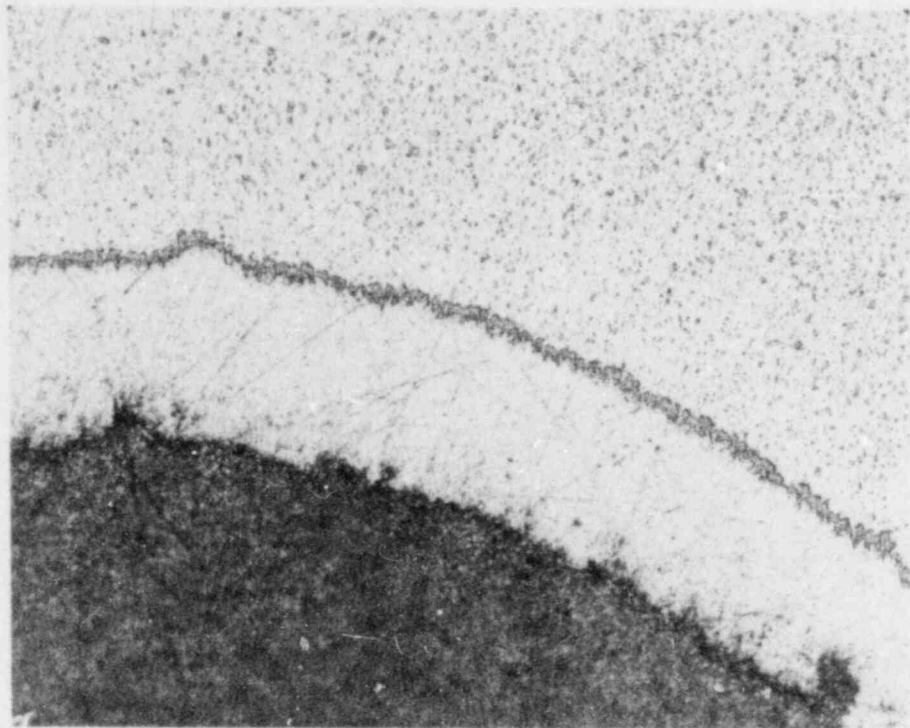


Figure 4.3-1. Example of Low-Oxygen Sponge Zirconium-Lined Tubeshell Showing the Zircaloy-Zirconium Interface Prior to Tube Reduction

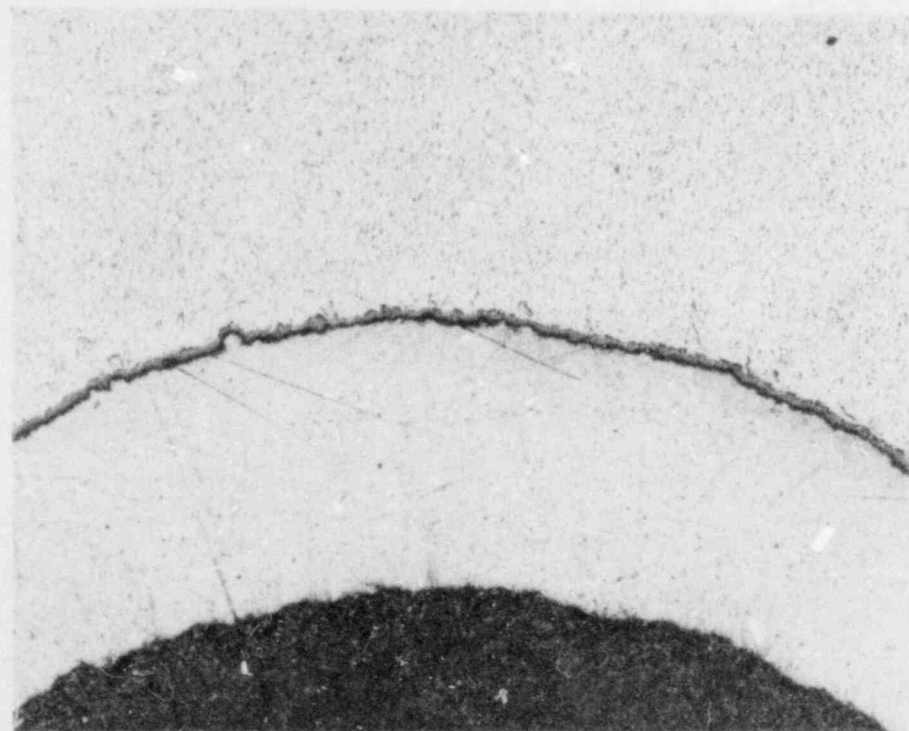
4.4 SUBTASK III. 3 IRRADIATION AND EVALUATION (J. R. Thompson, NFSED)

Power history data using the Fuel Performance Analysis and Data Acquisition System (FPADAS)³ will be collected for both the lead test assemblies in Quad Cities Unit 1 and the demonstration fuel planned for Quad Cities Unit 2. The fact that the Quad Cities is a dual unit station controlled by the same process computer allows the data from Units 1 and 2 to be collected on the same magnetic tape. Software modifications are currently being made so that the process computer will provide the power histories from both plants. The new software program will allow the core performance and detailed power history data from each plant to be separated and stored for later use.



(a)

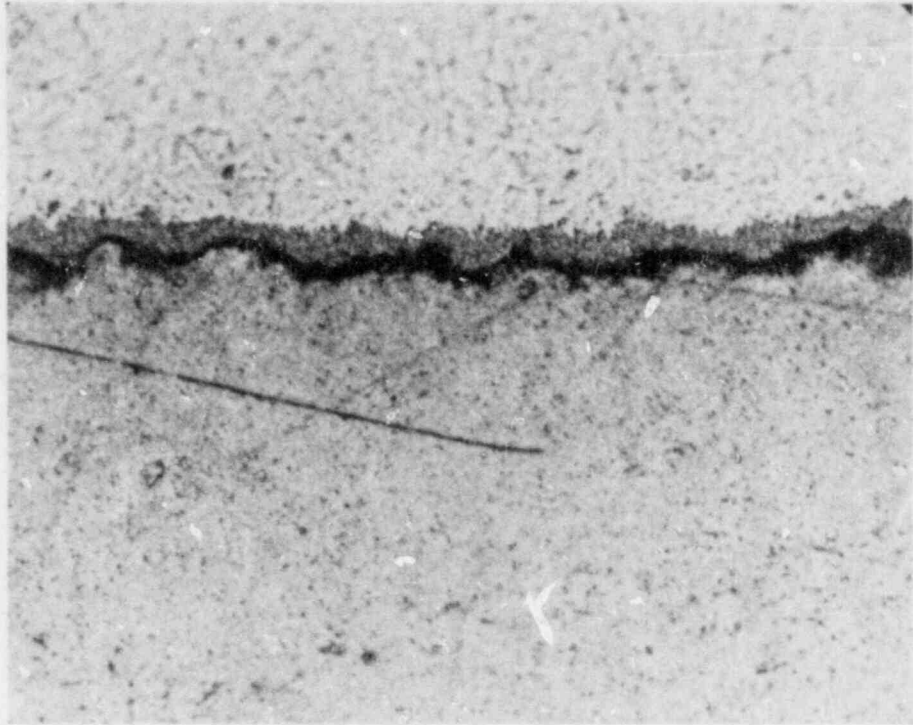
200X



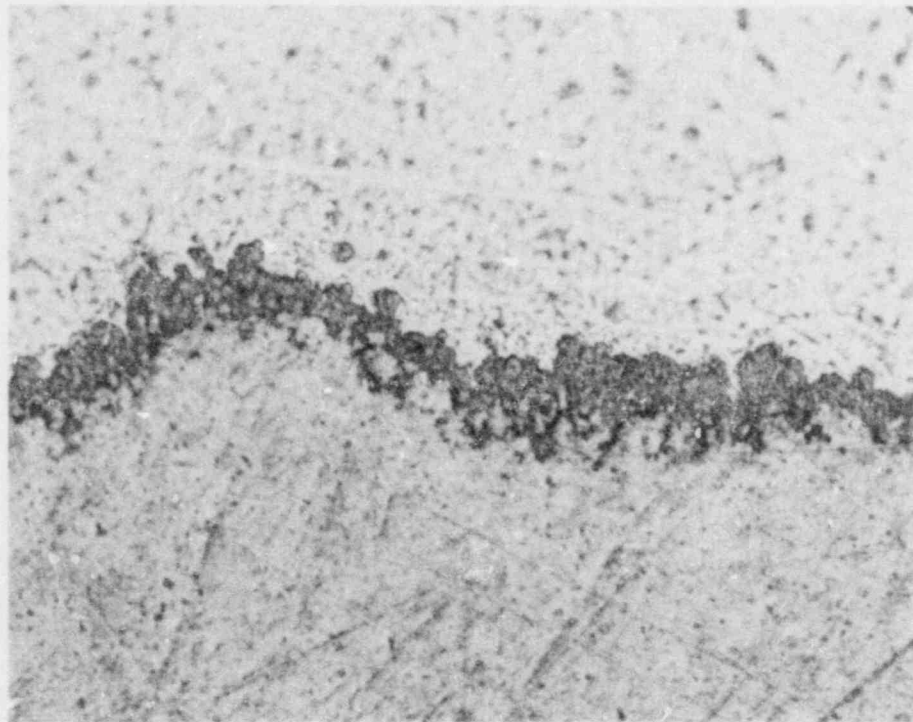
(b)

200X

Figure 4.3-2. Electroless Copper Plated on Oxidized Zircaloy, Viewed in Tapered Section. (a) WLM (b) CRD

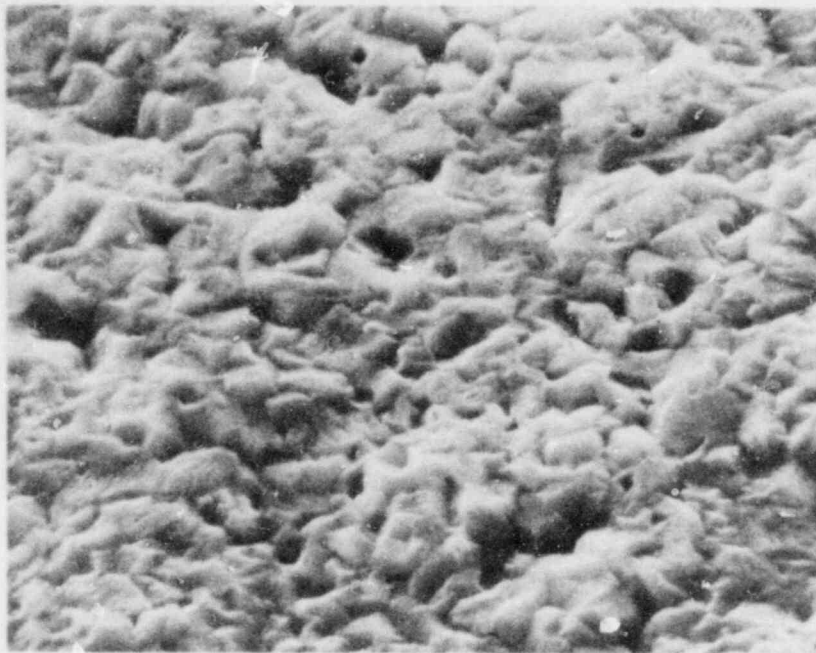


(a)



(b)

Figure 4.3-3. Same as Figure 4.3-2 at 1000x



(a)

5000X



(b)

5000X

Figure 4.3-4. Scanning Electron Micrographs of Copper Surfaces Electroless Plated on Oxidized Zircaloy. (a) WLM (b) CRD

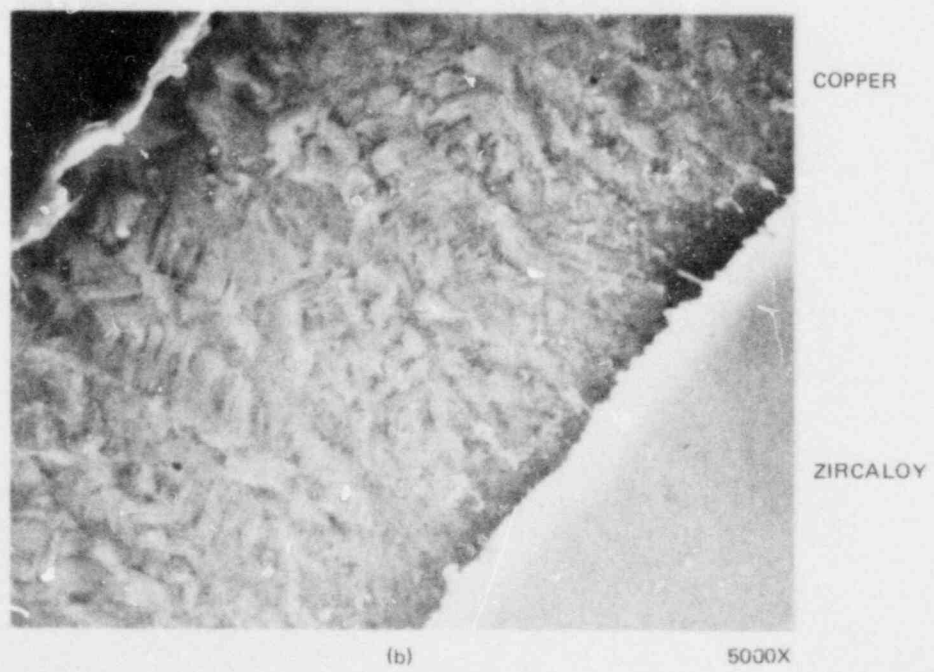
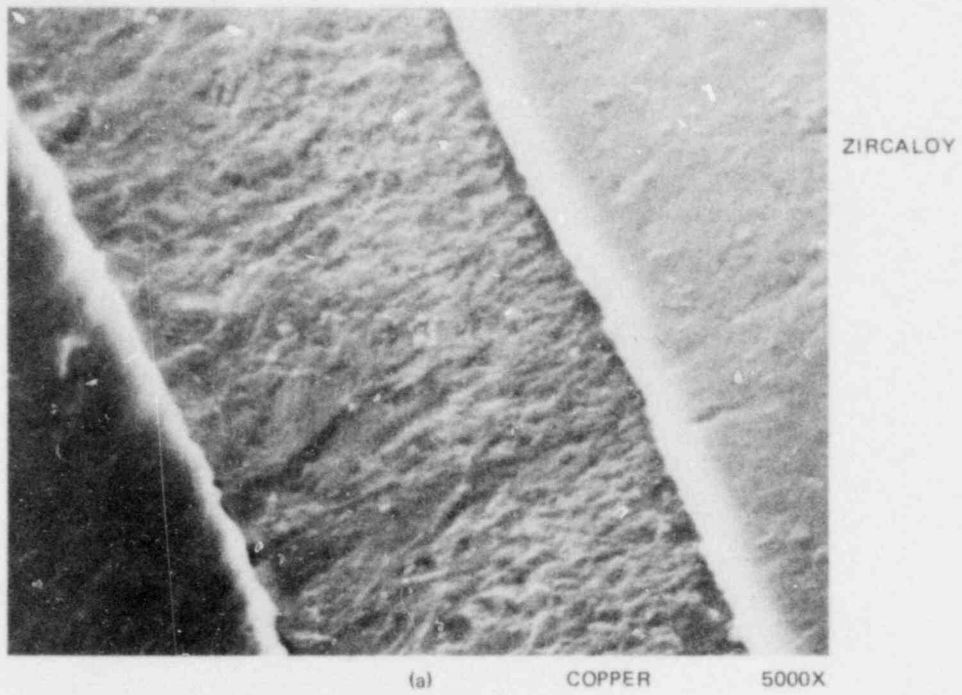
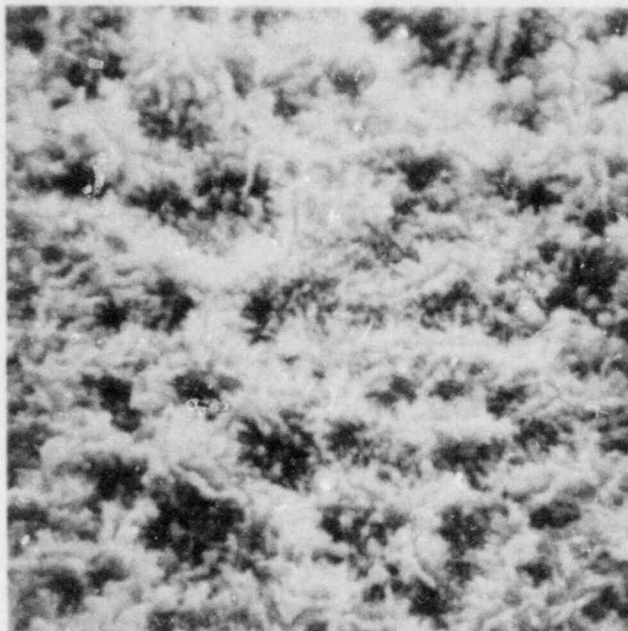
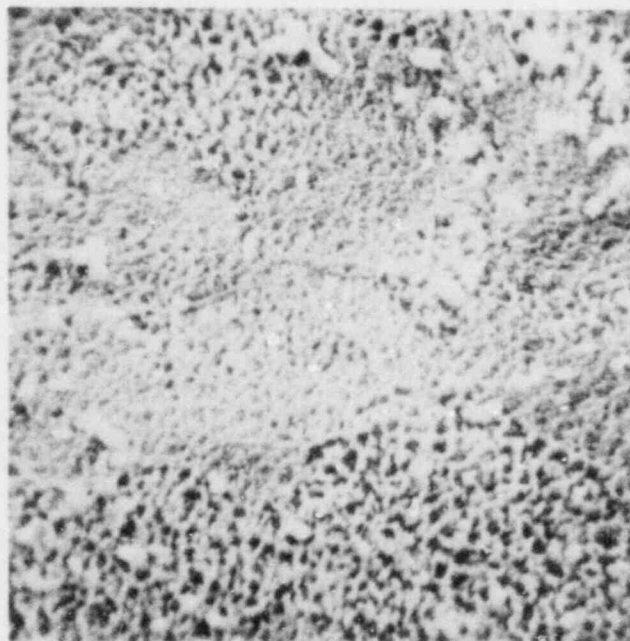


Figure 4.3-5. Copper Electroless Plated on Oxidized Zircaloy Viewed on Polished Cross Sectioned and Etched. (a) WLM (b) CRD



(a)

5000X



(b)

5000X

Figure 4.3-6. Zircaloy Tubing Surfaces After Removal of Copper in Dilute aq. HNO_3 , (a) WLM; (b) CRD

ACKNOWLEDGEMENTS

The contributing authors of Subsection 4.3 gratefully acknowledge the help of their colleagues:

J. C. Madore of WMD for ultrasonic test development

C. A. McKinney of WMD for planning and execution of tube reduction

R. S. Moore of WMD for invaluable guidance on barrier fabrication techniques

R. E. Strina of WMD for assisting with quality assurance

C. Robertson and N. Lewis of CRD for doing the scanning electron micrographs used in this report.

A. S. Holik, J. M. Grande and C. Rodd of CRD for metallography of the copper-plated Zircaloy

5. TASK IV LEAD TEST ASSEMBLIES (J. R. Thompson, NFSED)

Irradiation continues on the barrier lead test assemblies (LTA's) at Quad Cities Unit 1. Operating data is being collected and stored on magnetic tapes. The exposure through December 1979 is approximately 6.5 MWd/kg U.

The purpose of these assemblies is to precede the large scale demonstration fuel assemblies with significant exposures. (See Subtask III.3.) The LTA bundles will be inspected during the fall 1980 outage. (Shutdown is tentatively scheduled for October 15, 1980 for 15 weeks.)

ACKNOWLEDGEMENTS

The help of the following people is gratefully acknowledged by the author of Section 5:

W. A. Wong of NFSED for help in compiling and computing the power history data

C. Brown of the Quad Cities Nuclear Power Station, Commonwealth Edison Company for his cooperation and assistance in collecting the operating history data.

REFERENCES

1. Demonstration of Fuel Resistant to Pellet-Cladding Interaction, PHASE 2 First Semiannual Report, January-June 1979, compiled by H. S. Rosenbaum, GEAP-25163-1, August 1979.
2. Demonstration of Fuel Resistant to Pellet-Cladding Interaction, PHASE 1 Final Report, compiled by H. S. Rosenbaum, GEAP-23773-2, March 1979.
3. Demonstration of Fuel Resistant to Pellet-Cladding Interaction, Second Semiannual Report January-June 1978, compiled by H. S. Rosenbaum, GEAP-23773-1, September 1978.
4. Demonstration of Fuel Resistant to Pellet-Cladding Interaction, First Semiannual Report, July-December, 1977, compiled by H. S. Rosenbaum, GEAP-23773, February 1978.
5. S. R. Specker, L. E. Fennern, R. E. Brown, K. L. Stark, and R. L. Crowther, "The BWR Control Cell Core Improved Design", *Trans. Amer. Nucl. Soc.*, **30** (1978) 336.
6. B. Cox, "Oxidation of Zirconium and its Alloys", *Advances in Corrosion Science and Technology*, **5** (1976) 173.
7. R. S. Forsyth, W. H. Blackadder, K. Malen and G. Rönnerberg, "Fission Product Release to Loop Water from Operating Intentionally Defected Fuel", paper presented at IAEA Specialists Meeting on Defected Fuel Performance, Chalk River, Ontario, Canada, September 1979.
8. S. Junkrans and O. Värnild, "ASEA-ATOM Research on PCI", *Proceedings of Topical Meeting on Water Reactor Fuel Performance*, St. Charles, Ill., May 1977.
9. F. Garzarolli, R. Manzel, M. Peehs and H. Stehle, "KWU Observations and Hypothesis of PCI Failures", paper presented at IAEA Specialists Meeting on PCI, Vienna, Austria, June 1977.
10. H. Kleykamp, "The Chemical State of LWR High Power Fuel Rods under Irradiation", Karlsruhe Nuclear Research Center Report No. 2696, Jan. 1979 (in German).
11. D. H. Locke, "The Behavior of Defective Reactor Fuel", *Nucl. Eng. and Design* **21**, 318 (1972).

DISTRIBUTION

U.S. DOE Distribution (200)
 Category UC-78
 U.S. Department of Energy
 Technical Information Center
 P.O. Box 62
 Oak Ridge, TN 37830

J. S. Armijo
 General Electric Co.
 Nuclear Energy Division
 175 Curtner Avenue
 San Jose, CA 95125

D. E. Bessette
 Advisory Committee on Reactor
 Safeguards
 U.S. Nuclear Regulatory Commission
 1717 H. Street NW
 Washington, DC 20555

Gordon Bond
 GPU Service Corp.
 260 Cherry Hill Road
 Parsippany, NJ 07054

F. W. Buckman
 Consumers Power Company
 1945 Parnall Road
 Jackson, MI 49201

J. P. Cagnetta
 Northeast Utilities Service Co.
 P.O. Box 270
 Hartford, CT 06101

E. L. Courtright
 Battelle Pacific Northwest Laboratory
 Richland, WA 99352

C. E. Crouthamel
 Exxon Nuclear Company, Inc.
 Richland, WA 99352

G. F. Daebeler
 Philadelphia Electric Co.
 2301 Market Street
 P.O. Box 8699
 Philadelphia, PA 19101

R. N. Duncan
 Combustion Engineering, Inc.
 1000 Prospect Hill Road
 Windsor, CT 06095

M. D. Freshley (3)
 Battelle-Pacific Northwest Laboratory
 Richland, WA 99352

F. E. Gelhaus
 Electric Power Research Inst.
 P.O. Box 10412
 Palo Alto, CA 94303

D. J. Groetch
 Knolls Atomic Power Laboratory
 Box 1072
 Schenectady, NY 12301

R. M. Grube
 Yankee Atomic Electric Co.
 20 Turnpike Road
 Westboro, MA 01581

John Hallam
 Nuclear Services Corp.
 1700 Dell Avenue
 Campbell, CA 95008

C. R. Hann
 Battelle-Pacific Northwest Laboratory
 Richland, WA 99352

W. R. Harris
 Rand Corporation
 1700 Main Street
 Santa Monica, CA 90406

J. Horak
 Oak Ridge National Laboratory
 P.O. Box X
 Oak Ridge, TN 37830

William V. Johnston
 Chief, Fuel Behavior Research Branch
 Division of Reactor Safety Research
 U.S. Nuclear Regulatory Commission
 Washington, D.C. 20555

W. M. Kiefer (6)
 Commonwealth Edison Company
 P.O. Box 767
 Chicago, IL 06090

J. Korthever
 Duke Power Company
 P.O. Box 2178
 Charlotte, NC 28342

P. M. Lang (3)
 Nuclear Reactor Programs Branch
 Division of Nuclear Power Development
 U.S. Dept. of Energy
 Mail Stop B-107
 Washington, D.C. 20545

D. L. Larkin
 Washington Public Power Supply System
 P.O. Box 968
 Richland, WA 99352

M. L. Lee
 Consolidated Edison Company
 of New York
 4 Irving Place
 New York, NY 10003

Kashmiri Mahna
 Public Service Electric
 and Gas Co.
 80 Park Place
 Newark, NJ 07101

Tony Mansell
 Arkansas Power & Light
 P.O. Box 551
 Little Rock, AK 72203

R. O. Meyer
 Attn: M. Tokar
 Reactor Fuels Section
 Division of Systems Safety
 U.S. Nuclear Regulatory Commission
 Washington, D.C. 20555

R. S. Miller
 Westinghouse Electric Corp.
 Nuclear Fuel Division
 Box 355
 Pittsburgh, PA 15230

R. J. Mullin
 Tennessee Valley Authority
 1410 Commerce Union Bank Bldg.
 Chattanooga, TN 37402

D. R. O'Boyle
 Commonwealth Edison Co.
 P.O. Box 767
 Chicago, IL 60690

R. R. O'Laughlin
 Public Service Indiana
 1000 East Main Street
 Plainfield, IN 46168

R. Omberg
 Hanford Engineering Development
 Laboratory
 P.O. Box 1970
 Richland, WA 99352

B. A. Pasternak
 Booz-Allen Applied Research
 4330 East-West Highway
 Bethesda, MD 20014

J. T. A. Roberts
 Electric Power Research Inst.
 P.O. Box 10412
 Palo Alto, CA 94303

T. Row
 Oak Ridge National Laboratory
 P.O. Box X
 Oak Ridge, TN 37830

H. W. Schadler, Manager
 Metallurgy Laboratory
 General Electric Company
 Research and Development Center
 P.O. Box 8
 Schenectady, NY 12301

T. Snead
 Duke Power Company
 P.O. Box 2178
 Charlotte, NC 28342

Howard Sobel
 American Electric Power Service Corp.
 Nuclear Materials and Fuel
 Management Section
 2 Broadway
 New York, NY 10004

G. Sofer
 Exxon Nuclear Company, Inc.
 Richland, WA 99352

I. Spiewak
 Oak Ridge National Laboratory
 P.O. Box X
 Oak Ridge, TN 37830

E. Straker
Science Applications, Inc.
8400 Westpark Drive
McLean, VA 22101

J. R. Tomonto
Florida Power & Light Co.
P.O. Box 013100
Miami, FL 33101

J. Tulenko
Babcock & Wilcox Co.
Nuclear Power Generation Div.
P.O. Box 1260
Lynchburg, VA 24505

W. J. Tunney
Long Island Lighting Co.
175 E. Old Country Road
Hicksville, NY 11801

D. B. Wehmeyer
Detroit Edison Co.
2000 Second Avenue
Detroit, MI 48226

W. A. Weinreich
Bettis Atomic Power Laboratory
Box 79
West Mifflin, PA 15122

K. Woods
Exxon Nuclear Company, Inc.
Richland, WA 99352